Model for Studying the Physiological Role of Non-cell Autonomous Factors on Neuromodulation

Changho Chun

A dissertation
submitted in partial fulfillment of the
requirements for the degree of

Doctor of Philosophy

University of Washington

2022

Reading Committee:

David L. Mack, Chair
Andre Berndt
Ying Zheng
Alec S.T. Smith

Program Authorized to Offer Degree:

Bioengineering

University of Washington

Abstract

Model for Studying the Physiological Role of Non-cell Autonomous Factors on Neuromodulation

Changho Chun

Chair of the Supervisory Committee:

David L. Mack

Department of Rehabilitation Medicine

The intercellular communication in the ventral horn of the spinal cord is essential for the motor function to innervate skeletal muscle. Hence, the progressive pathologies of several neuromuscular diseases (NMDs) are likely to be driven by defects in more than one cellular subtype in the ventral spinal cord. However, current neuro-centric human NMD modeling efforts do not recapitulate the nature of non-cell autonomous neuromodulation occurring upstream of the disease, which significantly limits our pathologic understanding. Therefore, in spite of the recent advancement in developing human induced pluripotent stem cell (hiPSC)-derived neurons, the pathologic mechanism of non-cell autonomous neurodegeneration remains elusive. Moreover, the current differentiation process of iPSC-derived spinal motor neurons does not accurately mirror the transcriptomic trajectories of the native ventral spinal cord development, limiting the application of the differentiated neurons. To address these shortcomings, we studied the role of exogenous physiological inputs on neuromodulation using human iPSC-derived spinal motor neurons, spinal astrocytes, and inflammatory stress factors. We studied the neuroprotective mode of astrocytes in normal tissue and demonstrated that astrocyte-derived extracellular vesicles enhance the longevity and electrophysiological function of immature iPSC-neurons. Additionally, we showed that excessive exposure to the pro-inflammatory cytokine interferon-

γ, which is secreted from a broad range of immune cells, induces an extensive transcriptomic alteration of iPSC-derived motor neurons toward neurodegeneration, leads to the expression of pathologic hallmarks of ALS. Finally, we assessed the physiological relevance of the iPSC-derived motor neurons we used in this study. We performed a longitudinal transcriptomic analysis of differentiating iPSC-motor neurons at each critical time point of development, to compare it with that of the developing human spinal cord ventral horn. We expect this comprehensive transcriptomic mapping at a single-cell level will provide us invaluable guidance for improving our spinal neuron differentiation strategy. Together, we believe our findings contribute to understanding how the human motor circuit is developing and affected by surrounding factors in normal and diseased conditions, which could lead to developing more reliable human neuromuscular models eventually to identify future therapeutic targets of NMDs.

Table of Contents

Acknowledgement

I would first like to thank my advisor, Dr. David L. Mack. You gave me an invaluable chance to study in your lab and learn how to raise important scientific questions, run a wide range of projects to test interesting hypotheses, and collaborate with excellent scientists which all shaped me into the scientist I am today. You trusted me with considerable freedom to pursue various projects of my interest, while also supporting those works with your keen scientific insight and guidance which significantly helped me go through all of the difficulties in research. Moreover, I truly appreciate your personal mentorship offered every day which allowed me to stay motivated and be productive over the course of my training. It was an incredible privilege to work with you and I will forever be grateful for your support in my graduate experience and beyond.

I also owe great thanks to Dr. Alec S.T. Smith who has been my daily scientific mentor to carry out most of the research projects together, and Dr. Mark Bothwell for providing such great support with his rich insight on neurobiology. I highly appreciate both of your guidance on my research which could not have been made this far without your help. I would also like to thank my supervisory committee, Dr. Andre Berndt, Dr. Ying Zheng, Dr. Alec S.T. Smith, and Dr. Alshakim Nelson for their tremendous mentorship and guidance on my graduate studies. I am grateful for all of your support to make me grow as a big thinker, researcher, and a member of the scientific community.

I must also thank the members of the Mack lab and friends in ISCRM community for their friendship and support throughout my graduate study. Although not all of them are listed here, these are several individuals who have had a pleasant impact on my last 5 years of life. Justin Daho Lee, Dr. Jung Hyun Lee, Juyoung Seong, Yu Jung Shin, Dr. Jongseob Choi, Kyung-Hoon Kim, Dr. Ohjoon Kwon, Dr. Nisa M. Williams, Dr. Jonathan Tsui, Travis Moerk, Dr. Joy Su, Dr. SiWei Luo, Dr. Christian Mandrychy, Dr. Samantha Bremner, Saffie Mohran, Dr. Shawn Luttrell, Dr. Mike Rappleye, Dr. Hyejin Kim, Jaepil Jung, Dr. Yong Tae Kim, Kyungjoon Min, Dr. Dale W. Hailey, Dr. Mary Regier.

I would like to thank my family in Korea for their unconditional love and support throughout my life. I appreciate my parents and sister who encouraged and helped me find a way to pursue what I really want to do without hesitation. Thank you for being such great role models to me as a scientist and as a person. I love you.

Lastly, I would like to express my biggest gratitude to my lovely wife, Hyejin Ko for believing in my ability and deciding to take this challenge with me 5 years ago. You have always provided me with the best support in every aspect in every moment, which allowed me to keep pursuing this goal. I am very proud of what we have accomplished together and I will remember this time forever in my life as we grow old together. I would like to also thank my adorable babies Hyunu Chun and Whochu, for coming into my life and giving all of the unreplaceable emotional support to me. I love you all.

Chapter 1. Introduction

1.1 Neuromuscular disease and implications for human health

Neuromuscular diseases (NMD) collectively affect 250,000 patients in the United States, 160 per 100,000 people worldwide and the majority of them are incurable.[1] The diseases involve progressive degeneration of motor and sensory units in the nervous system, leading to severe skeletal muscle contraction or atrophy. The patients often exhibit respiratory weakness, foot deformities, gait disturbance, grip impairment, and loss of sensation, which worsen over time depending on the subtype of NMD.[2] Management of NMDs has been an intractable challenge since most of them are chronic, rapidly progressive, disabling, and most of all, etiologically heterogeneous.[3,4] Many complex genetic and non-genetic reasons are known to derive the NMD onset and progression, though the detailed pathologic mechanisms for most of them still remain elusive. The treatments are usually limited to physiotherapy, respiratory services, and clinical psychology, which all are not for ultimate therapeutics but auxiliary treatments. Due to the irreversible and progressive nature of those diseases, the financial burden is staggering with costs related to the patient exceeding $46 billion dollars annually.[4]

1.2 Amyotrophic Lateral Sclerosis

Amyotrophic Lateral Sclerosis (ALS) is one of the most devastating NMDs that primarily attacks motor neurons in the central nervous system (CNS).**[Figure 1.1]**[5,6] It begins with focal weakness but spreads relentlessly to most muscles including the diaphragm. The death is usually due to respiratory paralysis occurring within 3-5 years after the onset No therapy so far provides substantial clinical benefit against ALS. The only FDA-approved drugs are Riluzole and Edaravone, inhibiting glutamate-mediated excitotoxicity and reducing ROS-induced cellular stress respectively.[7] However, they all have been showing very limited improvement in neurodegeneration, extending life expectancy for just

several months after treatment without making functional recovery of neuromuscular tissue. 10% of ALS cases are familial type (fALS) caused by inherited genetic mutations, whereas the remaining 90% of cases are sporadic forms caused by a number of potential reasons. [5,6,8] SOD1 was the first ALS gene to be identified in the 1990s, and more than 120 genetic variants including C9orf72, TARDBP, FUS, UBQLN2 are known to be associated with ALS pathology.[7] There are a number of potential risk factors for sporadic ALS (sALS) development, such as smoking, environmental toxin exposure, traumatic brain injury, excessive use of skeletal muscle, or inflammatory stress and those acquired ALS cases often accompany post-translational gene modifications. Despite strikingly heterogeneous etiology, fALS and sALS have similarities in their pathologic features. Interestingly, it has an average onset age of mid-50s regardless of having an inherent genetic mutation, and the clinical symptoms appear nearly indistinguishable in both cases.[5] Thus, the critical questions unaddressed in ALS pathology are: 1) why the symptomatic stage comes so late in a patient's life even with the inherent mutation? 2) what triggers the rapid progression after the late onset? 3) Which exogenous stress factor mostly contributes to the sALS development?

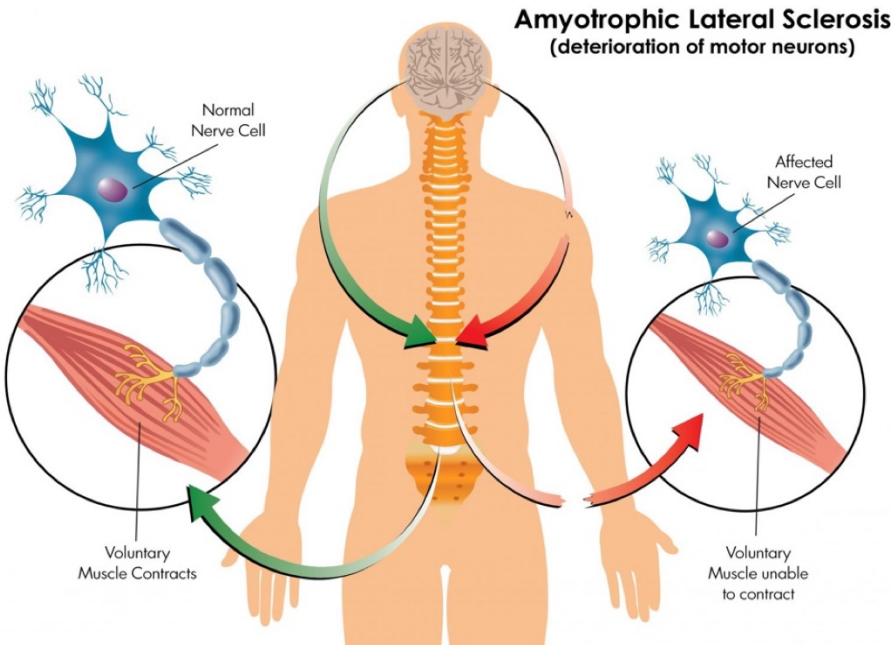

Figure 1.1 Schematic illustration of ALS' core pathology

The discovered hallmarks of ALS tissues are protein aggregation, mitochondrial dysfunction, endoplasmic reticulum stress, excessive neuronal excitability in the initial phase followed by motor neuron death, and altered protein homeostasis with axonal transport ability.[9] Among these, cytoplasmic aggregation of TDP-43 protein (encoded by the TARDBP gene) is one of the most common features observed over 97% of patient's post-mortem tissue in both fALS and sALS cases, indicating this highly

conserved nucleic acid-binding protein might play a critical role on ALS pathology.**[Figure 1.2]**[10] Forced expression of normal TDP-43 puncta by itself is known to trigger neurodegeneration, supports gain of aberrant TDP-43 expression is closely related to the disease development.[11–13] Given that TDP-43 is heavily involved in more than 2,000 gene expression processes including transcriptional regulation, alternative RNA splicing, mRNA migration and stabilization, TDP-43 malfunction is thought to be located at the upstream of the ALS pathology rather than just being a downstream phenotype of the disease, though the mechanism of the TDP-43 proteinopathy remains highly elusive.[11,14–17]

1.3 Non-neuron autonomous pathophysiology in ALS development

Neurons are just part of the ALS story. Although they are the major pathologic targets, it has been demonstrated that the neuro-centric approach has clear limitations in understanding the disease fundamentals. Glial cells such as astrocytes, Schwann cells, oligodendrocytes and microglia are potent neuromodulators that orchestrate neurogenesis, synaptogenesis, homeostasis and function from very early neurodevelopmental stage. [18,19] Increasing evidence points out those cells could be an initial target of degeneration to relay the pathological effect to neurons. Astrocytes are the most abundant glial cells in the CNS, particularly getting tremendous attention in ALS pathology given their indispensable role in neurophysiology. In normal conditions, they are heavily involved in the

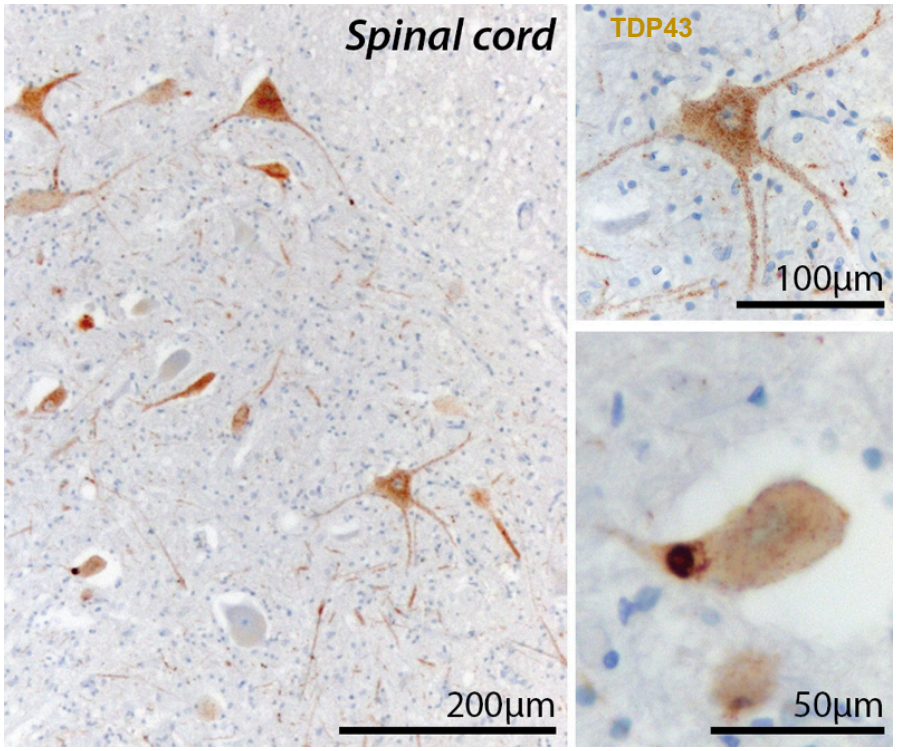

Figure 1.2 Cytoplasmic misallocation of TDP-43 in the spinal cord tissue harvested from a sporadic ALS patient.

neurotransmitter regulation in the extracellular microenvironment, CNS vascularization signaling, neurotrophic support, neurometabolites control and ionic regulation, all from the early stage of neurogenesis.[20–22] Neuron's significant dependence on astrocyte's input for initial development, maturation and function made the hypothesis that loss of neuroprotective roles of astrocytes and/or gain of neurotoxic function of diseased astrocytes to be marked as a powerful pathologic factor in ALS development reasonable.[23] **[Figure 1.3]**

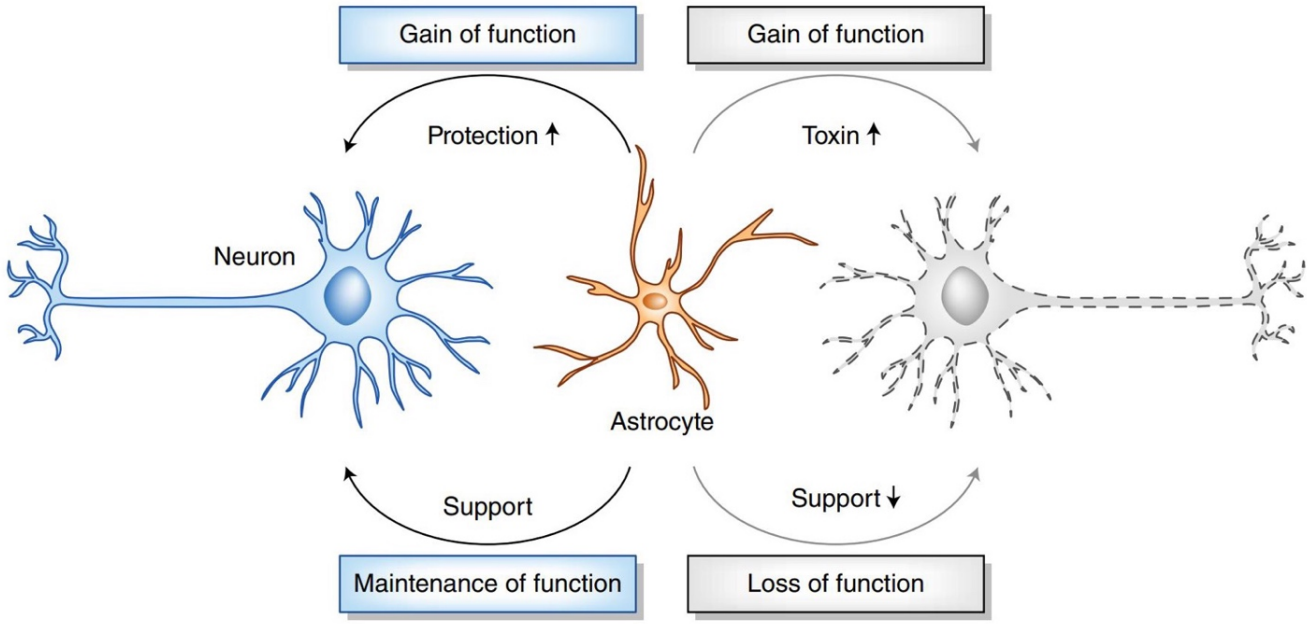

Figure 1.3 Graphical hypothesis about the bi-faced neuromodulation of astrocytes in normal and diseased condition

One of the known mechanisms involving astrocytes in early ALS pathology is a malfunction in glutamate regulation, which exerts excitotoxicity to neurons near the synaptic area. Astrocytes in normal condition uptakes the extra glutamates through glutamate transporter EAAT1,2 to buffer extracellular glutamate concentration for providing balanced excitatory neurotransmission to nearby neurons.[24] The astrocytic defect on extracellular glutamate clearance was proven to damage neurons in SOD1 mutant and sporadic ALS mouse models, and a number of clinical studies also implicated the elevated glutamate level in patient's body fluid was excitotoxic to motor neurons.[24–26] The downstream phenotypes of excitotoxic damage include disruption of intracellular calcium dynamics, generation of

reactive oxygen species (ROS), and mitochondrial dysfunction in ATP production, leading to progressive neuron loss. The hyperexcitation of neurons before death has been particularly evident in the pre-symptomatic stage of the disease, implying the pathologic input of malfunctioned astrocytes are a critical factor for relatively early phase of disease development.[27,28] Although the ablation of the diseased astrocytes made a dramatic improvement in neuronal survival, there still is missing information on which astrocyte-derived factor(s) induce neurodegeneration at each of the disease progression stages.[29–31]

Increasing number of studies imply the insoluble protein aggregation in neurons may be attributed to the pathologic input of impaired astrocytes. As mentioned in the previous section, cytoplasmic protein aggregation such as TDP-43, FUS, Ubiquitin is a characteristic feature penetrating etiologically heterogeneous ALS cases, postulated as a common pathologic factor as well as a potential therapeutic target for ALS treatment. Although protein inclusion has been observed in astrocytes as well, the role of astrocytes on TDP-43 proteinopathy is unclear. Moreover, contradictory results from recent studies regarding non-neuron autonomous TDP-43 proteinopathy hinder gaining clear insight into how protein inclusion contributes to ALS pathology. Serio *et a*l reported the TDP-43 mutant astrocytes (M337V) did not adversely affect the survival of co-cultured neurons, even with cytoplasmic TDP-43 localized in the astrocytes. The cumulative risk of death of WT motor neurons cultured on mutant astrocytes was not significantly different from that of the same neurons cultured on WT astrocytes, suggesting that mutant astrocytes are not directly inducing motor neuron death.[32] On the contrary, Tong *et al* reported the selective TDP-43 mutant expression in rat astrocytes caused a progressive loss of motor neurons and the subsequent skeletal muscle denervation, resulting in progressive paralysis.[33] In the study of Peng *et al*, the genetic ablation of TDP-43 in astrocytes exhibit A1-like reactive phenotype. Although the TDP-43$^{-/-}$ astrocytes did not affect the viability of co-cultured neurons, the manipulated mice showed motor deficits, implying the non-neuron autonomous functional impairment caused by the absence of astrocytic TDP-43.[34] The disagreement may come from the

difference in phenotypic severity of TDP-43 mutant astrocytes at the time of neuron co-culture, as the cytoplasmic accumulation of the protein granules is increasing as they age. Furthermore, the astrocyte proteinopathy might not be a direct trigger of neuron's significant death at the late stage of ALS, but enough to induce progressive functional impairment of neurons at the initial symptomatic phase. Finally, TARDBP mutation *per se* in astrocytes might not exert a neurotoxic effect directly but could be a secondary risk factor to trigger a detrimental immune response, which may lead to the neurodegeneration as a severe inflammatory response. Although with the different type of ALS causing mutation, recent transcriptomic study of SOD1 mutant astrocytes revealed the mutant astrocytes have significantly dysregulated expression of genes for coping with inflammatory stress. Since the increased vulnerability of astrocytes to the inflammatory cytokine attack was proven to induce their neurotoxic phenotype expression, the mutation might work as a trigger of astrocyte-mediated neurodegeneration by lowering the threshold to the inflammatory stress. [29] Interestingly, the stressed astrocytes were also proven to act as additional sources of pro-inflammatory cytokine release, such as type I and type II interferons upon initial stress, to exacerbate neurodegenerative phenotype expressions.

The intervention of immunity is in fact an important axis of the non-neuron autonomous neurodegeneration in ALS. Recent findings implicate the microglia and astrocytes which are responsible for defending nerves from infection in normal conditions may play a central role in rapid ALS progression at the symptomatic stage. Liddelow *et al* demonstrated that microglia under inflammatory stress secretes an excessive amount of cytokines (e.g. IL-1a, TNF, C1q) that primes astrocytes to express neurotoxic A1 phenotype.[29]A1 astrocytes are known to be abundant in various human neurodegenerative diseases including not only ALS but Alzheimer's, Huntington's, and Parkinson's disease. Since the survival of CNS neurons in those diseased tissues without A1 astrocytes was normal, the inflammatory stress-bearing 'microglia - astrocyte axis' may be a critical driver of rapid neurodegeneration at the late stage of the disease. Another recent study provided evidence of interferon-gamma (IFNγ) which is a potent inflammatory cytokine secreted from the diverse types of

immune cells in our body induced neurodegeneration that recapitulates phenotypes of neurodevelopmental disorders such as schizophrenia and autism.[35] Aebischer *et al* added an interesting discovery on this by showing ALS mutant (SOD1) astrocytes express a significantly elevated level of IFNγ for extracellular secretion, implying the cytokine could play a central role in the astrocyte's neurodegeneration mechanism.[36] In summary, ALS appears to be a multifactorial disease with complex pathological mechanisms but is likely to require the intervention of non-neuronal factors for inducing severe neurodegeneration that leads to the disease development toward the symptomatic stage. However, the majority of the non-neuron autonomous neurodegenerative mechanism and molecular drivers of ALS development still remain unclear.

1.4 Human Induced Pluripotent Stem Cells: Applications and Limitations to Model NMD

Animal models of ALS have been widely used to understand its pathologic mechanism. Transgenic ALS rodent models are usually generated by overexpressing human ALS-inducing mutant genes such as SOD1, TARDBP, c9orf72, FUS. Although these models provided invaluable resources for studying molecular cascades of pathogenic processes, their clear limitations of human relevance and low throughput initiated the development of human ALS model using induced pluripotent stem cells (hiPSCs). Since Yamanaka *et al* have shown that activating 4 different transcription factors (Myc, Oct3/4, Sox2, Klf4) can reprogram human adult somatic cells back in time to an embryonic-like pluripotent state, iPSC-based platforms have been widely used for deriving almost every cell type in the human body for developmental study and disease modeling.[37–39] To utilize iPSCs' merits to circumvent ethical issues while maintaining embryonic pluripotency, ALS research society has been putting an enormous effort to differentiate iPSCs into functional spinal motor neurons, glial cells, and skeletal muscle. The collective endeavor provided us the first opportunity to develop cell subtypes from actual ALS patients with known genotypes and phenotypes, which was not feasible with embryonic stem cells. [37]

Among those ALS-relevant cell types, spinal motor neuron differentiation has been mostly studied to recreate the upstream pathology of the disease. Chambers *et al* discovered that inhibition of BMP-4 and TGF-beta signaling by the combinatorial use of small molecules SB431542 and LDN193189 in the early phase of iPSC differentiation blocks endoderm and mesoderm fates, leads to the efficient generation of neuroectodermal cells in a few days.[40] The dramatic enrichment of neuroectodermal cells through this dual-SMAD inhibition was confirmed by high expression of paired box protein 6 (PAX6), sex-determining region Y-box2 (SOX2) and intermediate filament protein, Nestin.[41] As the neuroectoderm is specified, further signaling gradients act as morphogenic cues to establish rostro-caudal and dorso-ventral neural axes. The paraxial mesoderm surrounding the early neural tube secretes retinoic acid (RA), which induces caudalization and further directs neurogenesis. RA signaling gradually decreases caudally down the spinal cord, as indicated by the increased inhibitory activity of FGFs that are highly expressed in the lumbar spinal cord and tail bud. In addition to RA and FGFs, Wnts are also required for the induction of caudal hindbrain and spinal cord identities. Another key morphogen drives dorso-ventral spinal identity is Sonic Hedgehog (SHH). SHH is secreted from the notochord in a gradated manner along the dorso-ventral axis. High SHH concentrations promoted ventral spinal subtypes whereas SHH concentration faded out near the dorsal horn. Gradient patterning of SHH further controlled the population ratio of motor neuron and interneuron in the spinal ventral horn as well. [41,42] **[Figure 1.4]**

This initial breakthrough has led investigators to further pattern multipotent neural progenitors toward spinal neuron population by reducing the contaminating sensory neurons and glial cells in culture. Du *et al* demonstrated that combinatorial treatment of SB431542, LDN193189 and CHIR99021 (Wnt agonist) for a longer period than previous protocols together with CompoundE (anti-mitotic reagent) significantly depresses the proliferation of contaminating cells.[43] More than 20 published protocols so far demonstrated the differentiated cells consistently expressing pan-neuronal markers (e.g. MAP-2, TuJ1, Neurofilament) as well as 25-40% motor neuron-specific proteins (e.g. Islet-1, HB9)

by day 25-30 of differentiation.[42–47] The successful derivation of functional neurons was further demonstrated by running electrophysiological functional assessments, such as patch clamp and multi-electrode assay (MEA) assays.[48]

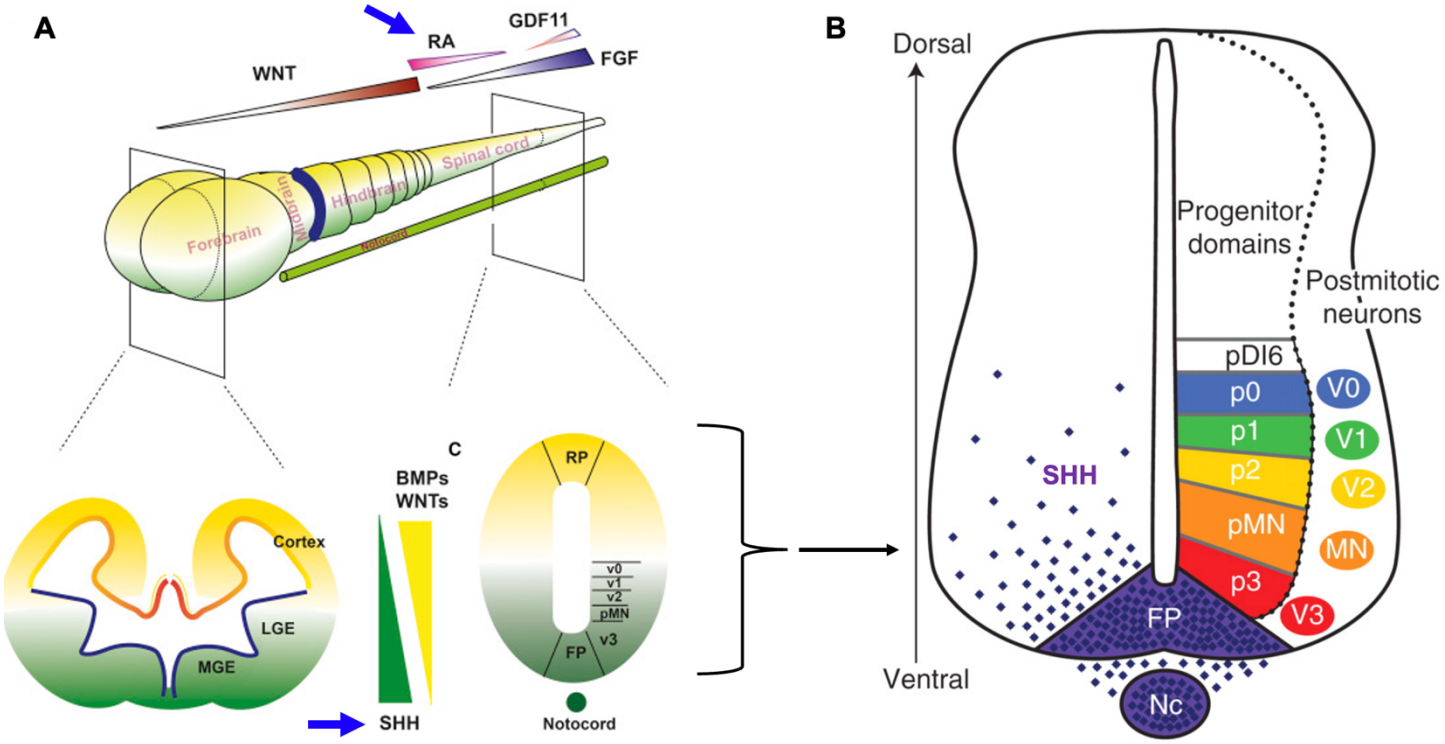

Figure 1.4 Major signaling pathways and morphogens for native CNS neuron development (A) Illustration of morphogen gradient forms each part of CNS. RA and SHH control the degree of caudalization and ventralization, respectively. (B) The cross-section of the spinal cord shows the developing location of ventral neuron subpopulations.

Despite this huge progress, iPSC-derived neurons obtained from a series of small molecule treatments exhibit immature physiology compared to their *in vivo* counterparts in the adult spinal cord. The biggest roadblock is coming from the lack of fundamental understanding about how the current *in vitro* differentiation process is spatiotemporally different from native spinal neurogenesis, particularly in terms of signaling kinetics occurring at each stage of development. As such, mutant iPSC-derived neurons might merely represent early-stage pathology rather than the late stage of neurodegeneration. Given that over 90% of ALS patients are sporadic cases with late-onset in the age of 50-60's, the iPSC-neuron model falls short of to model symptomatic stage's pathologic environment. Moreover, those motor neuron differentiation protocols produce a network of ventral spinal neurons as a whole, including

various subtypes of interneurons as well. However, we do not know how closely the differentiated culture represents the native spinal tissue in terms of subpopulation composition or transcriptional profiles. Studies in mice showed that ventral spinal cord motor circuits incorporate more than a dozen motor neuron and interneuron subtypes, but the composition and transcriptomic profiles of human spinal cord neurons are unknown and unlikely to be identical to that of the mouse. With iPSC-motor neuron differentiation protocol, Thiry *et al* recently reported the differentiating culture at day 28 is composed of 35% motor neurons, 28% interneurons and 22% glial cells without providing a further classification of cell subtypes, which could be highly dependent on differentiation schemes.[47] Therefore, available data does not provide a sufficient yardstick to assess the capacity for our differentiation protocols to produce populations that accurately represent the human spinal cord ventral horn, making the reliability of iPSC-based neurodegenerative disease modeling still questionable. To accurately model ALS pathophysiology, it is indispensable to generate neurons that express comparable transcriptomic profiles of native spinal neurons, as well as being receptive to the glial-derived cues to recapitulate neuroglial interactions that constitute the pathologic core of the symptomatic ALS tissue.

As mentioned, glial cells are potent upstream mediators of neurons, likely to be heavily involved in both neuroprotection and neurodegeneration in a number of neurodegenerative diseases. Despite their importance, it is not until very recently that glial cells are included in neurodegeneration studies while neurons have been getting tremendous attention. As such, developing differentiation protocols for various human iPSC-derived glia was not initiated until recently. However, as the increasing number of evidence has been implying their substantial role in nervous system development and degeneration under disease conditions, establishing reliable iPSC-glia differentiation protocols became a foremost important prerequisite to model neurodegeneration as a whole. Among those glial cell types, astrocytes are the most abundant cells in our nervous system with neurons (astrocytes to neurons population ratio in human cortex = 1.65:1) and their development is relatively well-studied than others. During mouse embryogenesis, astrocytes and neurons are generated from the same precursors, radial glia which is

the earliest cell type coming from the lateral wall of the neural tube.[21] Astrogenesis sequentially follows neurogenesis but does not initiate until the late embryonic stage to early postnatal period where radial glia differentiates into astrocyte progenitors. **[Figure 1.5]** [49]

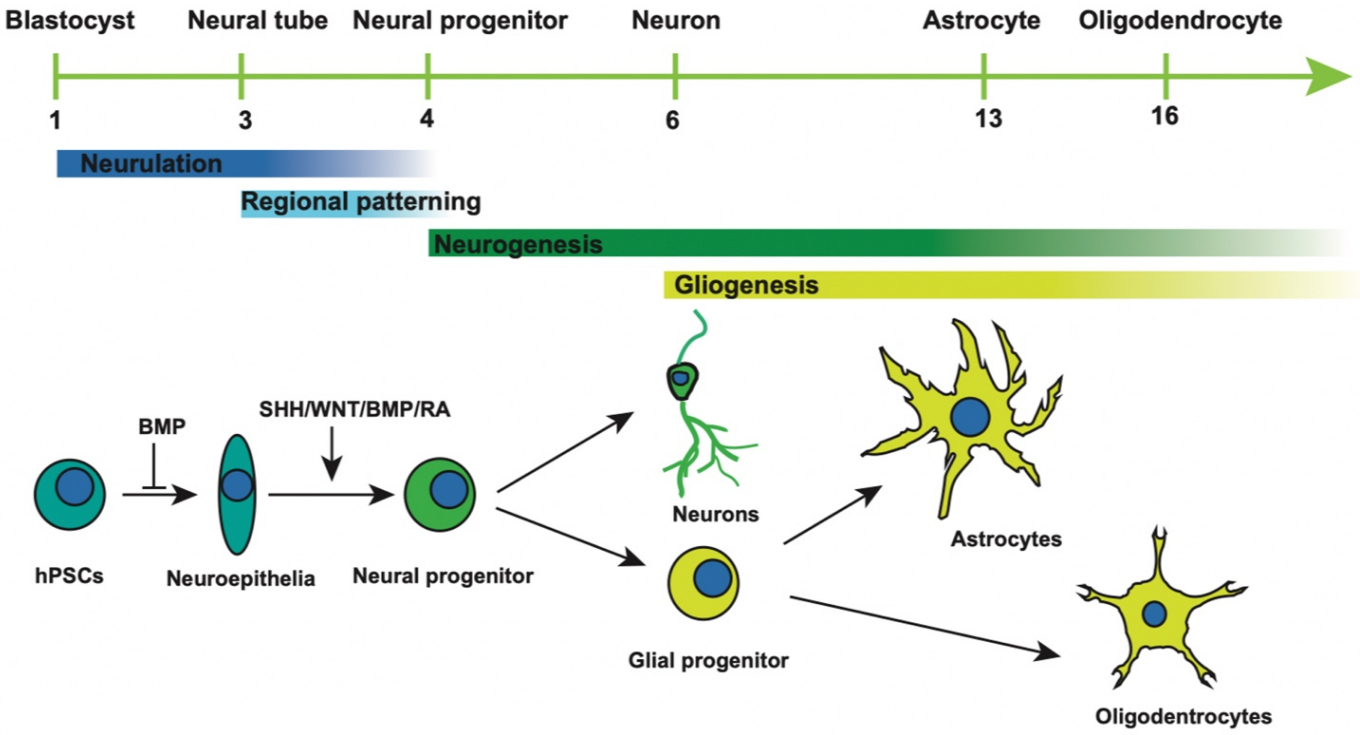

Figure 1.5 Developmental timeline (weeks) of neurogenesis and astrogenesis in mouse embryo

Over the first post-natal week, the astrocyte progenitor cells mature into astrocytes possessing resting phenotype with an average size of 150 μm (mouse). To mimic their native development, Krenick et al reported the first iPSC-derived astrocyte generation, and more than 15 different protocols were proven to produce cells expressing glia-specific markers since then. [50] Those protocols commonly apply Bone morphogenetic protein 4 (BMP4) and Leukemia inhibitory factor (LIF) to derive early neuroepithelial precursors to astrogenic lineage by blocking neurogenic transcriptions, followed by treating serum or Ciliary neurotrophic factor (CNTF) for maturation.[51–55] Evaluation of the generated culture is usually performed by immunocytochemistry with canonical glial markers such as GFAP, S100b, AQP4, GLAST, GLT1 and qPCR for gene expression analysis accompanied by functional

assessments such as glutamate uptake assay and ATP-mediated intracellular calcium release assay. Although the differentiated cells satisfied the current metrics for astrocyte validation, the culture is still heterogeneous with an unknown subpopulation of astrocytes and other glial cell types. Moreover, given their extreme plasticity upon exogenous stimulation, obtaining normal astrocytes in the resting state in culture is still challenging. Finally, the lack of astrocyte-specific markers for live cell sorting and immunostaining hinders efficient purification and verification of the culture, particularly at the late stage of differentiation. Although most of the canonical pan-glial markers allow excluding contaminating neurons in culture but leave intra-glial discrimination difficult. Recently, Barbar *et al* reported the CD49f as an effective mature-stage iPSC-astrocyte marker, but their sequencing data suggest the marker is non-specifically expressed in the early stage of native brain astrocytes as well, indicating the necessity of more reliable marker discovery for functional astrocyte use to recapitulating neuroglial interaction. [56]

1.5 Unmet Needs and Future Perspectives

Despite the initial advancement in human NMD modeling detailed in the previous sections, there still is dire need for accurately recapitulating NMD pathophysiology as a whole with human iPSC-derived cells. With current iPSC-NMD modeling approaches, it is difficult to elucidate how the neurodegenerative pathology occurs at the CNS upstream for subsequent muscle denervation. These shortcomings are likely due to the oversimplified 'neuro-centric' disease models which lack a comprehensive understanding of non-cell autonomous aspects of neurodegeneration, in addition to the use of immature neurons with unknown subpopulation identities. Consequently, studies often show inconclusive or contradictory results by using isolated iPSC-motor neurons from different sources or chemically purified neurons. Hence, there has recently been a targeted focus on developing strategies for recreating iPSC-derived human neuroglial tissues to study their pathological interaction in a dish. However, the comprehensive disease modeling and treatment studies with those tissues are still in their infancy mainly due to several roadblocks. First, there still is a significant lack of understanding about how the native neuroglial interaction occurs (e.g. signaling mode) in the normal spinal cord,

thereby lacking a reliable yardstick to compare and modify our neuroglial tissue generation scheme *in vitro*. Second, we still do not understand which mode of neuroglial interaction derives the pathologic characteristics of many NMDs including ALS, hindering the recapitulation of the actual disease progression in the culture plate. Finally, molecular drivers involved in the pathologic neuroglial crosstalk are yet identified, leaving the upstream therapeutic target of NMD unidentified. Therefore, the future NMD research perspectives for understanding the progression of neurodegeneration should include the mechanism of neuromodulation induced by the non-neuron autonomous factors, especially the glial input. We expect our proposed studies to provide significant insights into how the neurons are affected by the exogenous pathogenic factors thereby contributing to a better understanding of the disease progression mechanism and identifying potential therapeutic targets to combat the NMDs.

1.6 Dissertation of Specific Aims

The overarching goal of the research presented in this dissertation is to develop a human stem cell model for studying the role of non-cell autonomous factors on neuromodulation in both normal and diseased conditions. We sought to investigate the consequence and potential molecular drivers of neuromodulation mediated by astrocytes using iPSC-derived neurons. We believe our study provides an in-depth understanding of the physiological role of glia and their secreted factors, particularly for deriving neurodegenerative phenotypes in the spinal motor neurons that recapitulate the upstream pathology of NMD. This goal was accomplished by pursuing the following specific aims. **[Figure 1.6]**

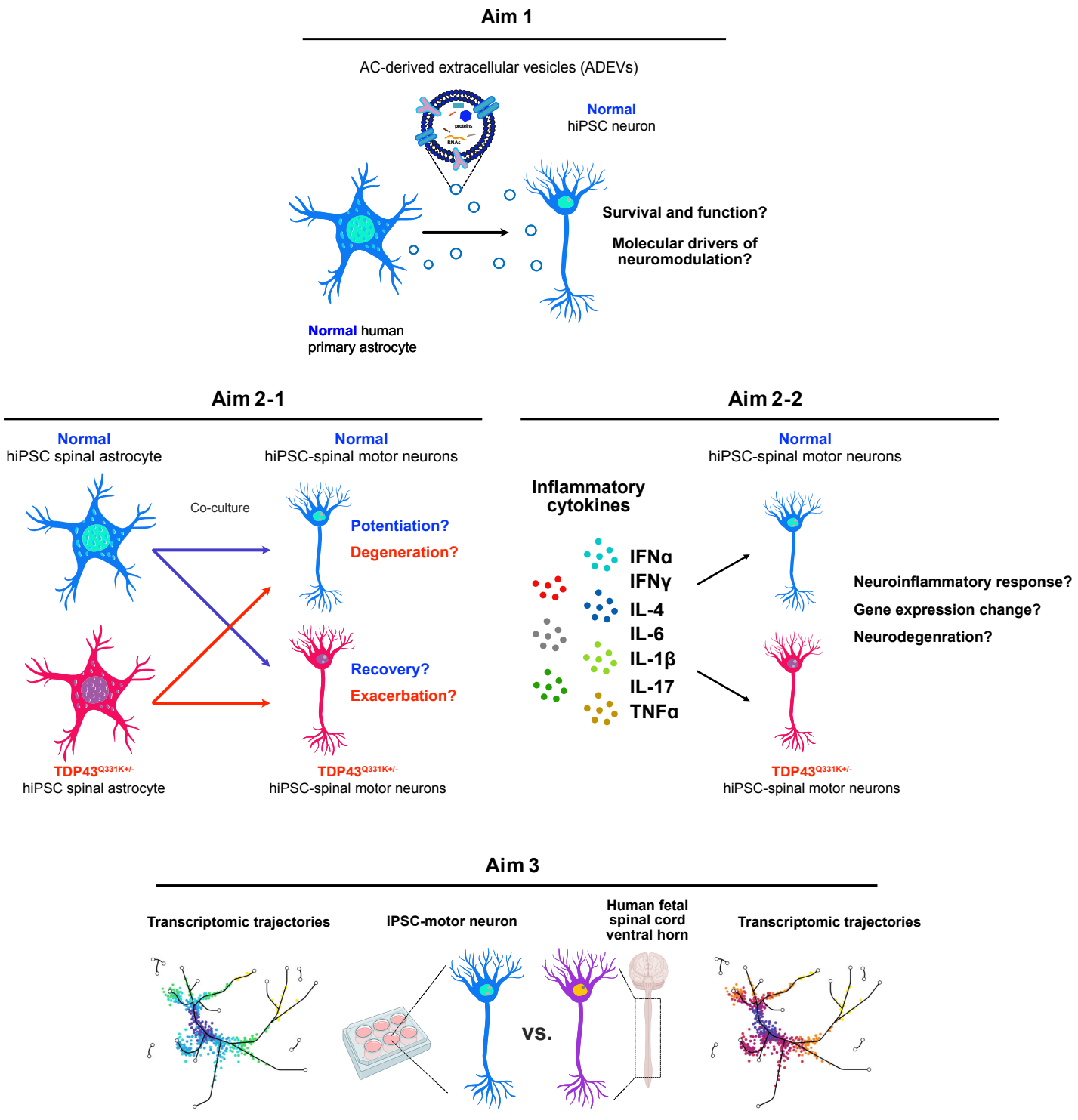

Figure 1.6 Graphical illustration of specific aims

Aim 1. Investigate the neuroprotective role of normal astrocyte-derived extracellular vesicles

Neuronal physiology is highly dependent on astrocytic modulation in both normal and diseased conditions, but their neuromodulation mode is not well understood. Specifically, it is unclear how the astrocytes relay their signals to neurons and which molecular drivers are mainly responsible for each of the altered neuronal phenotypes. We hypothesized that normal astrocytes use their extracellular vesicles (EVs) to carry neuroprotective molecules for enhancing the electrophysiological function and longevity of iPSC neurons. To test this hypothesis, we have collected EVs from normal human astrocytes for iPSC-neurons and monitored their physiological change. Additionally, we performed EV-cargo analysis using Exo-RNAseq and proteomics assays for identifying neuroprotective vesicular cargo molecules.

Aim 2-1. Study the astrocyte-mediated neurodegeneration in ALS using iPSC-derived spinal astrocytes and isogenic motor neurons

Given the normal neuron's significant dependence on astrocytes for their survival and function, we hypothesized the diseased astrocyte's continuous physiological input would cause severe neurodegeneration, resembling the late-stage of ALS phenotypes. To test this hypothesis, we first developed a differentiation protocol to generate both spinal astrocytes and spinal motor neurons from iPSCs reprogrammed from normal donors and its isogenic mutant TDP-43 (Q331K+/-) counterpart. Next, we analyzed the phenotypic difference between WT and TDP-43 mutant astrocytes and motor neurons, followed by comparing the electrophysiological impact of normal and mutant astrocytes on neurons by co-culturing the two cells.

Aim 2-2. Study the pathologic role of neuroinflammatory cytokines on ALS development using iPSC-derived spinal motor neurons

Since many recent studies have shown that the overly reactive peripheral immunity that is mainly comprised of astrocytes and microglia promotes neurodegeneration, we sought to understand how excessive exposure to inflammatory stress affects the physiology of the iPSC-motor neurons. We

screened 7 different cytokines known to be elevated in ALS patients' cerebrospinal fluid in terms of their ability to induce PD-L1 expression, which is a well-conserved immune-modulatory gene in most mammalian cells. We found that IFNγ, a pro-inflammatory cytokine secreted from immune cells including astrocytes, significantly upregulates the PD-L1 expression on iPSC-motor neurons. Thus, we hypothesized that excessive exposure of IFNγ to the spinal cord may promote neurodegenerative gene expressions of motor neurons, which could lead to manifesting severe pathologic phenotypes in motor neurons. To test this hypothesis, we ran a single-cell RNA sequencing analysis of iPSC-motor neurons with and without the IFNγ treatment and compared their transcriptomic profile, as well as their phenotype expressions such as cytoplasmic protein aggregation and electrophysiological impairment.

Aim 3. Assess the physiological relevance of the iPSC-spinal neurons by comparing transcriptomic trajectories of differentiating *in vitro* culture to that of the developing human spinal cord

Despite the progress in generating iPSC-derived spinal neurons, a fundamental gap is remaining unresolved to apply the result for downstream neuromuscular tissue engineering and disease modeling studies. First, the phenotypic immaturity of the iPSC-neurons is a critical roadblock for accurately recapitulating the actual nerve physiology. Second, we still do not understand how different the iPSC-neuron's transcriptomic profiles are from those of native counterparts, thereby having clear limitations in expanding their applications. In this last aim, we ran longitudinal single-cell RNA sequencing at each differentiation stages of iPSC neurons to perform a side-by-side comparison of the result to the data generated with native spinal neurons obtained from the fetal spinal cord at different gestational stages. The time-course transcriptomic data revealed that our iPSC-motor neuron differentiation protocol works well in terms of generating motor neuron-enriched culture by day 24, but at the same time, significant disparities with that of *in vivo* dataset which identifies problems of the current induction method to be resolved in the future. We expect this transcriptomic trajectory comparison will tell us how we should modify the current differentiation strategy to better mimic the cellular population and gene

expression profile of developing native spinal cord for generating reliable iPSC-neurons in a dish. Furthermore, this time-course transcriptomic dataset will also provide us important clues about how and when we should co-culture spinal neurons with iPSC-skeletal muscle to generate a functional neuromuscular junction in our later projects, to eventually model NMDs in a tissue level that encompasses upstream and downstream physiology of the disease.

1.7 Reference

1. Santoso, J. W. & McCain, M. L. Neuromuscular disease modeling on a chip. *DMM Disease Models and Mechanisms* vol. 13 (2020).
2. Mary, P., Servais, L. & Vialle, R. Neuromuscular diseases: Diagnosis and management. *Orthopaedics and Traumatology: Surgery and Research* vol. 104 S89–S95 (2018).
3. Morrison, B. M. Neuromuscular Diseases. *Seminars in Neurology* **36**, 409–418 (2016).
4. Larkindale, J. *et al.* Cost of illness for neuromuscular diseases in the United States. *Muscle and Nerve* **49**, 431–438 (2014).
5. Hardiman, O. *et al.* Amyotrophic lateral sclerosis. *Nature Reviews Disease Primers* vol. 3 (2017).
6. Valko, K. & Ciesla, L. Amyotrophic lateral sclerosis. *Progress in Medicinal Chemistry* **58**, 63–117 (2019).
7. Araki, T. *Amyotrophic lateral sclerosis*.
8. Niedermeyer, S., Murn, M. & Choi, P. J. Respiratory Failure in Amyotrophic Lateral Sclerosis. *Chest* **155**, 401–408 (2019).
9. Masrori, P. & van Damme, P. Amyotrophic lateral sclerosis: a clinical review. *European Journal of Neurology* vol. 27 1918–1929 (2020).
10. Halliday, G. M. *et al.* TDP-43 in the hypoglossal nucleus identifies amyotrophic lateral sclerosis in behavioral variant frontotemporal dementia. *Journal of the Neurological Sciences* **366**, 197–201 (2016).
11. Suk, T. R. & Rousseaux, M. W. C. The role of TDP-43 mislocalization in amyotrophic lateral sclerosis. *Molecular Neurodegeneration* vol. 15 (2020).
12. Lee, S. *et al.* The overexpression of TDP-43 in astrocytes causes neurodegeneration via a PTP1B-mediated inflammatory response. *Journal of Neuroinflammation* **17**, (2020).
13. Jo, M. *et al.* The role of TDP-43 propagation in neurodegenerative diseases: integrating insights from clinical and experimental studies. *Experimental and Molecular Medicine* vol. 52 1652–1662 (2020).
14. Walker, A. K. *et al.* ALS-associated TDP-43 induces endoplasmic reticulum stress, which drives cytoplasmic TDP-43 accumulation and stress granule formation. *PLoS ONE* **8**, (2013).
15. Prasad, A., Bharathi, V., Sivalingam, V., Girdhar, A. & Patel, B. K. Molecular mechanisms of TDP-43 misfolding and pathology in amyotrophic lateral sclerosis. *Frontiers in Molecular Neuroscience* vol. 12 (2019).
16. Velebit, J. *et al.* Astrocytes with TDP-43 inclusions exhibit reduced noradrenergic cAMP and Ca2+ signaling and dysregulated cell metabolism. *Scientific Reports* **10**, (2020).
17. Hergesheimer, R. C. *et al.* The debated toxic role of aggregated TDP-43 in amyotrophic lateral sclerosis: A resolution in sight? *Brain* vol. 142 1176–1194 (2019).
18. Fields, R. D. & Stevens-Graham, B. *New Insights into Neuron-Glia Communication*. http://science.sciencemag.org/.
19. Ullian, E. M., Sapperstein, S. K., Christopherson, K. S. & Barres, B. A. Control of synapse number by glia. *Science* **291**, 657–661 (2001).

20. Allen, N. J. & Eroglu, C. Cell Biology of Astrocyte-Synapse Interactions. *Neuron* vol. 96 697–708 (2017).

21. Farhy-Tselnicker, I. & Allen, N. J. Astrocytes, neurons, synapses: A tripartite view on cortical circuit development. *Neural Development* vol. 13 (2018).

22. Bayraktar, O. A., Fuentealba, L. C., Alvarez-Buylla, A. & Rowitch, D. H. Astrocyte development and heterogeneity. *Cold Spring Harbor Perspectives in Biology* **7**, (2015).

23. Shane A. Liddelow & Michael V. Sofroniew. Astrocytes usurp neurons as a disease focus. *Nature Neuroscience* **22**, 510–512 (2019).

24. Kim, K. *et al.* Role of Excitatory Amino Acid Transporter-2 (EAAT2) and glutamate in neurodegeneration: Opportunities for developing novel therapeutics. *Journal of Cellular Physiology* vol. 226 2484–2493 (2011).

25. Parkin, G. M., Udawela, M., Gibbons, A. & Dean, B. Glutamate transporters, EAAT1 and EAAT2, are potentially important in the pathophysiology and treatment of schizophrenia and affective disorders. *World Journal of Psychiatry* **8**, 51–63 (2018).

26. Bursch, F. *et al.* Altered calcium dynamics and glutamate receptor properties in iPSC-derived motor neurons from ALS patients with C9orf72, FUS, SOD1 or TDP43 mutations. *Human Molecular Genetics* **28**, 2835–2850 (2019).

27. Shaw, P. J. & Ince, P. G. *Glutamate, excitotoxicity and amyotrophic lateral sclerosis*. *J Neurol* (1997).

28. Lau, A. & Tymianski, M. Glutamate receptors, neurotoxicity and neurodegeneration. *Pflugers Archiv European Journal of Physiology* vol. 460 525–542 (2010).

29. Liddelow, S. A. *et al.* Neurotoxic reactive astrocytes are induced by activated microglia. *Nature* **541**, 481–487 (2017).

30. Yamanaka, K. & Komine, O. The multi-dimensional roles of astrocytes in ALS. *Neuroscience Research* vol. 126 31–38 (2018).

31. Guttenplan, K. A. *et al.* Knockout of reactive astrocyte activating factors slows disease progression in an ALS mouse model. *Nature Communications* **11**, (2020).

32. Serio, A. *et al.* Astrocyte pathology and the absence of non-cell autonomy in an induced pluripotent stem cell model of TDP-43 proteinopathy. *Proceedings of the National Academy of Sciences of the United States of America* **110**, 4697–4702 (2013).

33. Tong, J. *et al.* Expression of ALS-linked TDP-43 mutant in astrocytes causes non-cell-autonomous motor neuron death in rats. *EMBO Journal* **32**, 1917–1926 (2013).

34. Yi, A. *et al.* Loss of TDP-43 in astrocytes leads to motor deficits by triggering A1-like reactive phenotype and triglial dysfunction. doi:10.1073/pnas.2007806117/-/DCSupplemental.

35. Warre-Cornish, K. *et al. Interferon-γ signaling in human iPSC-derived neurons recapitulates neurodevelopmental disorder phenotypes*. *Sci. Adv* vol. 6 http://advances.sciencemag.org/ (2020).

36. Aebischer, J. *et al.* IFNγ triggers a LIGHT-dependent selective death of motoneurons contributing to the non-cell-autonomous effects of mutant SOD1. *Cell Death and Differentiation* **18**, 754–768 (2011).

37. Richard, J. P. & Maragakis, N. J. Induced pluripotent stem cells from ALS patients for disease modeling. *Brain Research* vol. 1607 15–25 (2015).

38. Berry, B. J., Smith, A. S. T., Young, J. E. & Mack, D. L. Advances and current challenges associated with the use of human induced pluripotent stem cells in modeling neurodegenerative disease. *Cells Tissues Organs* **205**, 331–349 (2019).

39. Takahashi, K. *et al.* Induction of Pluripotent Stem Cells from Adult Human Fibroblasts by Defined Factors. *Cell* **131**, 861–872 (2007).

40. Chambers, S. M. *et al.* Highly efficient neural conversion of human ES and iPS cells by dual inhibition of SMAD signaling. *Nature Biotechnology* **27**, 275–280 (2009).

41. Sances, S. *et al.* Modeling ALS with motor neurons derived from human induced pluripotent stem cells. *Nature Neuroscience* vol. 19 542–553 (2016).

42. Davis-Dusenbery, B. N., Williams, L. A., Klim, J. R. & Eggan, K. How to make spinal motor neurons. *Development (Cambridge)* **141**, 491–501 (2014).

43. Du, Z. W. *et al.* Generation and expansion of highly pure motor neuron progenitors from human pluripotent stem cells. *Nature Communications* **6**, (2015).

44. Hawrot, J., Imhof, S. & Wainger, B. J. Modeling cell-autonomous motor neuron phenotypes in ALS using iPSCs. *Neurobiology of Disease* vol. 134 (2020).

45. Winner, B., Marchetto, M. C., Winkler, J. & Gage, F. H. Human-induced pluripotent stem cells pave the road for a better understanding of motor neuron disease. *Human Molecular Genetics* vol. 23 (2014).

46. Fujimori, K. *et al.* Modeling sporadic ALS in iPSC-derived motor neurons identifies a potential therapeutic agent. *Nature Medicine* **24**, 1579–1589 (2018).

47. Thiry, L., Hamel, R., Pluchino, S., Durcan, T. & Stifani, S. Characterization of Human iPSC-derived Spinal Motor Neurons by Single-cell RNA Sequencing. *Neuroscience* **450**, 57–70 (2020).

48. Smith, A. S. T. *et al.* Human Induced Pluripotent Stem Cell-Derived TDP-43 Mutant Neurons Exhibit Consistent Functional Phenotypes Across Multiple Gene Edited Lines Despite Transcriptomic and Splicing Discrepancies. *Frontiers in Cell and Developmental Biology* **9**, (2021).

49. Tao, Y. & Zhang, S. C. Neural Subtype Specification from Human Pluripotent Stem Cells. *Cell Stem Cell* vol. 19 573–586 (2016).

50. Krencik, R. & Zhang, S. C. Directed differentiation of functional astroglial subtypes from human pluripotent stem cells. *Nature Protocols* **6**, 1710–1717 (2011).

51. TCW, J. *et al.* An Efficient Platform for Astrocyte Differentiation from Human Induced Pluripotent Stem Cells. *Stem Cell Reports* **9**, 600–614 (2017).

52. Roybon, L. *et al.* Human stem cell-derived spinal cord astrocytes with defined mature or reactive phenotypes. *Cell Reports* **4**, 1035–1048 (2013).

53. Clarke, B. E. *et al.* Human stem cell-derived astrocytes exhibit region-specific heterogeneity in their secretory profiles. *Brain* vol. 143 (2020).

54. Tchieu, J. *et al.* NFIA is a gliogenic switch enabling rapid derivation of functional human astrocytes from pluripotent stem cells. *Nature Biotechnology* **37**, 267–275 (2019).

55. Perriot, S. *et al.* Human Induced Pluripotent Stem Cell-Derived Astrocytes Are Differentially Activated by Multiple Sclerosis-Associated Cytokines. *Stem Cell Reports* **11**, 1199–1210 (2018).

56. Barbar, L. *et al.* CD49f Is a Novel Marker of Functional and Reactive Human iPSC-Derived Astrocytes. *Neuron* **107**, 436-453.e12 (2020).

Chapter 2. The Neuroprotective Role of Normal Astrocyte-derived Extracellular Vesicles

- This chapter has been published in the following manuscript

Changho Chun, Alec S.T. Smith, Hyejin Kim, Dana S. Kamenz, Jung Hyun Lee, Jong Bum Lee, David L. Mack, Mark Bothwell, Claire D. Clelland and Deok-Ho Kim*, **'Astrocyte-derived Extracellular Vesicles Enhance the Survival and Electrophysiological Function of Human Cortical Neurons *in vitro*'** *Biomaterials*, 271, 120700, (2021)

2.1 Abstract

Neurons derived from human induced pluripotent stem cells are powerful tools for modeling neural pathophysiology and preclinical efficacy/toxicity screening of novel therapeutic compounds. However, human neurons cultured *in vitro* typically do not fully recapitulate the physiology of the human nervous system, especially in terms of exhibiting morphological maturation, longevity, and electrochemical signaling ability comparable to that of adult human neurons. In this study, we investigated the potential for astrocyte-derived EVs to modulate survival and electrophysiological function of human neurons *in vitro*. Specifically, we demonstrate that EVs obtained from human astrocytes promote enhanced single cell electrophysiological function and anti-apoptotic behavior in a homogeneous population of human iPSC-derived cortical neurons. Furthermore, EV-proteomic analysis was performed to identify cargo proteins with the potential to promote the physiological enhancement observed. EV cargos were found to include neuroprotective proteins such as heat shock proteins, alpha-synuclein, and lipoprotein receptor-related protein 1 (LRP1), as well as apolipoprotein E (APOE), which negatively regulates neuronal apoptosis, and a peroxidasin homolog that supports neuronal oxidative stress management. Proteins that positively regulate neuronal excitability and synaptic development were also detected, such as potassium channel tetramerization domain containing 12 (KCTD12), glucose-6- phosphate dehydrogenase (G6PD), kinesin family member 5B

(KIF5B), spectrin-alpha non-erythrocytic1 (SPTAN1). The remarkable improvements in electrophysiological function and evident inhibition of apoptotic signaling in cultured neurons exposed to these cargos may hold significance for improving preclinical *in vitro* screening modalities. In addition, our collected data highlight the potential for EV-based therapeutics as a potential class of future clinical treatment for tackling inveterate central and peripheral neuropathies.

2.2 Introduction

The mammalian cerebral cortex is well organized with specific layers supporting distinct neuronal populations.[57–59] Within the cortex, neurons not only form connections with each other, but also with supporting glial cells. These neuroglial interactions are indispensable for ensuring neuron survival, differentiation, maturation, regeneration and proper coordination of motor and sensory information in the brain.[59–64] Astrocytes are the most abundant subtype of glial cells coexisting with neurons in the central nervous system (CNS). They are known to provide structural and trophic support to neurons, mediate synaptogenesis at early stages of neonatal brain development, maintain and eliminate neuronal synapses, and modulate excitability of associated neurons.[65] Animal studies have revealed that astrogenesis, which begins during the later stages of neurogenesis (around E18 in rodents), coincides with axon and dendrite outgrowth as well as synaptic initiation in neurons.[65,66] Although numerous studies have revealed a diverse range of astrocyte functionality on neurons, detailed mechanisms of how these nerve cells specifically interact with each other during development and beyond, and how their interactions are altered in diseased tissues, are not well understood. Recent studies using murine-derived cells have described EV-mediated neuronal modulation by astrocytes in response to inflammatory or oxidative stress[67–71], or from genetic mutation causing neurodegenerative disease.[72,73] These studies have significantly broadened our understanding of exosome-mediated control of neurons by astrocytes in pathologic conditions, but we still lack critical information on how astrocyte-derived EVs modulate neuronal physiology in the normal human nervous system. Given that

astrocytes show species-specific characteristics to exhibit significantly varied physiological features in different organisms, reliable human model study of EV-mediated astrocyte-neuron interactions will highly contribute to understanding neuroglial communication in normal human CNS development.

In this study, we utilized hiPSC-derived cortical neurons and human astrocyte-derived EVs to investigate the effect of EVs on the physiological behavior of human neurons, with a particular focus on their positive regulation of neuronal survival and electrophysiology. The data presented here highlight the neuroprotective role of astrocyte-derived EVs, as evidenced by reduced apoptotic signal expression and enhanced electrophysiological function in treated neurons. In addition, we analyzed the proteomic profile of astrocyte EVs in order to identify cargo molecules that may be responsible for the observed enhancement of neuronal survival and function.

2.3 Materials and Methods

2.3.1 Astrocyte cell culture

Commercially sourced human primary astrocytes were purchased from ScienCell Research Laboratories (Carlsbad, CA) and were stored, thawed and sub-cultured based on the manufacturer's protocol. Cultures were maintained in a 37 ºC / 5 % CO_2 incubator throughout the culture period and the astrocytes were used up to passage five, to maintain consistent cell quality. Initially, the astrocytes were cultured for 72 hours in a base medium with an astrocyte growth supplement and fetal bovine serum provided by the same manufacturer. After 72 hours of culture, the medium was replaced with an EV-free medium consisting of the base medium plus EV-depleted serum and supplement. The cells were then cultured for an additional 12 to 84 hours, allowing them to secrete a maximal number of EVs, while maintaining less than 90% cell confluency before collection of the conditioned medium.

2.3.2 Human iPSC maintenance and cortical neuron differentiation

WTC11 human induced pluripotent stem cells stably transduced with a doxycycline-mediated Ngn-2 overexpressing transgene were kindly provided by the Gladstone Institute (San Francisco, CA).

These cells were maintained and differentiated according to the Gladstone protocol published previously.[74,75] The hiPSCs were differentiated into human cortical neurons using a previously reported method with limited modifications. Specifically, 80% confluent hiPSC colonies on Matrigel-coated plates (Corning) were dissociated into single cells using Accutase (Thermo-Fisher) and transferred on to fresh Matrigel-coated plates. The cells were then treated with an induction medium including N2 supplement (100x, Thermo-Fisher), non-essential amino acids (100x, Thermo-Fisher), Glutamax (100x, Thermo-Fisher) and doxycycline (1000x, Sigma-Aldrich) to initiate differentiation. The cultures were maintained with the same induction medium replenished every day for 48 hours before being passaged and transferred to the final assay plate. Differentiated neurons at day 3 post-induction were transferred to 0.01% poly-L-ornithine (Sigma-Aldrich) and 5 µg/mL laminin (Sigma-Aldrich) coated glass coverslips for subsequent analysis. Cells were then fed with BrainPhys medium supplemented with B27 (Invitrogen), laminin (Sigma-Aldrich), and 10 ng/mL brain derived neurotrophic factor (BDNF; R&D Systems) every 3 days until endpoint analysis.

2.3.3 EV isolation and characterization

Astrocytes were cultured with vendor-provided base medium supplemented with EV-depleted serum. The culture medium in which cell-derived EVs were secreted was collected after 12, 24, 36, 48, or 84 hours of culture. A multi-step ultracentrifugation protocol was then applied to concentrate and purify the EVs. First, a spin at 300 rcf for 10 minutes was used to remove detached cells. 2,000 rcf for 10 minutes was then used to remove dead cells before a spin at 10,000 rcf for 30 minutes was applied to remove cell debris and apoptotic bodies. The EVs were then collected following 2 repeated ultracentrifugation steps at 30,000 rcf for 70 minutes. The EVs in the final solution were sterile filtered using a 0.2 µm filter, resuspended in 50 µL of BrainPhys medium (Stem cell technologies), and stored at -80 ºC for up to one month until use. The size distribution and density of the collected EVs were analyzed using a Nanoparticle Tracking Analyzer (Nanosight of Malvern Institute). Storage temperature-dependent changes in modal size and particle concentration were analyzed at different

temperatures (4 ºC, -20 ºC and -80 ºC) at day 3 and 7. The changes in physical properties and total protein concentration of EVs after repeated freeze-thawing cycles was analyzed using isolated EVs that were repeatedly incubated at -80 ºC and thawed at room temperature. After each cycle, EV proteins were quantified using the Micro BCA Protein Assay Kit (Thermo Fisher) and following the manufacturer's protocol. The modal size and particle concentrations were measure using Nanoparticle Tracking Analyzer.

2.3.4 TEM imaging

For transmission electron microscopy imaging of EVs, a Titan TM 80-300 (FEI) was employed at an accelerated voltage of 200 kV. The isolated EVs were resuspended in DPBS and the samples were deposited onto a Lacey Formvar/carbon-coated copper grids, then air-dried at room temperature before analysis.

2.3.5 Immunocytochemistry

To verify successful differentiation of cortical neurons and homogeneity of cultured astrocytes, cells were immunostained for expression of cortical neuron (layer 2 and 3) and glia specific markers. Briefly, cells were fixed in 4% paraformaldehyde for 15 minutes followed by permeabilization using 0.2% triton-X solution for 10 minutes. Cells were then blocked with 0.5% BSA in PBS for 1 hour at room temperature. After blocking, cells were incubated with primary antibodies diluted in 0.5% BSA solution in PBS overnight at 4ºC. The next day, cells were washed 3 times with PBS, and incubated for 2 hours in a secondary antibody solution containing secondary antibodies diluted in 0.5% BSA solution in PBS. Coverslips were mounted on microscope slides using Vectashield containing DAPI (Vector Labs) to counterstain samples for nuclei. Images were taken at the Garvey Imaging Core at the University of Washington's Institute for Stem Cell and Regenerative Medicine using a Nikon A1 Confocal System on a Ti-E inverted microscope platform. Antibodies used in these experiments were as follows: rabbit anti-MAP-2 (1:1000, Millipore), mouse anti-CUX-1(1:500, Thermo-Fisher), chicken anti-GFAP (1:1000, Invitrogen), mouse anti-S100B (1:500, Sigma-Aldrich), Alexafluor-594 conjugated goat-anti-mouse

secondary antibody (1:500, Invitrogen), Alexafluor-594 conjugated goat-anti-chicken secondary antibody (1:500, Invitrogen) Alexafluor-488 conjugated goat-anti-mouse secondary antibody (1:500, Invitrogen) and Alexafluor-647 conjugated goat-anti-rabbit secondary antibody (1:200, Invitrogen).

2.3.6 EV labeling and uptake study

An ExoGlow-protein EV labeling kit (System Biosciences, Palo Alto, CA) was used for live cell EV imaging. Collected EVs were incubated for 20 minutes with the labeling dye (1:500) at 37 ºC to induce vesicular protein conjugation with the dye molecules. Then the solution was treated with the ExoQuick-TC solution and incubated for 2 hours at 4 ºC, followed by centrifugation at 10,000 rcf for 10 minutes to remove unlabeled reagent molecules and collect labeled EVs only. The labeled EVs were resuspended in neuronal maintenance medium and added to neurons 72 hours post-differentiation at various concentrations. A live cell imaging microscope (Eclipse T1, Nikon) was used to image fluorescently labeled EV uptake by the cultured neurons. In these experiments, images were collected at multiple locations from examined culture wells every 5 minutes for 2 hours. Additionally, neurons treated with unlabeled EVs were fixed after 2 hours of treatment and immunostained with a mouse anti-CD81 antibody (1:100, Thermo-Fisher) to quantify the relative amount of internalized EVs based on fluorescence intensity. CD81 labeling was coupled with fluorescently-labelled phalloidin (for F-actin visualization; 1:200, Invitrogen) to confirm the correct positioning of CD81 expression relative to the cell cytoskeleton.

2.3.7 Cell senescence and apoptosis assay

To quantify the population of senescent neurons in each culture condition, a β-galactosidase staining kit (Sigma-Aldrich) was used. The cells were fixed at day 4 with 4% paraformaldehyde (PFA) for 15 minutes. The staining solution was prepared by mixing 25 µL of the X-gal solution with 475 µL of iron buffer to make a total of 500 µL for each well. The staining solution was added to the culture and kept at 37 °C for 3 hours before assessment. The number of cells exhibiting blue dye accumulation in their cytoplasm under bright field microscope was then compared for each group. To quantify apoptotic cells in these cultures, Annexin 5 (Thermo-Fisher) with propidium iodide (PI, Thermo-Fisher) was used to label cells for flow cytometry analysis (BD Canto II). Specifically, 200,000 cells per condition were treated with fluorescently labelled Annexin V and propidium iodide for 15 minutes at room temperature. These cells were then immediately washed before flow cytometry analysis to minimize cell death during the assay process. The number of cells expressing Annexin V and/or PI in each group was then analyzed and quantified using FlowJo software (BD Biosciences).

2.3.8 Morphological assessment of neurons

To examine the effect of astrocyte-derived EV treatment on axon outgrowth, cultured neurons were imaged 2 hours, 6 hours and 12 hours after plating. The length of the longest neurite segment for each neuron was measured for every image taken at each time point. Additionally, neurons from each group were fixed at each timepoint and stained with anti-neurofilament to enable comparative assessment of axon length. The axon morphologies were analyzed using the Simple Neurite Tracer plugin in ImageJ. To measure axon branching, the neurons immunostained for neurofilament expression were individually analyzed using the NeuronJ plugin for ImageJ to identify the divergence of axon terminals.

2.3.9 Electrophysiological assessment of neurons

Electrophysiological function of neurons in each group was recorded using whole-cell patch clamp techniques. Recordings were performed on an inverted DIC microscope (Nikon) connected to an EPC10 patch clamp amplifier and computer running Patchmaster software (HEKA). Coverslips supporting cultured neurons were loaded onto the microscope stage and bathed in a Tyrode's solution containing 140 mM NaCl, 5.4 mM KCl, 1.8 mM $CaCl_2$, 1 mM $MgCl_2$, 10 mM glucose, and 10 mM HEPES. The intracellular recording solution (120 mM L-aspartic acid, 20 mM KCl, 5 mM NaCl, 1 mM $MgCl_2$, 3 mM Mg^{2+}-ATP, 5 mM EGTA, and 10 mM HEPES) was loaded into borosilicate glass patch pipettes (World Precision Instruments) with a resistance in the range of 2–6 MΩ. Offset potentials were nulled before formation of a gigaΩ seal. Suction was then applied to disrupt the cell membrane in contact with pipette end. This process allowed electrical and molecular access to the intracellular space, and membrane potentials were then corrected by subtraction of the liquid junction potential, calculated by Patchmaster. The current clamp mode was used for recording action potential behavior of neurons. Specifically, a 2 nA depolarizing single pulse was applied for 5 ms to induce single action potentials, and stepwise current injections of 10 pA from -30 to +70 pA for 500 ms were applied to trigger repetitive action potential firing. The action potential duration at 90% repolarization (APD90), depolarization speed and repolarization speed were recorded for each group of neurons by the Patchmaster software. Inward and outward currents were evoked in voltage clamp mode, by providing 500 ms depolarizing steps from -120mV to +30mV in 10 mV increments. To measure resting membrane potential of neurons in each group, gap-free recordings of spontaneous activity in patched neurons were performed in current-clamp mode with 0 pA current injection. The analyses of action potential waveforms and currents were performed using the Patchmaster software suite. All reagents used in this protocol were obtained from Sigma-Aldrich.

2.3.10 Proteomics analysis

The protein cargo profile of astrocyte-derived EVs was analyzed using a commercial proteomics service (System Biosciences). Astrocyte conditioned medium was sampled after 84 hours of culture for EV collection followed by protein isolation and mass spectrometry. Raw data was analyzed using Proteome Discoverer (Thermo-Fisher). Protein function was then evaluated using the gene ontology browser DAVID (version 6.8).

2.3.11 Statistical analysis

All experiments were performed using at least 3 independently cultured neuron populations. EV treatments were derived from 4 independent batches of cultured astrocytes. Significant differences between groups were evaluated using either unpaired, two-tailed t-tests or Mann Whiney-U tests depending on whether the data was normally distributed. One-way analysis of variance (ANOVA), or ANOVA on ranks depending on data normality, with *post hoc* tests for multiple comparisons were used to compare data sets with more than two experimental groups. For analysis of repetitive firing via patch clamp, contingency tables were constructed and used to run chi squared tests to determine whether the distribution of data was dependent on cell type. In all experiments, a p value of less than 0.05 was considered significant. All statistical tests were performed using the GraphPad Prism statistics software (GraphPad Software Inc.).

2.4 Results

2.4.1 Doxycycline-mediated overexpression of Neurogenin-2 is sufficient to drive cortical neuron differentiation from hiPSCs

Human cortical neurons were obtained following the previously developed protocol that uses an iPSC line harboring a doxycycline-inducible neurogenin-2 (Ngn2) transgene; a transcription factor that drives rapid conversion of stem cells to neurons.[75] Briefly, neuronal differentiation was induced by applying doxycycline for 24 hours after single cell dissociation of iPSCs and completed by exposing the early stage neurons to a specific induction medium for an additional 48 hours. This was then followed by a change to medium supplemented with BDNF, B27, and laminin from day 3 onwards [**Figure 2.1A].**

In the first 24-hour period following induction, stem cells rapidly became polarized and began to exhibit growth cones indicative of initial neurite outgrowth. By day 3, neurite growth was more apparent and distinct axon outgrowth in each cell was observed. Cells at day 7 gained a typical neuronal morphology characterized by long axons with branched dendrites approaching those of adjacent cells and small, well-defined soma **[Figure 2.1B].** Differentiated neurons were transferred to laminin-coated assay plates at day 3 for further maturation and analysis. The overall differentiation period (3 days) was dramatically shorter than that required in conventional human iPSC-derived neuron differentiation, which can take 4-6 weeks.[63,76,77] Immunocytochemistry data collected from these cells demonstrated a high degree of homogeneity of cortical neurons for each experimental batch (n = 5), indicating significant enhancements in reproducibility and yield, compared to conventional, small molecule-mediated differentiation of human neurons. In particular, the uniform expression of CUT-like homeobox 1 (CUX-1) observed in the majority of examined cells verified the successful generation of pyramidal cortical neurons specific to upper layers of the cerebral cortex. The immunocytochemistry results highlight the reliability of the described method for producing differentiated neurons with which to study the effect of internalized EVs. **[Figure 2.1C]**

2.4.2 Ultracentrifugation of human astrocyte conditioned medium leads to isolation of consistent and highly-uniform EVs

The homogeneity of the cultured astrocyte population was confirmed using immunostaining for two glial cell-specific protein markers, GFAP and S100B, which are known to be primarily expressed in the astrocyte cytoplasm. [**Figure 2.2A, 2.2B]** Astrocyte-EVs were collected by serial ultracentrifugation**.** TEM images of negative stained EVs. **[Figure 2.2C]** and the Brownian motion observed from laser-scattered particles in the assay solution demonstrate the successful isolation of EVs from the conditioned medium. The mean mode size of collected EVs was 124 nm, with a density of $1.5x10^9$

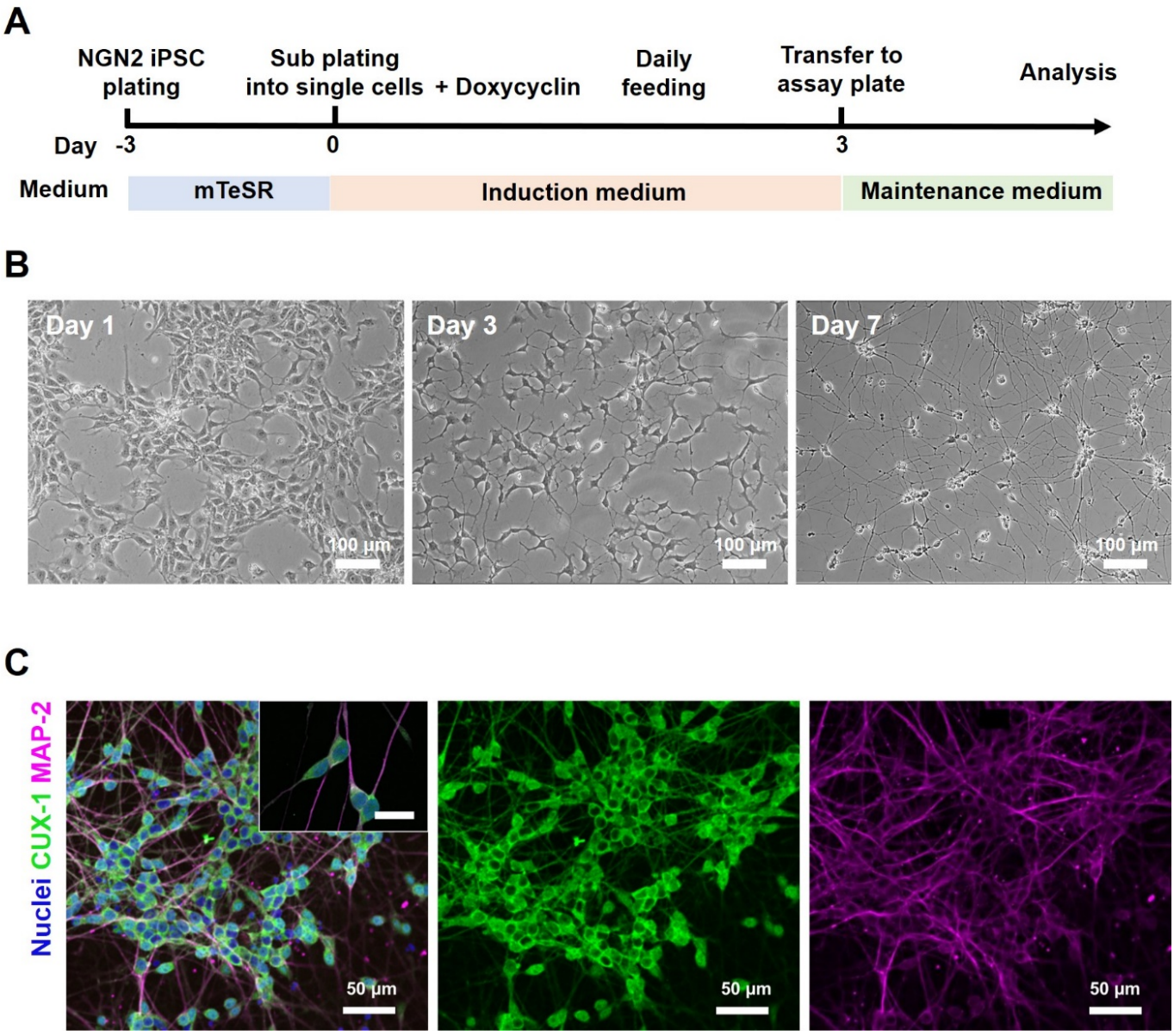

Figure 2.1 Differentiation of cortical neurons from Ngn 2 overexpressing hiPSCs. (A) Differentiation protocol highlighting the use of doxycyclin to initiate Ngn 2 transcription. (B) Morphological changes observed between initial stages of differentiation and the later stages of culture. (C) Human iPSC-derived cortical neurons immunostained using antibodies against CUX-1 (neuronal marker in cerebral cortex layers 2 and 3) and MAP2 (pan-neuronal marker) with DAPI-stained nuclei. Inset shows clear expression of CUX-1 in the cell cytoplasm. Scale bar of inset image: 20 µm.

particles/mL, and minimal batch-to-batch variation. **[Figure 2.2D, 2.2E]** The number of collected EVs were linearly proportional to the incubation time of the astrocytes, as they continuously proliferate in culture but presumably maintain their EV secretion rates. Although there was no significant difference in the number of collected EVs between 48 and 84 hours of astrocyte culture, we maintained all subsequent cultures to 84 hours to obtain the maximum number of EVs for use in downstream experiments before cells became overconfluent and started to deteriorate. **[Figure 2.2F]** Long-term EV storage at temperatures below 4 °C and repeated freeze-thawing procedures did not cause significant change in their mode size, particle concentration, or total protein concentration, **[Figure 2.2G, 2.2H, 2.2I]** indicating their stable nature in response to environmental changes. The mean zeta potential of the collected EVs was -10.37 mV, which indicated that the vesicles possessed a negative net surface charge. **[Figure 2.2J]** The uniform surface charge prevented the aggregation of particles due to their electrical repulsion, leading to a stabilized nanoparticle suspension in the described system. Quantitative proteomics revealed that extracellular matrix proteins were the most abundant protein type inside the astrocyte-EVs, including fibronectin1 and collagen subtypes. **[Figure 2.2K]**

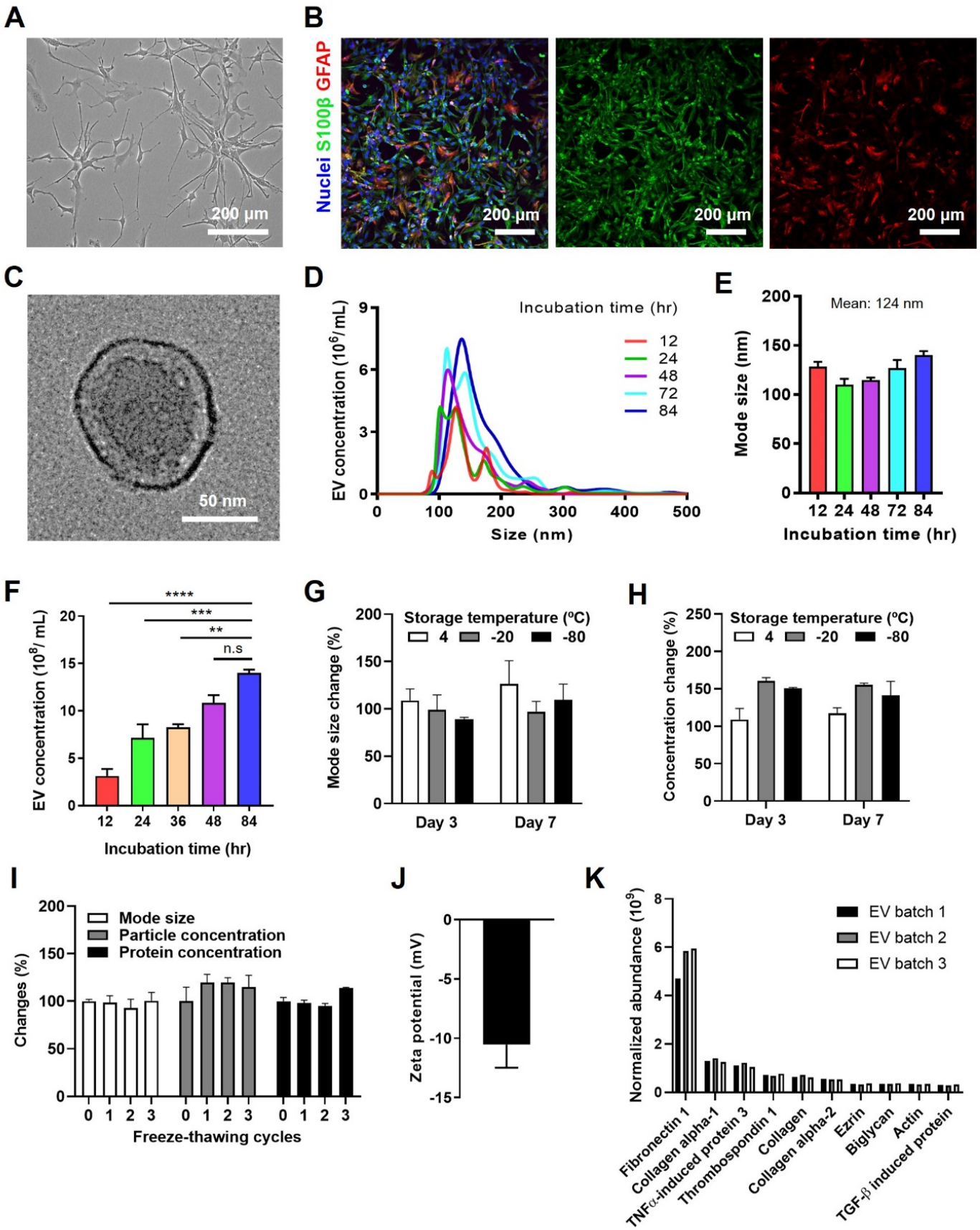
A
200 μm
B
Nuclei S100β GFAP
200 μm
200 μm
200 μm
C
50 nm
D
Incubation time (hr)
12
24
48
72
84
EV concentration (10^6/mL)
Size (nm)
E
Mean: 124 nm
Mode size (nm)
Incubation time (hr)
F
****
***
**
n.s
EV concentration (10^8/ mL)
Incubation time (hr)
G
Storage temperature (ºC)
4
-20
-80
Mode size change (%)
Day 3
Day 7
H
Storage temperature (ºC)
4
-20
-80
Concentration change (%)
Day 3
Day 7
I
Mode size
Particle concentration
Protein concentration
Changes (%)
Freeze-thawing cycles
J
Zeta potential (mV)
K
EV batch 1
EV batch 2
EV batch 3
Normalized abundance (10^9)
Fibronectin 1
Collagen alpha-1
TNFα-induced protein 3
Thrombospondin 1
Collagen
Collagen alpha-2
Ezrin
Biglycan
Actin
TGF-β induced protein

Figure 2.2. Astrocyte identification and EV characterization (A) Bright field image of human primary astrocytes at day 3 of culture. (B) Astrocyte culture immunostained using antibodies against GFAP and S100β; glial cell markers primarily expressed in astrocytes. (C) TEM images of EVs collected from primary astrocytes. (D) Size distribution of collected EVs with various cell incubation time before EV collection. (E) Mode size of collected EVs with various incubation time measured by NTA (Nanoparticle Tracking Analysis). Incubation times on the x axis indicate the time elapsed following EV-free medium change at day 4. (F) Number of particles per mL in the EV solution with the various astrocyte incubation times. Effect of long-term storage at different temperatures on EV mode size change (G) and particle concentration change (H). (I) Effect of repeated freeze-thaw cycles on EV mode size, particle concentration, and total protein concentration. (J) Zeta-potential of collected EVs after 84 hours of cell incubation. (K) The ten most abundant proteins detected in the EVs. In all presented data, error bars are SD and **p< 0.005 ***p<0.0005 ****p<0.0001, ns not significant (n=3).

2.4.3 Differentiated cortical neurons readily uptake astrocyte-derived EVs

For the next step, we investigated whether astrocyte-derived EVs can be internalized by human cortical neurons in culture. Antibodies against CD81 and the ExoGlow-protein EV labeling kit, which covalently label internal EV proteins, were used to cross-check EV-specific protein expression in the neuronal cytoplasm after EV treatment. The fluorescence signal from ExoGlow was optimized to monitor the neuronal uptake of EVs in a live cell culture environment. After 1 hour of EV treatment, followed by medium washing, 83.3% of neurons expressed fluorescence signal localized to their cell bodies, indicating successful uptake of astrocyte-derived EVs to the cytoplasm of cortical neurons. **[Figure 2.3A]** However, due to the short duration of the activated fluorescence moiety, the fluorescence signal decayed rapidly after 2 hours of labeled EV treatment. To fluorescently quantify the amount of internalized EVs, we instead immunostained neurons with antibodies against CD81 (a common transmembrane protein on EV surface) after treating EVs with various cell to EV ratios. CD81 expression analysis revealed that EV-treated neurons exhibited significant increases in cytoplasmic fluorescence intensity in a dose-dependent manner, providing further evidence of successful internalization of EVs into the cultured neurons. **[Figure 2.3B]** Fluorescence intensity dramatically increased when treating up to 25 EVs per cell and then reached a plateau, indicating that EV uptake saturated near the 25 EV particles per cell ratio. **[Figure 2.3C, 2.3D]** Untreated neurons did not show CD81 positivity, not only indicating the absence of EVs in the cell but also negligible levels of endogenous CD81 expression in the cultured neurons. **[Figure 2.3D]**

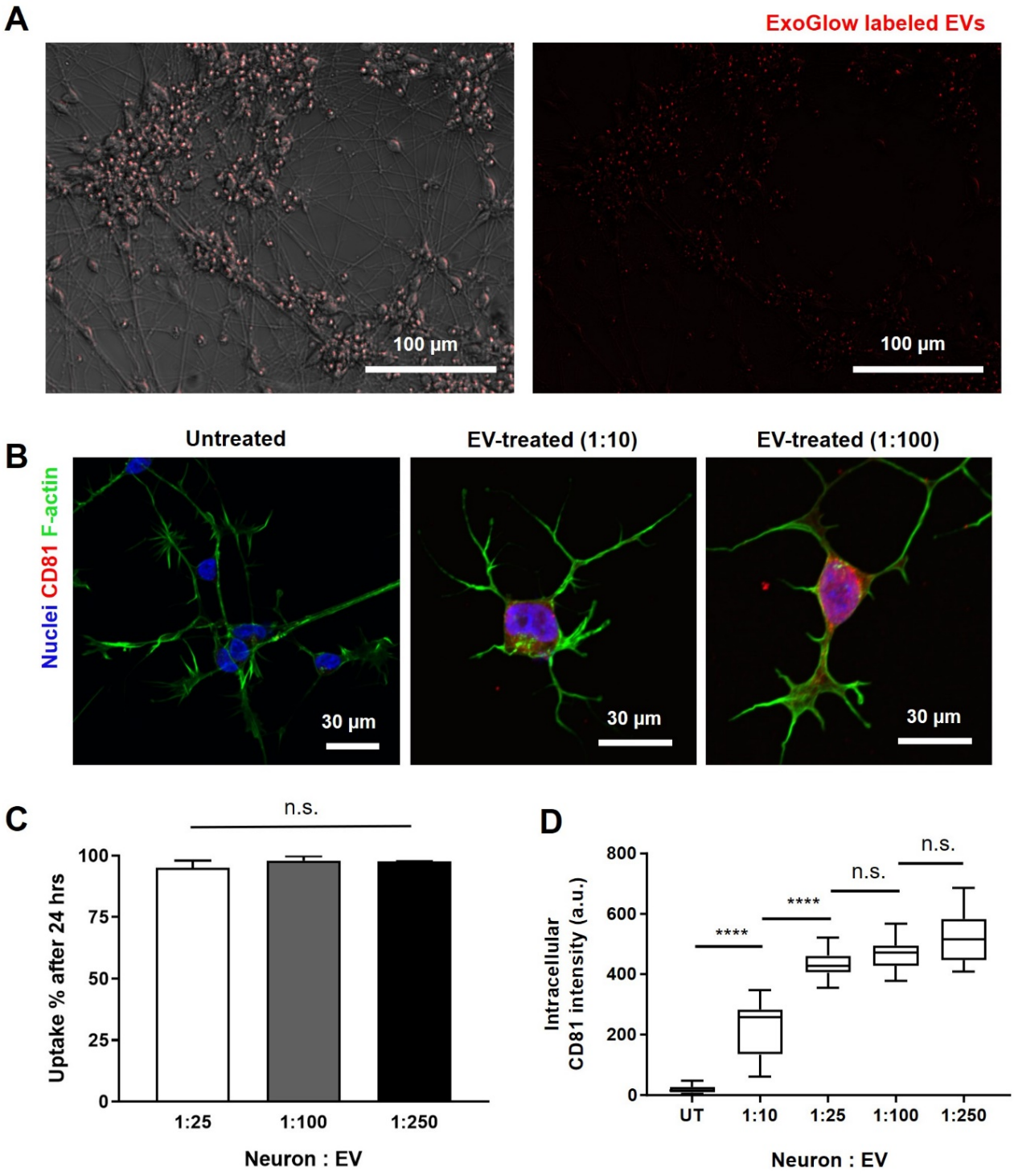

Figure 2.3. EV internalization assay using EV-specific markers (A) Live cell images of cortical neurons illustrating localization of EVs stained with the ExoGlow EV-protein staining kit for 1 hour. (B) Representative cortical neurons double immunostained with antibodies against CD81 and F-actin to demonstrate cytoplasmic internalization of differing amounts of EVs. (C) The uptake efficiency of EVs at different neuron to EV ratios obtained by quantifying fluorescently labeled EVs. (D) The relationship between CD81 fluorescent intensity in EV-treated cells with different cell to EV ratio. The fluorescence intensity is expressed as relative values normalized to an untreated sample. In all presented data, **p< 0.005 ***p<0.0005 ****p<0.0001, ns not significant (n = 3).

2.4.4 Astrocyte-derived EV treatment inhibits neuronal apoptosis and senescence in cultured neurons

Since differentiation of cells in culture is an intrinsically stressful process, it is perhaps not surprising that the rapid (3 day) differentiation of neurons from hiPSCs in response to Ngn-2 overexpression produced high numbers of apoptotic cells. 92% of neurons without EV treatment expressed at least one of the apoptotic markers examined, whereas EV treated neurons contained a reduced population of early apoptotic cells. Increasing concentrations of EV treatments were found to correlate closely with the percentage of healthy living cells identified from each group, strongly implying a role for astrocyte-derived EVs in inhibiting neurons from entering the apoptotic pathway. Although the EVs did not effectively rescue cells already undergoing late stage apoptosis, an apparent trend towards a gradual reduction in the number of cells entering early stage apoptosis in all EV-treated groups suggests that bioactive molecules encapsulated in the EVs were able to rescue these cells from responding to pro-apoptotic signals in differentiating cultures. **[Figure 2.4A, 2.4B]**

We also studied the effect of astrocyte-derived EVs on morphological degeneration in low density cultures to quantify any effect of the treatment on neuritic development. We plated early stage differentiated neurons (day 3) at 10,000 cells/cm^2, which constitutes 10% of our typical neuron plating density for long term culture. EVs were applied 1 hour after neuron plating and medium was replenished with fresh EV-supplemented medium every three days thereafter until the assay date. Untreated groups quickly began to show significant neuritic deterioration and cells did not survive beyond day 8 of culture. Conversely, EV-treated cultures showed normal axonal projections at day 4 and retained their robust morphology until day 8. **[Figure 2.5A]** Additionally, we tested whether low-density cortical neurons were susceptible to unusual cell senescence, and whether astrocyte-derived EVs could inhibit activation of senescent pathways in these cells. β-galactosidase (β-gal) is a hydrolase enzyme that catalyzes the hydrolysis of β-galactosides into monosaccharides in senescent cells that normally contain hyperactive lysosomes.[78,79] The cleavage of a chromogenic substrate (X-gal) solution by upregulated galactosidase activity results in the precipitation of a purple dye in the senescent cell cytoplasm. We used a β-gal

solution kit on each group of neurons and analyzed the expression of X-gal cleavage-mediated dye precipitation in their cytoplasm. Low density neurons on day 4 without EV treatment clearly expressed dark blue aggregates in their cell bodies, strongly indicating that the cells had adopted a senescent state**.** The number of β-gal positive neurons in the EV-treated group (1:100) were significantly less than that of untreated controls at day 4 of culture, indicating that the vesicular cargo was able to inhibit early neuronal senescence as well. **[Figure 2.5B]**

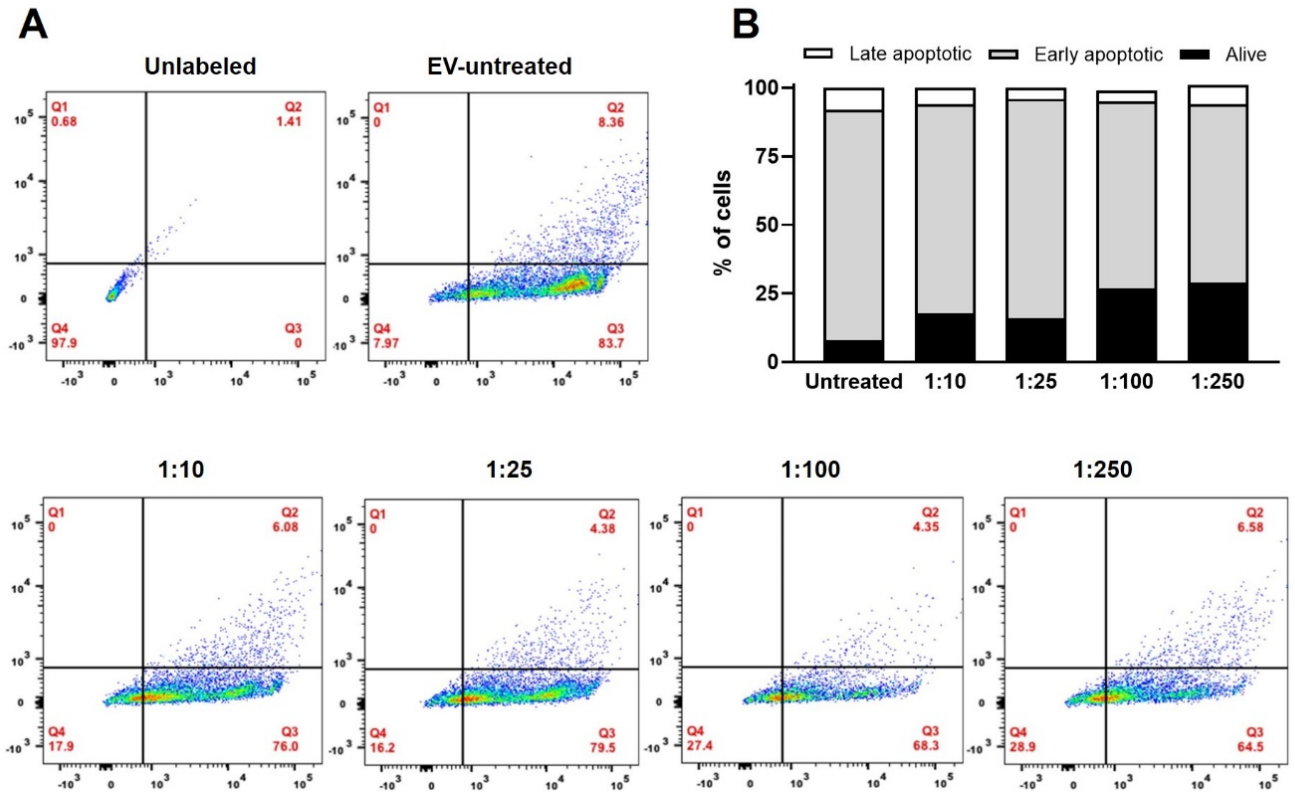

Figure 2.4. Analysis of apoptotic neurons in response to treatment with various concentrations of astrocyte-derived EVs (A) Flow cytometry analysis of neurons at day 6 using Annexin V (y axis) and propidium iodide (x axis). The inset numbers indicate the percentage of cells occupying each quadrant. Q1 = early-stage apoptotic cells (PI positive), Q2 = late-stage apoptotic cells (both PI and Annexin V positive), Q3 = early-stage apoptotic cells (Annexin V positive), Q4 = alive cells (PI and Annexin V negative). 10,000 cells per condition were used for this assay. (B) Quantification and comparison of the number of analyzed cells correspond to each condition. A contingency table comparing EV treatment conditions against apoptosis found that the two factors are significantly related ($p = 0.008$, Chi squared test), suggesting that the occurrence of neuronal apoptosis is dependent on the amount EVs added in the culture medium.

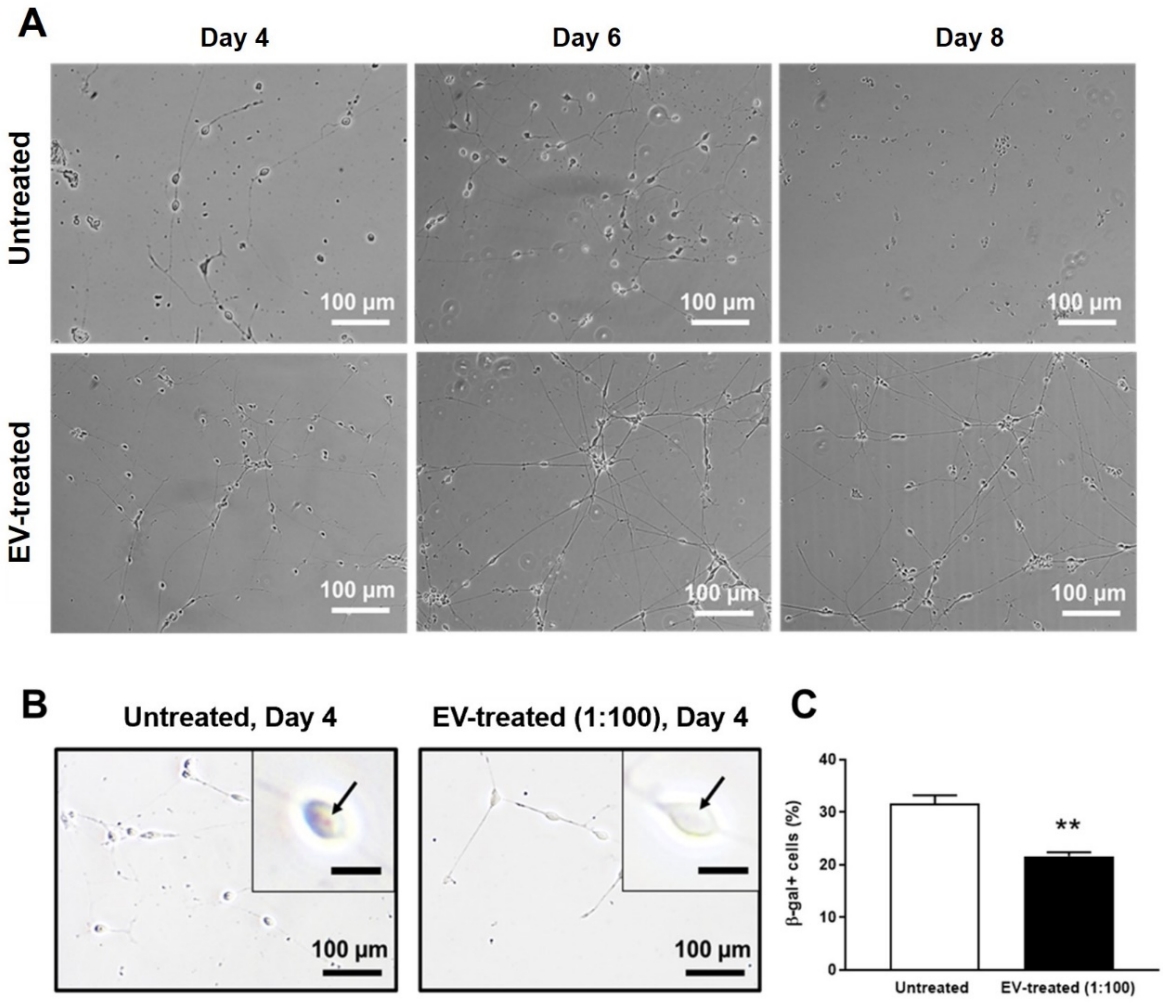

Figure 2.5 Neuronal senescence assay comparing untreated and EV-treated neurons at day 3 post-induction. (A) Bright-field images taken from different time points in culture with and without EV treatment. (B) Bright-field images taken after cells were stained with a β-galactosidase solution that produces a precipitate in the cytoplasm of senescent cells supporting hyperactive lysosomes. Scale bars of inset images: 20 µm (C) Quantification of the number of β-galactosidase-stained cells in treated and untreated cells at day 4 of each culture. Error bars represent the standard error of the mean. **p<0.005 (n = 3).

2.4.5 Astrocyte-derived EV treatment enhances single cell electrophysiology of neurons

Since astrocytes are actively involved in regulating electrochemical behavior of neurons in the CNS, we hypothesized that neuronal electrophysiology may be modulated by means of secreted astrocyte-derived EVs, based on the fact that the astrocytic coverage is limited to adjacent neurons, while consistent electrochemical regulation is required for neurons throughout the CNS. We therefore used whole cell patch-clamp techniques to investigate electrophysiological behavior in 4-weeks old

cortical neuron cultures with or without astrocyte-derived EV treatment. Evoked action potential firing in neurons treated with EVs was significantly improved compared with untreated controls, in terms of repetitive firing behavior and action potential amplitude. **[Figure 2.6A]** The population of neurons exhibiting repetitive firing behavior in response to 500 ms depolarizing current injections was much higher in the EV-treated group (50% of total) compared with that of untreated controls (30% of total). **[Figure 2.6B]** Due to the higher number of repetitive firing cells in astrocyte-derived EV treated cultures, treated neurons also exhibited a significant increase in average action potential firing frequency compared with untreated controls. **[Figure 2.6C]** Similarly, we observed shorter action potential durations at 90% of repolarization (APD_{90}) in the EV treated neurons (5.61±0.08 ms) compared with untreated controls (6.89±0.33 ms). **[Figure 2.6D]** Together, these results indicate that the EV-treated neurons were more responsive to the input stimulus than neurons cultured without the aid of astrocyte-derived EVs**.** Specifically, the improvement in action potential firing frequency may indicate that the intracellular protein cascade (e.g. voltage-gated ion channels) that processes electrochemical stimuli in EV-assisted neurons was more highly developed than those of untreated control cells. In particular, the data suggest that activity of voltage-gated potassium channels might be affected by EV treatment since a significant improvement in action potential repolarization was observed in treated cells whereas the depolarization speed was consistent. **[Figure 2.6E, 2.6F]** Finally, we compared resting membrane potential (RMP) between EV-treated and untreated neuronal populations. In these experiments, the average RMP of EV treated neurons was -61.6±2.0 mV, whereas untreated neurons exhibited an average RMP of -50±1.76 mV. **[Figure 2.6G]** This significant decrease in RMP may indicate a greater capacity for transmembrane proteins in EV-treated cells to mediate passive K^+ membrane permeability, though further investigation of the mechanism is required. Another possible speculation is that the internalized EV cargos promoted the development of a more physiological K^+ gradient in the intracellular region of the cultured neurons. Such a result would therefore suggest that EV treated neurons promote the expression of more functional ion pumps and/or transporters.

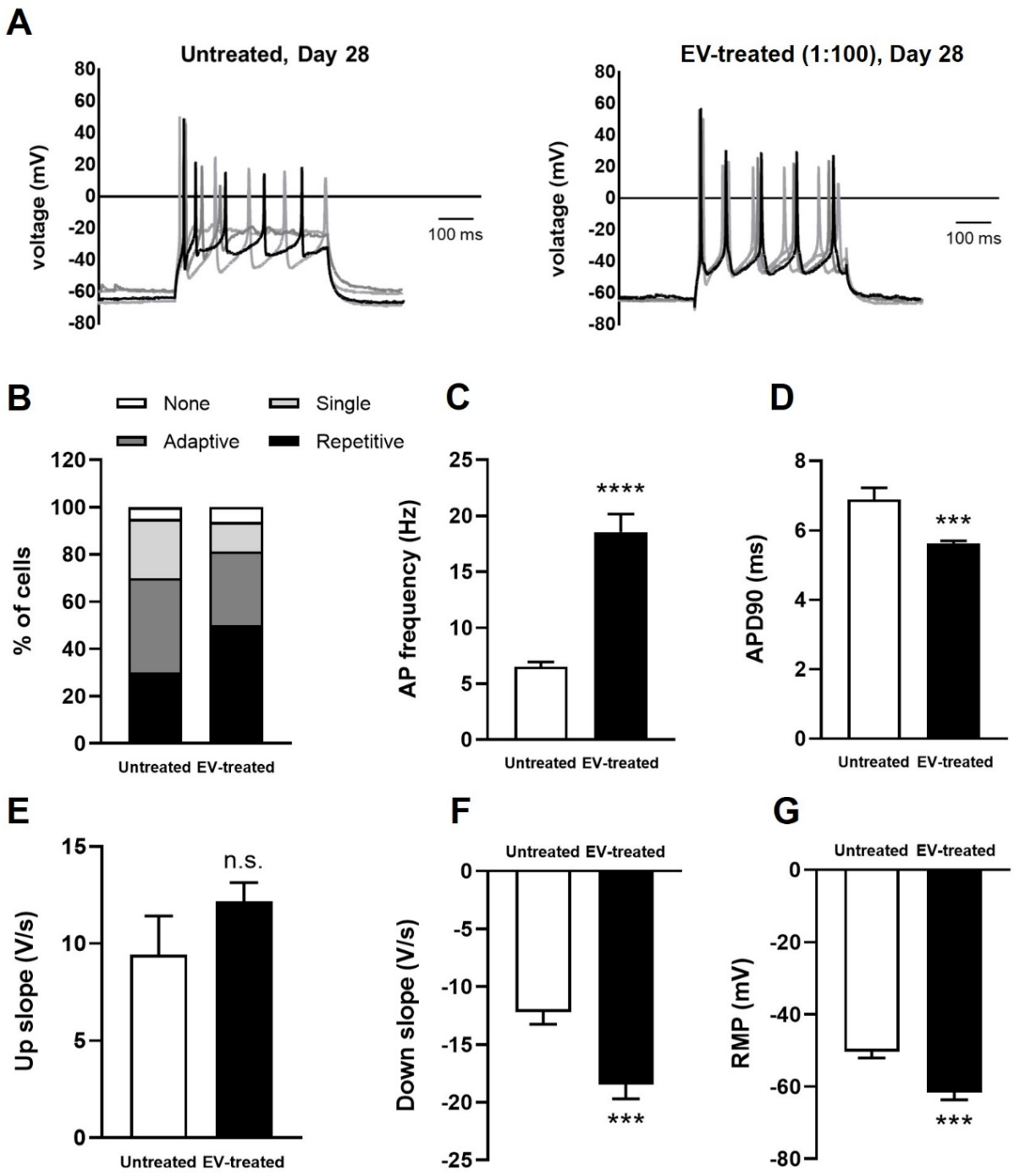

Figure 2.6. Single cell electrophysiology of EV-treated and untreated neurons. (A) Representative action potential traces recorded from EV-treated and untreated neurons. (B) Number of patched neurons exhibiting different action potential firing patterns, categorized as 'repetitive', 'adaptive', 'single', and 'none'. A contingency table comparing EV treatment condition against firing behavior found that the two factors are significantly related ($p = 0.018$), suggesting that the frequency of firing type occurrence is dependent on the presence or absence of EVs in the culture medium. (C) Maximum action potential firing rate in each group of neurons measured in response to a 500 ms depolarizing current injection. (D) The action potential duration at 90% of repolarization (APD90). Depolarization speed (E) and repolarization speed (F) of neurons relative to the apex of the recorded action potential. (G) Resting membrane potential measured from unstimulated neurons with 0 pA current injection. In all presented data, error bars represent standard error of the mean, and ***$p<0.0003$ ****$p<0.0001$, ns not significant. n = 20 (untreated), n = 16 (EV-treated) for each data set.

2.4.6 Proteomics analysis identify EV cargo proteins that promote neuronal survival, oxidative stress management, and electrophysiological function

To identify molecular contributors to the above-mentioned physiological enhancement in EV treated cortical neurons, we performed a quantitative EV-proteomics assay. Mass spectrometry data processed with Proteome Discoverer produced a list of 875 proteins detected from three biological replicates of astrocyte conditioned medium. We then used gene ontology (GO) analysis to categorize the detected proteins in three major GO terms: cellular component, molecular function, and biological process. Nearly 60% of the detected proteins originated from extracellular exosomes while the rest were from cytoplasm, cytosol, and cell membrane**.** This result directly confirms that most of the proteins we analyzed were from an exosomal origin, since exosomes themselves are cytoplasm/cytosol derived. **[Figure 2.7A]** This analysis further specifies that the EVs we collected are highly likely to be exosomes. A large portion of the listed proteins function for protein binding and cell-cell adhesion, likely indicating that many of the EV-associated proteins detected were involved in facilitating EV binding and uptake into the target cell, thus enabling its role as a potent intercellular transporter. **[Figure 2.7A-1, 2.7A-2]** Using a list of common EV proteins reported by Choi *et al.* as a background, we then performed protein enrichment analysis by comparing astrocyte-derived EV protein levels to the background. Proteins identified from astrocyte-derived EVs were more heavily associated with integrin binding and extracellular matrix organization than common proteins found generally in EVs. **[Figure 2.7B]** We then further characterized astrocyte-derived EVs specifically for their cohort of membrane proteins by referring to an up-to-date list of EV surface proteins reported by Wu *et al.*[80] CD81 was the most abundant membrane protein expressed on astrocyte-derived EVs, justifying our method of using CD81 as a reasonable marker for the identification and verification of neuronal EV uptake. **[Figure 2.7C]** Although the majority of identified proteins work to support fundamental EV physiology and function, we sought to find neuroprotective proteins and proteins potentially involved in neuronal electrophysiology from the cargo protein profile. We found 40 proteins previously reported to negatively regulate cell apoptosis (10 of them were neuron-specific) such as HSP90AB1, α-synuclein, LRP1, and

APOE. **[Figure 2.7D]** Additionally, we found several cargo proteins that could potentially affect hiPSC-derived neuron electrophysiological function. These include Potassium channel tetramerization domain containing 12 (KCTD12), Glucose-6- phosphate dehydrogenase (G6PD), Kinesin family member 5B (KIF5B), Spectrin-alpha non-erythrocytic1 (SPTAN1). **[Figure 2.7E]**

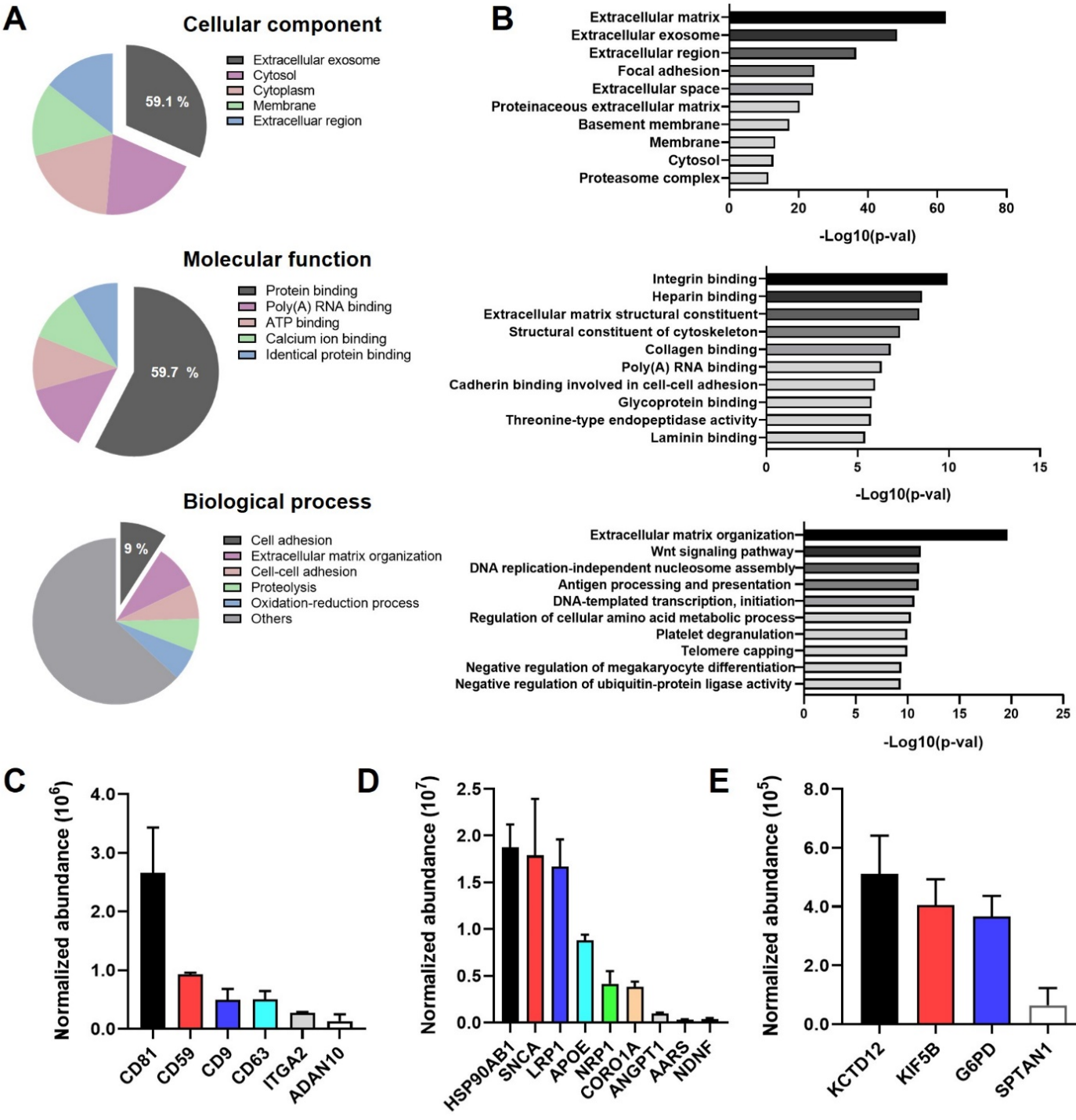

Figure 2.7 Proteomics analysis of astrocyte-derived EVs. (A) Top 5 GO terms ordered by protein % for the following categories: cellular component, molecular function and biological process. (B) The most enriched GO terms for each of the GO categories using the normal EV cargo protein list as a background.[81] (C) Normalized abundance of astrocyte-EV membrane proteins discovered. The most up-to-date list of EV surface proteins as a reference is obtained from literature.[80] (D) Normalized abundances of astrocyte-EV proteins involved in the negative regulation of neuronal apoptosis. (E) Normalized abundances of astrocyte-EV proteins that may be involved in neuronal ion channel and membrane excitability modulation. In all presented data, error bars represent the standard deviation.

2.5 Discussion

One possible mechanism of remote interaction between astrocytes and neurons is EV-mediated signaling. EVs such as exosomes are generated as intraluminal vesicles through inward budding of the multivesicular body; a subtype of late-stage endosomes.[82–89] Endogenously programmed intracellular trafficking of multivesicular bodies can either fuse them with lysosomes for subsequent degradation, or with the plasma membrane to facilitate the release of their vesicular contents into the extracellular space in the form of EVs.[82,88,89] In addition to the cellular 'waste disposal' role of EVs, they are now regarded as major carriers of soluble factors that mediate paracrine communication between various types of cells within the CNS.[82,85] EVs encapsulate numerous proteins and transferrable mRNA, miRNA, lncRNA and lipids in order to modulate recipient cell behavior through post-transcriptional gene regulation, direct protein expression, or expression of transferred inhibitory RNAs[89]. For a detailed description of these vesicles, please see recent reviews (Zhang *et al.* 2019, Basso *et al*. 2016).

The role of astrocyte-derived EVs in different neuronal subtypes has been studied in several *in vitro* and animal model studies. These previous studies focused on phenotypic changes that occur in EV secreting cells in response to various extracellular stimuli, such as inflammatory cytokine treatment, which can result in significant changes to their EV profile and in turn induce remarkable degeneration in neurons taking up these EVs.[67,69,72,73,90] Despite these studies significantly expanded our understanding of how astrocyte-derived EVs regulate their function to modulate neuronal physiology, phenotypic disparity of astrocytes in the CNS of human and murine models has meant that a reliable understanding of human astrocyte EV-based neuroglial communication remains elusive. Moreover, previously published studies have primarily investigated the effect of astrocyte-derived EVs on neuronal survival, morphological development, and population level electrophysiology using murine-derived cells and multi-electrode array systems.[69] While informative as a means to widen our basic understanding of EV-mediated neuroglial communication, such studies are insufficient to delineate astrocyte-EV's comprehensive effect on the electrophysiological function of single neurons, and more importantly, to

define the EV cargo molecules that drive the reported physiological effects in treated cells. In this study, we sought to elucidate the effect of astrocyte-derived EVs on hiPSC-derived neurons, focusing on their role in enhancing electrochemical function. Moreover, we analyzed the cargo protein profile using EV-proteomics to identify those proteins likely responsible for the physiological enhancements we observed.

We first confirmed the identity of hiPSC neurons differentiated for this study. The Ngn2 overexpressing i^{3}N iPSCs developed by Wang *et al*. were used for rapid differentiation into highly homogeneous human cortical neurons.[74] Doxycycline-induced differentiation generated CUX-1 and MAP-2 positive cortical neurons after just 3 days in culture and these neurons were found to be capable of absorbing EVs from the culture medium, likely via standard EV uptake mechanisms described elsewhere.[84,91] Although the majority of the population in culture exhibited a cortical neuron identity, as determined by expression of the above mentioned markers, the survival and function of these cells following Ngn2 overexpression was not yet determined. Therefore, we measured their baseline health and function using apoptotic markers, a senescence marker, and single cell electrophysiological analysis in the absence of glial-derived support. Flow cytometry results using two different apoptosis markers (Annexin V and propidium iodide) illustrated that the majority of these neurons at 3 days post-induction were already apoptotic. Though the signaling mechanisms controlling neuronal apoptosis in adult nerve tissue are not fully understood, previous studies have suggested a lack of paracrine trophic factors such as neurotrophins and IGF-1 may lead to apoptotic cell death.[92,93] Other previous observations have led to the hypothesis that deregulation of the cell cycle can directly trigger apoptosis or oxidative stress can affect cell cycle machinery to promote apoptosis.[94,95] Insufficient provision of growth factors and/or tolerance of oxidative stress are potent factors in driving the onset of neurodegenerative disease. As such, the lack of direct support from glial cells in purified cultured neurons may lead to misinterpretation of assay results, especially in neurodegenerative disease modeling studies. Given that neuronal apoptosis is not a cell-autonomous behavior, we treated astrocyte-derived EVs to early stage (day 3) cultured neurons to check whether the vesicular cargos

could enhance neuron survival in culture. We confirmed that neuronal apoptosis was evidently ameliorated following EV treatment and that survival improved in dose dependent manner. Our results may imply that astrocyte-derived EV cargoes function to prevent initiation or early progression of neuronal apoptosis but cannot reverse late stage progression in cells that are already committed to apoptotic cell death. Our results correlate with a previous study using a rodent model that showed expression of various neuroglobins in astrocytes exhibited an anti-apoptotic effect and suggested that such factors might function as neuroprotective against endogenous and environmental stressors.[96,97] We then tried to define the cargo proteins responsible for this improvement by running EV-proteomics analysis. Gene ontology analysis of the identified astrocyte-EV proteins identified 40 proteins that were previously reported to negatively regulate the cell apoptosis signal. 10 of these proteins were neuron-specific, including heat shock protein HSP90AB1, alpha-synuclein (SNCA), and low-density lipoprotein receptor-related protein 1 (LRP1). Heat shock protein 90AB1, which functions as a molecular chaperone to counteract cellular stress, was the most abundant among the anti-apoptotic regulator proteins present in the EVs. Carnemolla *et al.* showed that astrocytes and oligodendrocytes transcribe the HSP90aa1 and HSP90ab1 genes especially under heat shock response inhibited proteotoxic condition. Additionally, Batulan *et al.* reported the inability of differentiated neurons to transcriptionally induce endogenous heat shock responses after external stress in rodent model experiments.[98] These results, coupled with those presented here, suggest that astroglial heat shock protein support (rather than endogenous HSP expression in neurons) helps alleviate stress in neurons and that this interaction is mediated via EVs.

Additionally, EV treatment on low density neurons induced notable decreases in senescence marker expression. Proteomic analysis revealed calreticulin (CRT) expression in the EV cargoes. CRT is a highly conserved chaperone protein that predominantly resides in the endoplasmic reticulum. CRT has been reported to block the translation of p21 via stabilization of the 5' region of its mRNA, leading to the repression of p21 protein expression.[99] P21 is known to drive cell growth arrest and senescence,

therefore its suppression should also repress senescent behavior. Taken together, our data highlight a neuromodulatory function for astrocyte-EV cargo proteins that inhibits neuronal apoptosis and senescence triggered by stressful conditions in culture.

We next evaluated neuritic outgrowth speed and neurite length in EV treated neurons. A recent study using 3D co-cultures of neurons and astrocytes showed an interdependent structural development in these cell populations.[100] Astrocyte addition promoted denser dendrite development and longer axons in neurons while astrocytes also benefitted in terms of enhanced cytoskeletal outgrowth and proliferation. The study additionally illustrated that the degree to which astrocytic aid contributed to neuronal axon and dendrite development was highly dependent on the distance between the two cell types in culture. Astrocyte's structural support was significantly reduced in distal neurons, indicating their close contact is required for astrocyte-aided neurite development in neurons.[100] Similar to this result, we did not see meaningful enhancement of neuritic outgrowth speed nor axon length in EV treated neurons, reconfirming that astrocyte's structural support on developing neurons is unlikely to be provided via remote, EV-mediated interaction.

Since the major physiological function of neurons in the cerebral cortex is their inter-neuronal electrochemical signal transmission, considerable effort has been made to elucidate the role of astrocytes in promoting synaptogenesis and synapse maturation. Rodent model studies found that neurogenesis precedes astrogenesis in the cortex, but neuronal synapses do not form until the end of astrogenesis.[101] They also form 'tripartite' synapses with pre-synapsed neurons, increasing synaptic diversity and buffering neurotransmitter concentrations within the synaptic cleft to maintain electrochemical homeostasis. Although their critical role in intercellular synapse development is well defined in rodents, it has yet to be defined how astrocytes modulate the functional maturation of developing neurons, particularly in the human cortex. Here, we hypothesized that secreted factors from astrocytes contribute to the maturation of electrophysiological function in human cortical neurons, and

demonstrated that astroglial-derived EVs significantly enhance single neuron electrophysiology as determined by whole-cell patch clamp experiment.

Whole cell patch-clamp recording enables comprehensive electrophysiological assessment of individual neurons, by measuring resting membrane potential, input resistance and capacitance, and waveform analysis for evoked or spontaneous action potentials.[102] The characteristics of action potentials, such as depolarization and repolarization speed, action potential amplitude and frequency, action potential duration, along with the amplitude of sodium and potassium currents, are all important criteria for the validation of the functional maturity of neurons. Maximum frequency of action potential firing indicates how well neurons can repeat the action potential firing cycle in response to protracted depolarizing stimuli and depends on the strength of stimulus applied to the neurons. The nervous system in our body is frequency-modulated, rather than amplitude modulated, meaning that the intensity of a stimulus does not affect the action potential amplitude but it's frequency. With these metrics, we examined whether astrocyte-EVs act to enhance any aspects of electrophysiological maturation in cultured cortical neurons. We observed extensive improvement in the majority of examined electrophysiological metrics in EV treated neurons. EV-treated neurons exhibited more repetitive and consistent firing of action potentials in response to protracted depolarizing stimuli as well as significantly lower resting membrane potentials than untreated neurons. Previous studies have shown that addition of rat astrocytes to hiPSC-neural cultures induces dramatic enhancement of functional development in neurons, in terms of dendritic arborization, electrochemical excitability, and synapse formation. However, the underlying intercellular mechanism facilitating this positive regulation was not elucidated. Based on our results, we can postulate that ion channel expression in early stage hiPSC neurons may depend on the support of astroglial proteins and/or RNAs provided through remote molecular transmission.

To investigate the molecular drivers of the electrophysiological improvement observed in this study, we analyzed the cargo proteins collected within astrocyte-derived EVs. Proteomic analysis found

the presence of proteins promoting excitability of neurons, such as KCTD12, KIF5B, G6PD, and SPTAN1. Potassium channel tetramerization domain containing 12 (KCTD), an important protein for neuronal excitability control, is known to increase $GABA_B$ receptor expression in neurons, which acts in an excitatory manner during early stages of neuron development in contrast to their inhibitory role in the mature CNS.[103,104] Kinesin family member 5B (KIF5B) is a subtype of homologous kinesin 1 proteins with the primary role of mediating long-distance molecular transport in neurons. Most of the previous studies focused on their role as molecular motors, but a recent study showed KIF5B has distinct functions in excitatory synapse and ion channel development and function. Knock-out of KIFB (but not other KIF5s) induced significant reduction in the frequency of excitatory current generation in rodent models.[105] Additionally, Su *et al.* reported the KIF5B regulates the axonal transport of voltage-gated sodium channels, thereby indirectly controlling the excitatory electrochemical activity of neurons in the CNS.[106]

Increased activity of Glucose-6- phosphate dehydrogenase (G6PD) is known to protect neurons from Parkinsonism, mainly by protecting them from oxidative damage. Experiments conducted by Loniewska *et al*. demonstrated that G6PD deficient mice exhibit significant cognitive abnormalities and fail to replenish antioxidant glutathione, which detoxifies neurodegenerative reactive oxygen species (ROS) in neurons.[107] Neurons are one of the most vulnerable cell types to oxidative stress and reactive oxygen metabolites are known to act to modify ion transport mechanisms via ion transport pathway proteins.[108] As such, stable ROS handling ability in neurons may constitute a critical prerequisite to facilitate normal ion channel activities associated with electrophysiological function. Previous studies have revealed that ROS can attack ion channel transporters directly or indirectly through lipid peroxidation.[109] The disruption caused by accumulation of ROS stress on neuron membranes has been reported to alter membrane potential and current, ionic gradient, action potential duration and amplitude, spontaneous excitability, and even resting membrane potentials.[110] Hool *et al.* also demonstrated that ROS stress targets voltage-gated Na^+, K^+, Ca^{2+}, and Ca^{2+}-gated K^+ channels, and interferes with ATP-

sensitive K^+ currents and L-type Ca^{2+} currents.[111,112] The fact that CNS neurons have a limited antioxidant capacity, and rely heavily on astroglial support to deal with oxidative stress, makes inclusion of G6PD in the astrocyte-derived EVs a reasonable mechanism to facilitate remote support for neuronal ROS handling. Interestingly, one of the most prominent ROS (hydrogen peroxide) is known to delay the inactivation of sodium currents through altering K^+ channel activity.[110] Since we observed a dramatic ability for EV treatment to improve repolarization of cortical neurons but exerted little modulating effect on the depolarization speed, we postulate that antioxidant support from astrocyte-EVs may contribute to the restoration of a neuron's repolarization function. Given that ROS mediated stress is known to be involved in the pathology of numerous neurodegenerative diseases, these results highlight the importance of further in-depth study into the molecular mechanisms that underlie ROS stress-induced ion channel disruption. Such future work could help define common pathologic mechanisms across multiple disease states and identify potential therapeutic targets with which to combat neurodegeneration in the human CNS.

We also found small quantities of alpha II-spectrin within astrocyte-EV cargoes, that potentially work to stabilize Na^+ channels. Galiano *et al.* reported the alpha II-spectrin stabilizes nascent sodium channel clusters in cortical neurons and regulates the assembly of the node of Ranvier.[113] Mutations in alpha II-spectrin are a known cause of early infantile epileptic encephalopathies, and have been shown to alter the sensitivity of voltage-gated sodium channels, leading to abnormal action potential thresholds in infant nerves.[114] Additionally, the presence of EHD3 proteins in astrocyte-EVs, which has been shown to regulate membrane excitability in neurons, could help explain the observed improvement in action potential firing behavior in EV-treated neurons.[115] EHD3 in known to be differentially expressed in pyramidal neurons of the pre-frontal cortex in patients with schizophrenia, further underscoring its physiological role in modulating electrochemical behavior in cortical neurons.[116]

2.6 Conclusion

In this study, we have investigated the extensive physiological effects of EVs secreted from human astrocytes on hiPSC-derived cortical neurons. Treatment with an optimized EV concentration was found to have a significant impact on the inhibition of neuronal apoptosis, presumably due to the presence of anti-apoptotic proteins within the EVs. Additionally, we showed that EV treatment prevents early senescence and improves the longevity of cortical neurons in culture. EVs also remarkably altered the electrophysiology of single neurons. We observed a 40% increase in the number of neurons exhibiting repetitive action potential firing behavior, three times higher maximum frequency in action potential firing, and an 18.5% reduction in the APD_{90} of EV-treated neurons compared with untreated controls. EV-treated neurons also showed a significant reduction in resting membrane potential and faster repolarization speed, which all indicate a positive effect of astrocyte-derived EVs on their functional maturation. We also characterized the protein profile of astrocyte-derived EVs to identify protein cargos responsible for this dramatic enhancement of electrophysiological function. Several astrocyte proteins known to be involved in regulating neuronal ion channel maturation, membrane excitability, and oxidative stress handling were detected, which could explain the functional enhancement of cultured neurons post EV treatment. The observations presented here provide useful insights on the diverse modes of neuron-glia communication in the human CNS. These data may inform on the use of EVs for developing more physiologically relevant nerve-on-a-chip assays for preclinical screening applications, enhancing our capacity to model various types of neuropathies, and even the development of novel therapies or biomarkers critical for combating neurodegenerative diseases in the future.

2.7 Reference

1. Farhy-Tselnicker, I. & Allen, N. J. Astrocytes, neurons, synapses: A tripartite view on cortical circuit development. *Neural Dev.* **13**, 1–12 (2018).
2. Molnár, Z. *et al.* New insights into the development of the human cerebral cortex. *J. Anat.* 432–451 (2019). doi:10.1111/joa.13055
3. Rakic, P. & Lombroso, P. J. Development of the cerebral cortex: I. Forming the cortical structure. *J. Am. Acad. Child Adolesc. Psychiatry* **37**, 116–117 (1998).
4. Harris, K. D. & Mrsic-Flogel, T. D. Cortical connectivity and sensory coding. *Nature* **503**, 51–58 (2013).
5. Douglas, R. J. & Martin, K. A. C. Neuronal Circuits of the Neocortex. *Annu. Rev. Neurosci.* **27**, 419–451 (2004).
6. Dzyubenko, E., Gottschling, C. & Faissner, A. Neuron-Glia Interactions in Neural Plasticity: Contributions of Neural Extracellular Matrix and Perineuronal Nets. *Neural Plast.* **2016**, 5214961 (2016).
7. Shi, Y., Kirwan, P. & Livesey, F. J. Directed differentiation of human pluripotent stem cells to cerebral cortex neurons and neural networks. *Nat. Protoc.* **7**, 1836–1846 (2012).
8. Luarte, A. *et al.* Astrocytes at the Hub of the Stress Response: Potential Modulation of Neurogenesis by miRNAs in Astrocyte-Derived Exosomes. *Stem Cells Int.* **2017**, (2017).
9. Bellot-Saez, A., Kékesi, O., Morley, J. W. & Buskila, Y. Astrocytic modulation of neuronal excitability through K+spatial buffering. *Neurosci. Biobehav. Rev.* **77**, 87–97 (2017).
10. Hansen, M. G., Tornero, D., Canals, I., Ahlenius, H. & Kokaia, Z. In vitro functional characterization of human neurons and astrocytes using calcium imaging and electrophysiology. *Methods Mol. Biol.* **1919**, 73–88 (2019).
11. Ibáñez, F., Montesinos, J., Ureña-Peralta, J. R., Guerri, C. & Pascual, M. TLR4 participates in the transmission of ethanol-induced neuroinflammation via astrocyte-derived extracellular vesicles. *J. Neuroinflammation* **16**, 1–14 (2019).
12. Hira, K. *et al.* Astrocyte-derived exosomes treated with a semaphorin 3A inhibitor enhance stroke recovery via prostaglandin D2 synthase. *Stroke* **49**, 2483–2494 (2018).
13. You, Y. *et al.* Activated human astrocyte-derived extracellular vesicles modulate neuronal uptake, differentiation and firing. *J. Extracell. Vesicles* **9**, (2020).
14. Pascua-Maestro, R. *et al.* Extracellular vesicles secreted by astroglial cells transport apolipoprotein D to neurons and mediate neuronal survival upon oxidative stress. *Front. Cell. Neurosci.* **12**, 1–13 (2019).
15. Datta Chaudhuri, A. *et al.* Stimulus-dependent modifications in astrocyte-derived extracellular vesicle cargo regulate neuronal excitability. *Glia* **68**, 128–144 (2020).
16. Varcianna, A. *et al.* Micro-RNAs secreted through astrocyte-derived extracellular vesicles cause neuronal network degeneration in C9orf72 ALS. *EBioMedicine* **40**, 626–635 (2019).
17. Silverman, J. M. *et al.* CNS-derived extracellular vesicles from superoxide dismutase 1 (SOD1)G93A ALS mice originate from astrocytes and neurons and carry misfolded SOD1. *J. Biol. Chem.* **294**, 3744–3759 (2019).
18. Wang, C. *et al.* Scalable Production of iPSC-Derived Human Neurons to Identify Tau-Lowering

Compounds by High-Content Screening. *Stem Cell Reports* **9**, 1221–1233 (2017).

19. Fernandopulle, M. S. *et al.* Transcription Factor-Mediated Differentiation of Human iPSCs into Neurons. *Curr. Protoc. Cell Biol.* **79**, e51 (2018).
20. Gunhanlar, N. *et al.* A simplified protocol for differentiation of electrophysiologically mature neuronal networks from human induced pluripotent stem cells. *Mol. Psychiatry* **23**, 1336–1344 (2018).
21. Patani, R. *et al.* Retinoid-independent motor neurogenesis from human embryonic stem cells reveals a medial columnar ground state. *Nat. Commun.* **2**, (2011).
22. de Mera-Rodríguez, J. A. *et al.* Senescence-associated β-galactosidase activity in the developing avian retina. *Dev. Dyn.* **248**, 850–865 (2019).
23. Tominaga, T., Shimada, R., Okada, Y., Kawamata, T. & Kibayashi, K. Senescence-associated-β-galactosidase staining following traumatic brain injury in the mouse cerebrum. *PLoS One* **14**, 1–17 (2019).
24. Wu, D. *et al.* Profiling surface proteins on individual exosomes using a proximity barcoding assay. *Nat. Commun.* **10**, 1–10 (2019).
25. Basso, M. & Bonetto, V. Extracellular vesicles and a novel form of communication in the brain. *Front. Neurosci.* **10**, 1–13 (2016).
26. Gangoda, L., Boukouris, S., Liem, M., Kalra, H. & Mathivanan, S. Extracellular vesicles including exosomes are mediators of signal transduction: Are they protective or pathogenic? *Proteomics* **15**, 260–271 (2015).
27. Mulcahy, L. A., Pink, R. C., Raul, D. & Carter, F. Routes and mechanisms of extracellular vesicle uptake. **1**, 1–14 (2014).
28. Paolicelli, R. C., Bergamini, G. & Rajendran, L. Cell-to-cell Communication by Extracellular Vesicles: Focus on Microglia. *Neuroscience* **405**, 148–157 (2019).
29. Saeedi, S., Israel, S., Nagy, C. & Turecki, G. The emerging role of exosomes in mental disorders. *Transl. Psychiatry* **9**, 122 (2019).
30. Lee, Y., El Andaloussi, S. & Wood, M. J. A. Exosomes and microvesicles: Extracellular vesicles for genetic information transfer and gene therapy. *Hum. Mol. Genet.* **21**, 125–134 (2012).
31. Frühbeis, C., Fröhlich, D. & Krämer-Albers, E. M. Emerging roles of exosomes in neuron-glia communication. *Front. Physiol.* **3 APR**, 1–7 (2012).
32. Hessvik, N. P. & Llorente, A. Current knowledge on exosome biogenesis and release. *Cell. Mol. Life Sci.* **75**, 193–208 (2018).
33. Keir, M. E., Butte, M. J., Freeman, G. J. & Sharpe, A. H. PD-1 and Its Ligands in Tolerance and Immunity. *Annu. Rev. Immunol.* **26**, 677–704 (2008).
34. Holm, M. M., Kaiser, J. & Schwab, M. E. Extracellular Vesicles: Multimodal Envoys in Neural Maintenance and Repair. *Trends Neurosci.* **41**, 360–372 (2018).
35. Johnson, F., Hohmann, S. E., DiStefano, P. S. & Bottjer, S. W. Neurotrophins suppress apoptosis induced by deafferentation of an avian motor-cortical region. *J. Neurosci.* **17**, 2101–2111 (1997).
36. Lindholm, D., Carroll, P., Tzimagiorgis, G. & Thoenen, H. Autocrine-paracrine regulation of hippocampal neuron survival by IGF-1 and the neurotrophins BDNF, NT-3 and NT-4. *Eur. J. Neurosci.* **8**, 1452–1460 (1996).
37. Redza-Dutordoir, M. & Averill-Bates, D. A. Activation of apoptosis signalling pathways by reactive

oxygen species. *Biochim. Biophys. Acta - Mol. Cell Res.* **1863**, 2977–2992 (2016).

38. Elmore, S. Apoptosis: A Review of Programmed Cell Death. *Toxicol. Pathol.* **35**, 495–516 (2007).
39. Guidolin, D., Tortorella, C., Marcoli, M., Maura, G. & Agnati, L. F. Neuroglobin, a Factor Playing for Nerve Cell Survival. *Int. J. Mol. Sci.* **17**, 1–16 (2016).
40. Baez, E. *et al.* Protection by neuroglobin expression in brain pathologies. *Front. Neurol.* **7**, 1–10 (2016).
41. Batulan, Z. *et al.* High threshold for induction of the stress response in motor neurons is associated with failure to activate HSF1. *J. Neurosci.* **23**, 5789–5798 (2003).
42. Iakova, P. *et al.* Competition of CUGBP1 and calreticulin for the regulation of p21 translation determines cell fate. *EMBO J.* **23**, 406–417 (2004).
43. Fang, A. *et al.* Effects of astrocyte on neuronal outgrowth in a layered 3D structure. *Biomed. Eng. Online* **18**, 1–16 (2019).
44. Farhy-Tselnicker, I. & Allen, N. J. Astrocytes, neurons, synapses: A tripartite view on cortical circuit development. *Neural Dev.* **13**, 1–12 (2018).
45. Petersen, C. C. H. Whole-Cell Recording of Neuronal Membrane Potential during Behavior. *Neuron* **95**, 1266–1281 (2017).
46. Li, M. *et al.* KCTD12 modulation of GABA(B) receptor function. *Pharmacol. Res. Perspect.* **5**, 1–9 (2017).
47. Teng, X. *et al.* KCTD: A new gene family involved in neurodevelopmental and neuropsychiatric disorders. *CNS Neurosci. Ther.* **25**, 887–902 (2019).
48. Zhao, J. *et al.* Specific depletion of the motor protein KIF5B leads to deficits in dendritic transport, synaptic plasticity and memory. *Elife* **9**, 1–34 (2020).
49. Su, Y. Y. *et al.* KIF5B promotes the forward transport and axonal function of the voltage-gated sodium channel Nav1.8. *J. Neurosci.* **33**, 17884–17896 (2013).
50. Loniewska, M. M. *et al.* DNA damage and synaptic and behavioural disorders in glucose-6-phosphate dehydrogenase-deficient mice. *Redox Biol.* **28**, 101332 (2020).
51. Wang, X. & Michaelis, E. K. Selective neuronal vulnerability to oxidative stress in the brain. *Front. Aging Neurosci.* **2**, 1–13 (2010).
52. Kiselyov, K. & Muallem, S. ROS and intracellular ion channels HHS Public Access. *Cell Calcium* **60**, 108–114 (2016).
53. Jovanovi, Z. Effects of Oxidative Stress on the Electrophysiological Function of Neuronal Membranes. *Oxidative Stress Dis.* (2012). doi:10.5772/33580
54. Hermann, A., Sitdikova, G. F. & Weiger, T. M. Oxidative stress and maxi calcium-activated potassium (BK) channels. *Biomolecules* **5**, 1870–1911 (2015).
55. Sahoo, N., Hoshi, T. & Heinemann, S. H. Oxidative modulation of voltage-gated potassium channels. *Antioxidants Redox Signal.* **21**, 933–952 (2014).
56. Galiano, M. R. *et al.* Controls Axon Initial Segment Assembly. *Cell* **149**, 1125–1139 (2013).
57. Tohyama, J. *et al.* SPTAN1 encephalopathy: Distinct phenotypes and genotypes. *J. Hum. Genet.* **60**, 167–173 (2015).
58. EHD3-Dependent Endosome Pathway Regulates Cardiac Membrane Excitability and Physiology. *Circ Res* **23**, 1–7 (2008).

59. Prabakaran, S. *et al.* Mitochondrial dysfunction in schizophrenia: Evidence for compromised brain metabolism and oxidative stress. *Mol. Psychiatry* **9**, 684–697 (2004).

60. Choi, D. S., Kim, D. K., Kim, Y. K. & Gho, Y. S. Proteomics, transcriptomics and lipidomics of exosomes and ectosomes. *Proteomics* **13**, 1554–1571 (2013).

Chapter 3. Human stem cell model of astrocyte-mediated neurodegeneration in ALS

3.1 Abstract

To understand ALS pathology as a whole, recent research efforts try to add glial components to the conventional neuro-centric disease model. Glial cells' extensive roles in neuronal development, survival, and function in the CNS environment make the idea of glia-derived neurodegeneration reasonable. Among those glial cells, astrocytes have been getting particular interest due to their significant involvement in neurotransmission, intracellular stress management, homeostatic maintenance, and immune responses in CNS. Studies of neuron-astrocyte communication in ALS rodent models and clinical observations of patients' post-mortem tissue implicated the diseased astrocytes' involvement is attributed to the diverse aspect of neurodegeneration. Although increasing evidence equivocally points out that neurodegeneration is highly attributed to the aberrant astrocytic reactivity, molecular drivers and mechanism of astrocyte-mediated neurodegeneration are not well understood. Moreover, the lack of reliable human 'astrocyte-neuron models' that recapitulate the progression of ALS pathophysiology has been a roadblock to understanding the symptomatic stage of neurodegeneration as a whole. In this study, we generated iPSC-derived astrocytes and isogenic spinal motor neurons from normal and ALS mutant lines (TDP43Q331K+/-) to investigate the pathologic effect of mutant ALS astrocytes on the neurons as well as the therapeutic potential of normal astrocytes' physiological input to the diseased neurons. We first compared the phenotype of motor neurons derived from WT and ALS mutant iPSCs to understand the difference in their baseline physiology before adding any astrocytic component. Then we co-cultured each group of neurons with WT and ALS mutant iPSC-derived astrocytes to make 4 pairs of comparison, to understand how the different astrocytic input alters the neurophysiology, to build a more comprehensive model of human neurodegenerative diseases.

3.2 Introduction

Understanding the pathologic role of astrocytes in ALS development is one of the critical milestones in the ALS study. An increasing number of recent studies have been demonstrating the progressive neurodegeneration that occurs upstream of the disease is highly attributed to the neurotoxic astrocyte inclusion.[30,33,117–120] Significant infiltration of reactive astrocytes near neurons at the symptomatic stage of ALS, and remarkable slow-down of motor and cognitive deficits after their removal in animal models imply that astrocyte pathologies are mainly responsible for the disease progression.[30,121,122] Given that ALS has an extremely heterogeneous etiology including more than 20 genetic causes with a number of exogenous risk factors, aiming to effectively prevent its progression before entering the symptomatic stage would be a more feasible way to treat the disease rather than targeting the entire removal of all of the initial risk factors. Thus, understanding the progressive pathologic mechanism by identifying the triggering factor(s) for the explosive development of neurodegeneration is an indispensable task to achieving the goal.

Previous efforts to model astrocyte-neuron interaction in ALS tissue have been highly reliant on rodent models bearing human mutant SOD1 transgene ($SOD1^{G93A}$), which encodes enzymes that convert superoxide into oxygen or hydrogen peroxide. The SOD1 mutation was identified in the early 1990s, takes 2.3% of total ALS cases, and the studies with this rodent model provided enormous amounts of initial insights of pathologic neuroglial interactions. Those studies showed normal neurons in the chimeric mice acquired an ALS phenotype when surrounded by SOD1 mutant astrocytes.[117,123] Further studies showed the genetic ablation of mutant SOD1 in astrocytes significantly delayed the motor function impairment and extended the lifespan of treated mice, implicating the critical pathologic mechanism that goes through astrocytes to exert neuron damage.[30,124] The SOD1 mutant astrocytes were abnormally proliferative with enlarged protoplasmic morphology, and showed an elevated level of mitochondrial ROS, downregulated EAAT2 expression which is supposed to uptake the excessive extracellular glutamate for neuroprotection.[25] Another recent study of mutant SOD1 mouse models

revealed the SOD1 mutant astrocytes have a lower threshold against inflammatory stress, induced by IL-1a, TNF-a, and C1qa that generates reactive astrocytes. Guttenplan *et al* reported the significant upregulation of reactive astrocyte markers (complement 3) in SOD1 mutant astrocytes with smaller amounts of the exogenous inflammatory stress than for WT. The animals with reactive astrocytes showed dramatically shortened lifespans and motor deficits, which was not the case for the immune-compromised (knocked out of cytokine-releasing genes) mice. The significant delay of neurodegeneration but similar onset age in the knocked-out model agrees with the idea that inflammatory astrogliosis is highly involved in the disease progression phase, but not in the very initial pathologic stage.[31]

Despite the previous information collected from numbers of $SOD1^{G93A}$ rodent model studies, research of pathologic astrocyte-neuron interaction in ALS is still in its infancy. The SOD1 mutation case has been dominating the previous ALS studies by virtue of having the G93A SOD1 mouse model developed in the 1990s, but it takes only 2% of entire ALS subclasses. More importantly, ALS with SOD1 mutation exceptionally does not exhibit TDP-43 proteinopathy which is a hallmark of over 97% of ALS cases, making its disease representativeness low.[11,14,125] Thus, understanding the contribution of TDP-43 proteinopathy to ALS pathology by using a relevant astrocyte-neuron model would be a critical prerequisite to resolving the secret of the common ALS pathology, for the development of widely applicable ALS drugs. Finally, the murine model's lack of physiological relevance to the human ALS pathophysiology requires the development of a reliable human model to accurately mirror the TDP-43 dysfunction and severe neurodegeneration that occurs in actual patients.

In this study, we generated human iPSC-derived spinal cord astrocytes and isogenic motor neurons from both WT and ALS mutant ($TDP43^{Q331K+/-}$) stem cells, to investigate the pathologic role of the diseased astrocytes on non-cell autonomous neurodegeneration. Specifically, we investigated the physiologic effect of a mutation in TARDBP gene in astrocytes by hypothesizing the misregulation of this RNA-binding protein will extensively alter the expression of the thousands of downstream genes

that control astrocyte physiology, leading to the expression of severe neurotoxic phenotypes. We compared the phenotype of WT and ALS mutant iPSC-derived astrocytes and also motor neurons separately, to first analyze their baseline physiological difference which stems from the cell-autonomous mutation. Then we evaluated the neuron's electrophysiological function after co-culturing with the two different groups of astrocytes, to understand how the different astrocytic input alters the neuron's electrophysiological function.

3.3 Materials and Methods

3.3.1 Motor neuron differentiation from iPSCs

WTC11 iPSCs from a normal donor were provided by the Conklin lab (Gladstone Institute, CA) for normal motor neuron differentiation. Working with the University of Washington's Institute for Stem Cell and Regenerative Medicine Ellison Stem Cell Core, heterozygous *TDP-43*^{Q331K} mutations were introduced into the WTC11 iPSC line, using methods described previously.[48] Both the WT and mutant iPSCs were passed onto Matrigel-coated 6-well plates and incubated at 37°C / 5% CO_2 in mTeSR until they reached 50~60% confluency. At this point, cultures were differentiated into regionally unspecified neural progenitor cells using a monolayer differentiation method adapted from Du et al.[17] The cultures were single-cell passaged onto fresh Matrigel-coated 6-well plates on day 5 and 11, and kept in the induction medium until day 18. On day 18, the cultures were passaged on 0.01% poly-L-ornithine (Sigma-Aldrich) & 50 mg/mL Laminin (Sigma-Aldrich)-coated assay plates or frozen down in mFreSR medium (Stem cell Technologies). From day 18, the cells were exposed to culture conditions promoting motor neuron maturation, essentially as described by Amoroso *et al*.[18] The day 25 neurons were re-plated to the fresh laminin plate and co-cultured with astrocytes until the end of each assay.

3.3.2 Spinal astrocyte differentiation from iPSCs

The same line of iPSCs were used to generate human astrocytes. The undifferentiated cells were treated with the same induction medium of motor neuron differentiation until day 11, to obtain neural progenitor cells with spinal cord lineage. At day 11, the cells were exposed to glial-induction

medium mainly composed of Leukemia inhibitory factor replenished every day until day 18 passage. At day 18, cells were dissociated for replating on Matrigel-coated 6-well plate with Leukemia Inhibitory Factor (LIF) and BMP4 with the same concentrations for further differentiation. The culture was passaged every 6 days on Matrigel plate until day 40. The day 40 culture were sorted with CD44 and CD49f antibodies, to obtain mature astrocytes and expanded on the poly-ornithine / Laminin treated culture substrate for downstream assays.

3.3.3 Co-culture of astrocytes and motor neurons generated from WT and Q331K+/- iPSCs

The day25 of iPSC-motor neurons were co-cultured with the day 45 of iPSC-derived astrocytes on the laminin-coated 24 well culture plate and 48 well MEA plate. The neurons and astrocytes were plated with the density of 100,000 cells/well. For MEA experiment, neurons were plated to form compact monolayer to cover the embedded electrodes before adding the same number of astrocytes on top of neurons. The mixed populations were fed with half-neuronal and half-astrocyte maintenance medium after plating, and the fresh medium was supplied every day for the rest of the culture.

3.3.4 Immunocytochemistry

The cells were fixed in 4% paraformaldehyde for 15 minutes and blocked with 0.5% BSA in PBS for 1 hour at room temperature. Cells were then incubated with primary antibodies diluted in 0.5% BSA in PBS overnight at 4°C. The next day, cells were washed 3 times with PBS. They were then incubated in a secondary antibody solution containing secondary antibodies diluted in 0.5% BSA in PBS overnight at 4°C. Counterstaining was performed with Vectashied containing DAPI (Vector Labs). Images were taken at the Garvey Imaging Core at the University of Washington's Institute for Stem Cell and Regenerative Medicine using a SP8 Leica Confocal System on an inverted microscope platform. 12-bit 1024x1024 pixel images were acquired with LAS X Leica software. Antibodies used in this study were as follows: mouse anti-S100β (1 in 500, Thermo-Fisher), chicken anti-GFAP (1 in 1000, Thermo Fisher), rabbit anti-EAAT1 (1 in 200, Thermo Fisher), rabbit anti-microtubule associated protein-2 (1 in 1000, Millipore), mouse anti-Islet-1 (1 in 10, DSHB), rabbit anti-TDP43 (1 in 200, Thermo-Fisher),

mouse anti-TuJ1 (1 in 500, Thermo-fisher), rabbit anti-TuJ1 (1 in 200, Thermo-Fisher), Alexafluor-594 conjugated goat-anti-mouse secondary antibody (1:500, Invitrogen), Alexafluor-594 conjugated goat-anti-chicken secondary antibody (1:500, Invitrogen), Alexafluor-647 conjugated donkey-anti-mouse secondary antibody (1:500, Invitrogen), and Alexafluor-488 conjugated goat-anti-rabbit secondary antibody (1:500, Invitrogen). Quantitative analysis of fluorescence images was performed with ImageJ software.

3.3.5 Fluorescence Activated Cell Sorting (FACS)

Cells were lifted by incubation with TrypLE (Stem Cell Technologies) for 15 minutes. Cell suspension was triturated 8-10 times and passed through a 70mm cell strainer (Sigma; CLS431751) then diluted > 3x with PBS with calcium and magnesium. Cells were spun in a 15mL conical tube at 300 g for 5 minutes at room temperature. The cell pellet was resuspended in FACS staining buffer (DMEM/F12, 1% FBS, 1mM EDTA) with 1:50 PE Rat Anti-Human CD44 (for astrocytes, BD Biosciences), APC Mouse Anti-CD271 (for neurons, BD Biosciences) and APC Rat Anti-Human CD49f antibody (for astrocytes, BD Biosciences) and incubated on ice for 20 minutes. The IgG-PE and IgG-APC control dye was used for making secondary control groups. Cells were then washed twice in FACS wash buffer (PBS, 1% FBS, 1mM EDTA) by spinning down at 300 g for 5 minutes and resuspended in the culture medium. The CD44- & CD271+ cells (for neurons), CD44+ & CD49f + double-positive cells (for astrocyte) were isolated via FACS on an ARIA-3 Cell Sorter (BD Biosciences) using the 70μm nozzle, at 20 or 23 psi. Data were analyzed using FlowJo version 9.

3.3.6 ATP-stimulated intracellular Ca^{2+} imaging

Neurons at day 25, 32 and day 40 were treated with Fluo4-AM (Thermo-Fisher) for 30 minutes at 37°C, washed twice with PBS without calcium and magnesium and imaged in the live cell imaging solution. Live fluorescence imaging of the ATP induced Ca^{2+} activity was done with an ArrayScan XTi high-content imager (Thermo-Fisher). The whole field of view images at 20x magnification were acquired with Photometrics X1 cooled CCD camera (Thermo-Fisher) at 4 Hz for 60 seconds with ATP

(100μM, Thermo-Fisher) treatment. For quantification of the change in intensity over time, the cells in each experiment group were outlined as regions of interest (ROIs) and analyzed with ImageJ software. Ca^{2+} transients are expressed in the form of $\Delta F(t)/F0$, where F0 is a baseline fluorescence of a given region of interest and ΔF is the difference between the current level of fluorescence F(t) and F0. Fluctuations of $\Delta F(t)/F0$ of less than 0.05 were considered non-responses. The $\Delta F(t)/F0$ traces were presented with the original R script of the author.

3.3.7 Glutamate uptake assay

CD49f+ astrocytes (WT and $TDP43^{Q331K+/-}$) were incubated with 100 μM glutamate (Sigma-Aldrich) in the maintenance medium. The cell-free wells were equally treated with the same concentration of glutamate as a control. The conditioned medium was collected after 3 hours and analyzed with a colorimetric glutamate assay kit (Sigma-Aldrich), following the manufacturer's instruction. The same culture medium without glutamate were also used as negative controls. The absorbance of each well was quantified based on that of the glutamate standard solution. Three biological replicates per condition were used for the final analysis.

3.3.8 Mitochondrial trafficking analysis

For mitochondria movement recording, neurons at day 32 were stained with Mitotracker Orange CMTMRos (Thermo-Fisher) for 30 min. The stained cells were then washed twice with PBS without calcium and magnesium and imaged via a confocal microscope (Nikon A1, 40x oil lense) equipped with a live cell module maintaining 37°C, 5% CO 2 and > 90% relative humidity environment during recording. Time-lapse recordings were taken with an exposure time of 500 ms interval between image capture for 2 minutes. All images were analyzed using the TrackMate plugin in the ImageJ software to calculate instantaneous velocity of individual mitochondria. Each mitochondrion present in the axons of cells within the field of view were captured as individual particles and tracked frame by frame. The instantaneous velocity of each mitochondrion at each time point was then plotted as a histogram with 0.5 μm/second intervals. The data were normalized so that the relative velocity in *WT* cells was 1. In

so doing, the mitochondrial speed in neurons in all other experiment groups was calculated as a single relative value. GraphPad Prism 8 (GraphPad Software, San Diego, CA, USA) was then used for *post hoc* counting and plotting the frequency of instantaneous velocities.

3.3.9 Multi-Electrode-Array assay

Population-level of electrophysiological function in motor neuron cultures was assessed by a 48-well multielectrode array (MEA) system using the Maestro MEA system (Axion Biosystems). The day 21 cells were plated on the Cytoview 48 well plate (Axion Biosystems) at the density of 100,000 cells per well followed by adding the same number of iPSC-astrocytes (Day 50) on top of neurons. The maintenance medium was replaced every day. The recording was taken every day from day 22 to day 40 for all experiment groups. During data acquisition, standard recording settings for spontaneous neuronal spikes were used (Axis software, version 2.5), and cells were maintained at 37°C/ 5% CO_2 throughout the 2-minute recording period. The standard settings have 130 × gain, and record from 1 to 25 000 Hz, with a low-pass digital filter of 2 kHz for noise reduction. In all experiments, spike detection was set at 5x the standard deviation of the noise and network burst detection was recorded if at least 25% of the electrodes in a given well showed synchronous activity. Reported results were calculated by averaging all of the electrodes in each well, then averaging data from duplicate wells.

3.4 Results

3.4.1 Spinal motor neuron are successfully differentiated from WT and TDP43$^{Q331K+/-}$ iPSCs

Human iPSC cultures (WT and TDP43$^{Q331K+/-}$) were differentiated to regionally unspecified neural progenitor cells using a monolayer-based protocol adapted from Du *et al.* **[Figure 3.1]**

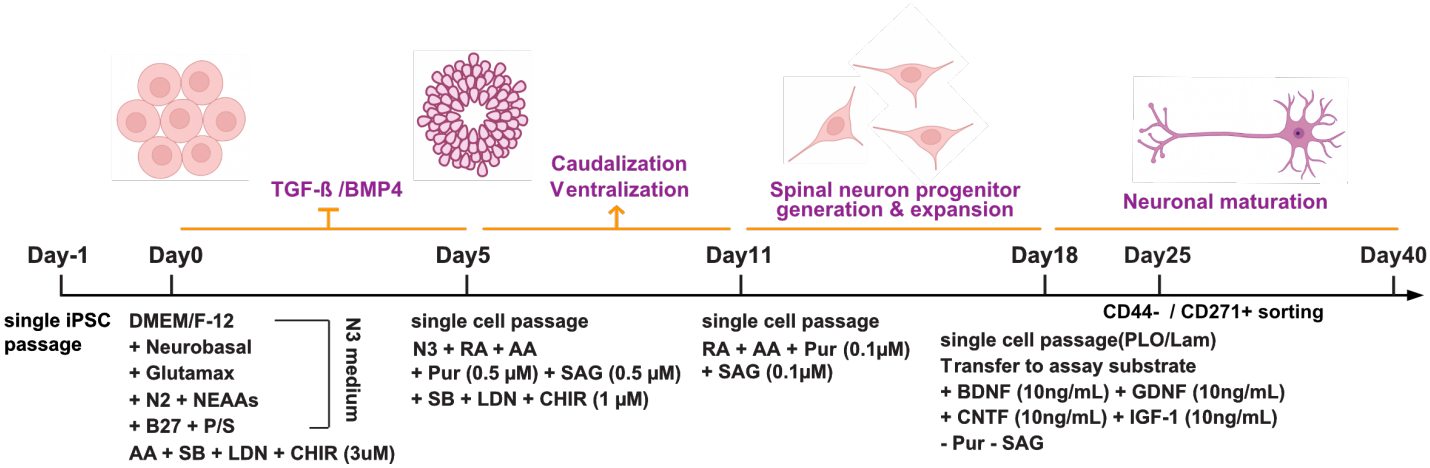

Figure 3.1 The protocol for ventral spinal motor neuron differentiation adapted from Du *et al*

The cells were subsequently exposed to differentiation conditions toward a caudal and ventral spinal phenotype, essentially as described by Amoroso *et al*.[18] The differentiating cells were bearing distinct neuronal morphology, characterized as multi-polar cell bodies with evident neuritic outgrowth. **[Figure 3.2A]** The day18 progenitors were positive for Nestin and PAX6 staining, the early marker of neurogenesis. **[Figure 3.2B]** The day 25 cells of both groups were highly expressing neuronal marker CD271 (P75NTR) on their surface but a negligible amount of CD44, which stains the glial cell population in this lineage of culture. **[Figure 3.2C, 3.2D]** The 39 % of day 25 WT cells expressed motor neuron specific transcription factor Islet-1 and all of them expressed a pan-neuronal marker TuJ1 (β III tubulin). Similarly, 42 % of the TDP43$^{Q331K+/-}$ cells on the same day were positive for the Islet-1 staining, and all of them expressed TuJ1. The expression levels of both Islet-1 and TuJ1 in WT and the mutant culture were not significantly different. **[Figure 3.2E, 3.2F]**

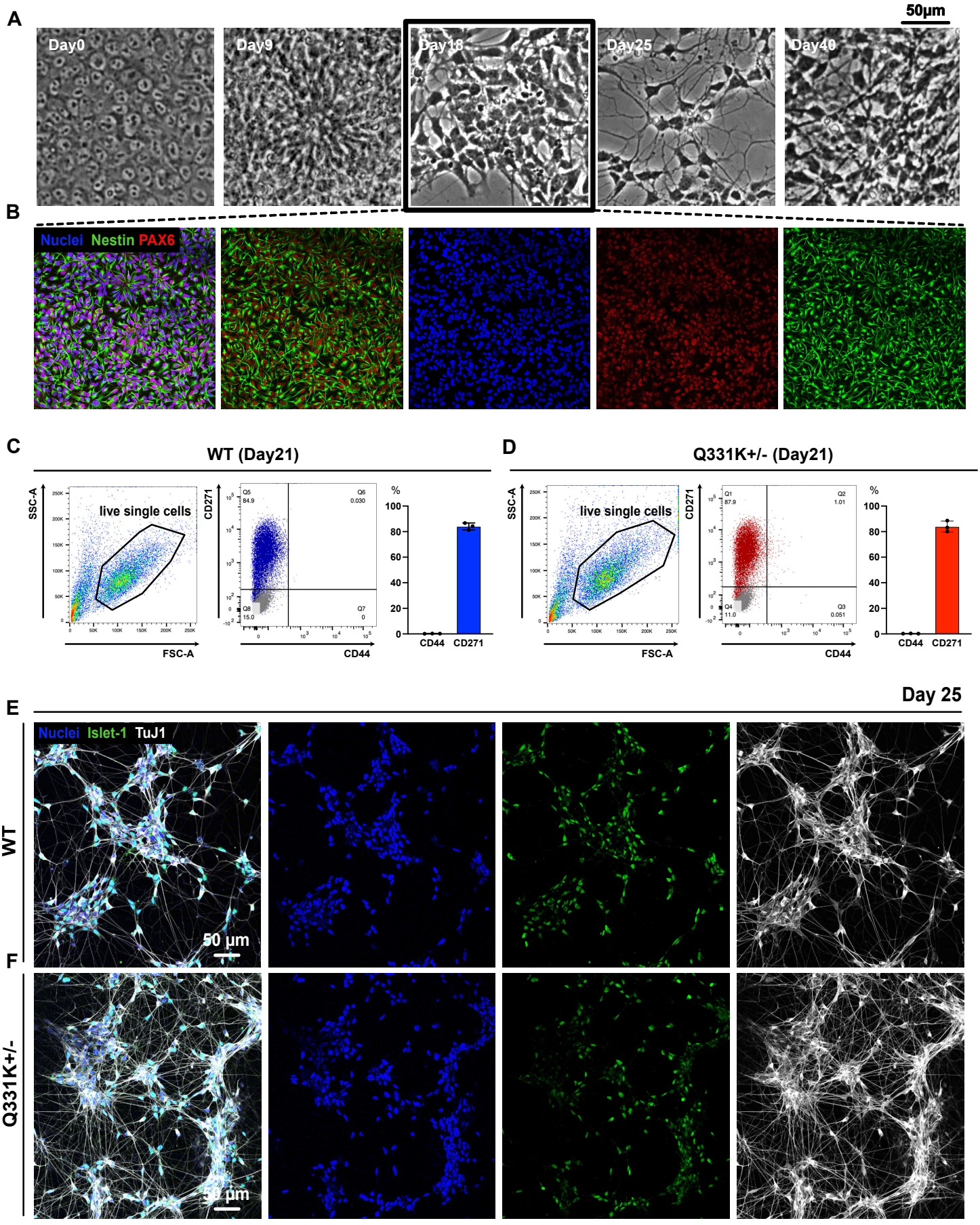
A
50μm
Day0
Day9
Day18
Day25
Day40
B
Nuclei Nestin PAX6
C
WT (Day21)
SSC-A
live single cells
FSC-A
CD271
CD44
Q5 84.9
Q6 0.030
Q8 15.0
Q7 0
%
CD44 CD271
D
Q331K+/- (Day21)
Q1 87.9
Q2 1.01
Q4 11.0
Q3 0.051
E
Day 25
WT
Nuclei Islet-1 TuJ1
50 μm
F
Q331K+/-
50 μm

Figure 3.2 The differentiating cells highly express neural progenitor and spinal motor neuron markers while exhibiting distinct morphological development (A) The cells exhibit dramatic morphological change along the differentiation. Day25 cells have distinct morphology of neurons with extended neurites (B) Day 18 cells express Nestin and PAX6, which are canonical markers for neural progenitors. The FACS result of day 25 culture. The cells are stained with antibodies against CD271 and CD44 for (C) WT and (D) Q331K+/- mutant group. (E) (F) Similar % of the WT and TDP-43 mutant culture at day 25 express Islet-1 and TuJ1, indicating the successful motor neuron differentiation from both groups of iPSCs.

3.4.2 WT and TDP43$^{Q331K+/-}$ iPSC-derived motor neurons showed a phenotypic difference in their electrophysiology but not in other functional aspects

The two groups of differentiated neurons from WT and TDP43$^{Q331K+/-}$ iPSCs were compared in terms of the TDP43 expression pattern, axonal mitochondria movement, and electrophysiologic functionality to investigate the neuron-autonomous disease phenotypes. We postulated the mutation in TARDBP gene could cause the increase of TDP-43 protein expression level as a compensation mechanism, as well as induce cytoplasmic mislocalization which is commonly observed in nerve cells with diverse neurodegenerative diseases. However, we did not observe a significant difference in TDP-43 localization pattern between the normal and mutant groups. The TDP-43 protein was dominantly expressed in the neuronal nuclei in both groups with a similar co-localization value (Pearson's R-value), indicating the TARDBP mutation in neurons *per se* is not a direct cause of the protein mis localization or aggregation. **[Figure 3.3A, 3.3B, 3.3C]** However, the entire gene expression level of TDP-43 in both groups became significantly different after the development, implying the compensation mechanism might be applied to make up the dysfunctional TDP-43 expression in neurons. **[Figure 3.3D]**

We also compared the intracellular calcium release ability of WT and mutant neurons at day 27. Both groups of cells did not show significant difference in terms of % cells responding to the ATP stimulation and average fluorescence intensity change, indicating the TDP-43 mutation might not impair intracellular calcium release ability upon extracellular stimulation. **[Figure 3.4A, 3.4B]** Furthermore, we compared the axonal trafficking speed of mitochondria which is an important function to maintain axon physiology, especially in motor neurons with extremely long axons. We did not observe any significant

difference the mitochondria trafficking speed in mutant neurons than that of WT neurons. **[Figure 3.4C, 3.4D]**

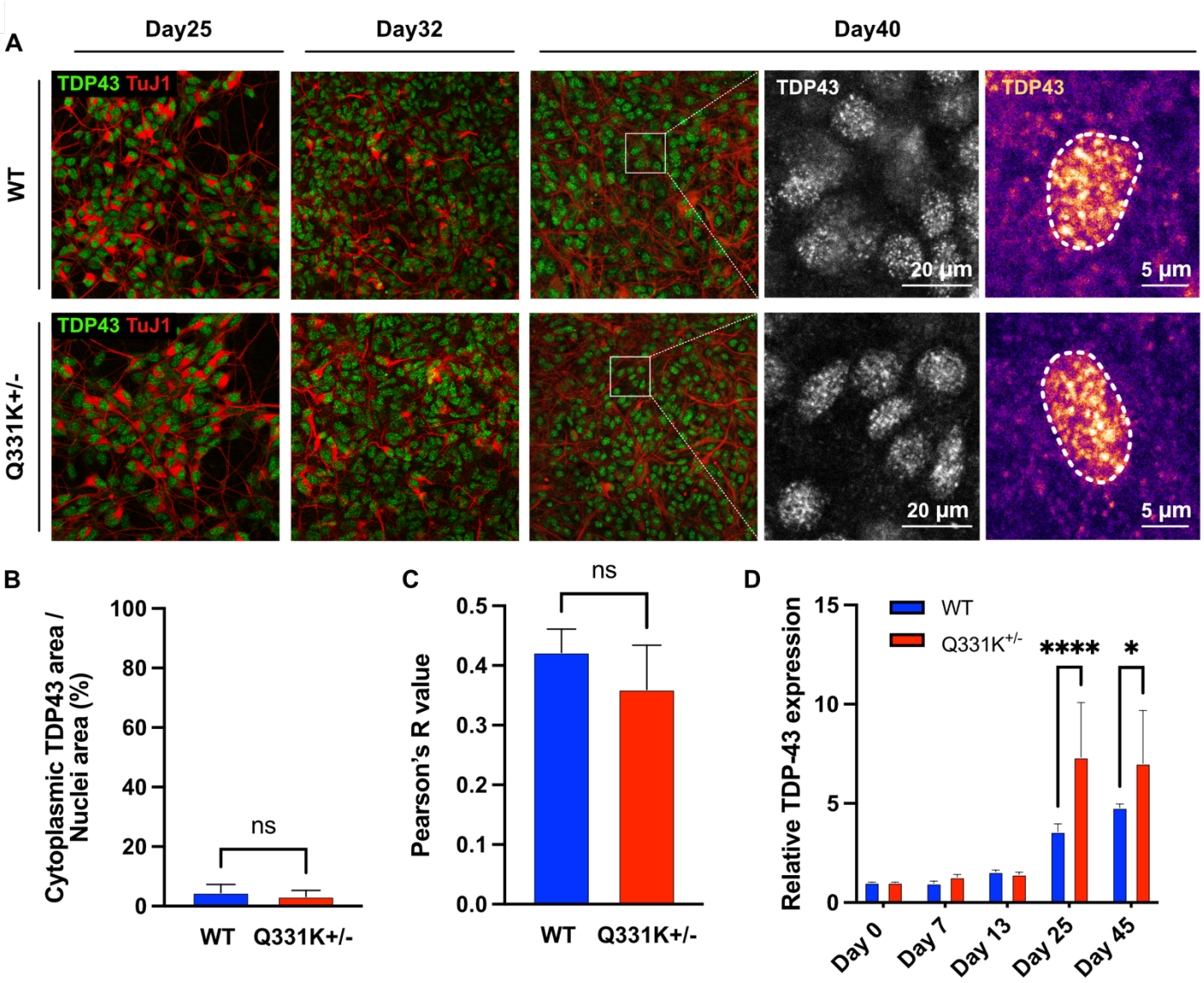

Figure 3.3 The TDP-43 expression pattern in WT and Q331K+/- iPSC-derived neurons. (A) The immunocytochemistry image of TDP-43 expression in WT and Q331K+/- mutant neurons at three different time points of differentiation. (B) The quantitative comparison of cytoplasmic TDP-43 allocation in WT and mutant neurons at day 40. (C) The quantified degree of co-localization for TDP-43 and DAPI expression in both groups at day 40 (D) The overall level of TDP-43 RNA (qPCR) at various developmental time points in both groups of neurons. In the presented data, error bars represent standard deviation, and *p<0.05, ****p<0.0001, ns not significant.

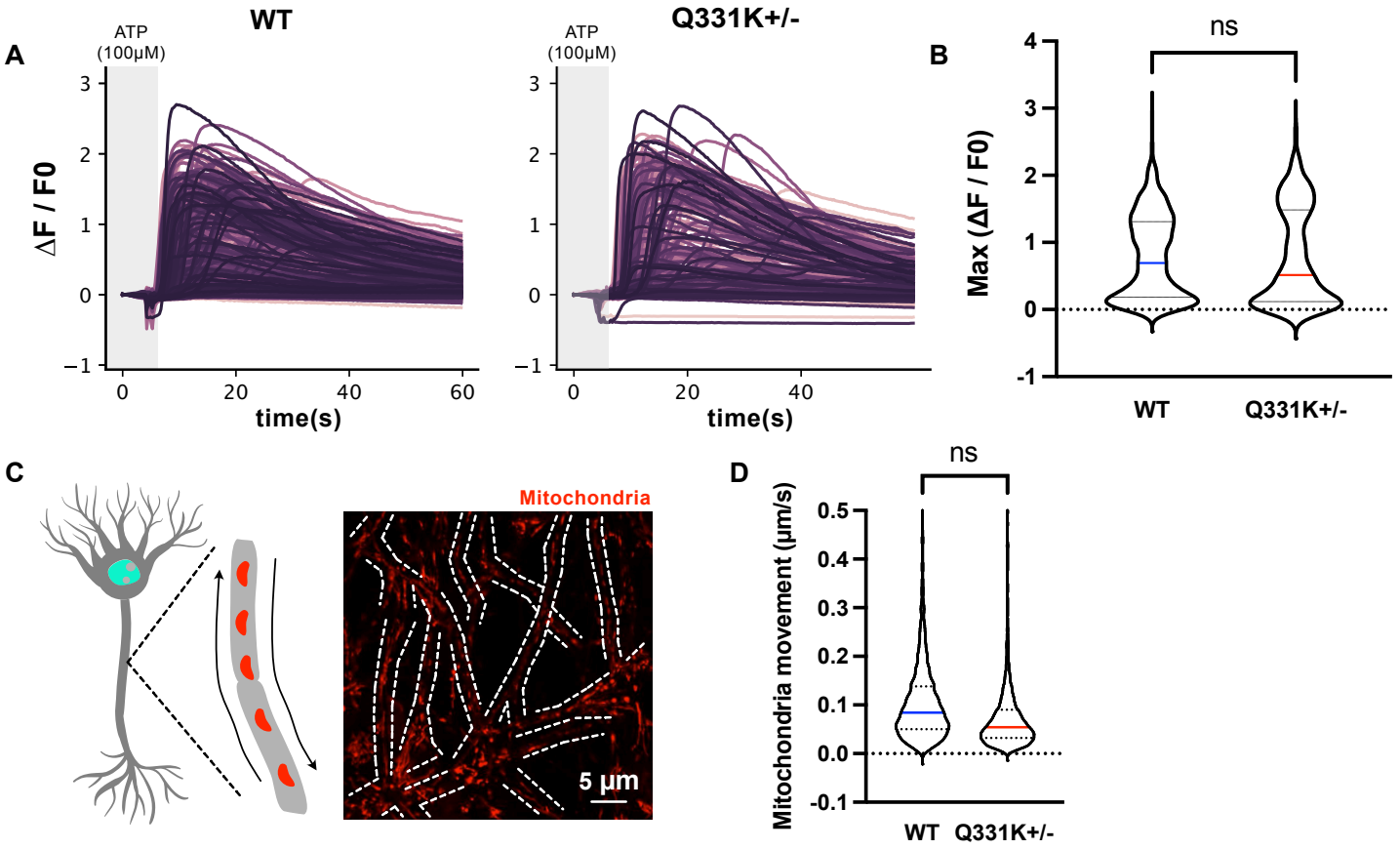

Figure 3.4 The comparison of intracellular calcium release and axonal mitochondria trafficking between WT and Q331K+/- mutant neurons at differentiation day 27. (A) The trace of fluorescence change recorded for individual cells upon exogenous ATP stimulation using Fluo-4. (B) The maximum fluorescence intensity changes under the ATP treatment in each group (C) Schematic and example fluorescence image of axonal mitochondria trafficking (D) Quantitative summary of mitochondria trafficking speed compared in each group. (ns not significant)

However, the electrophysiological functions of the neurons in each group were significantly different in terms of action potential firing rate, burst frequency, burst duration, and network burst frequency. The time-course MEA recordings with both groups of neurons all showed a gradual increase in the action potential firing frequency until day 30. However, the WT neurons showed a dramatic increase in firing frequency from day 31 whereas that of mutant neurons drew a plateau from the same time point. On the day of peak functionality, WT neurons showed significantly higher firing rates, a number of burst firings and their duration, and network burst firing frequencies than those of mutant neurons. **[Figure 3.5]**

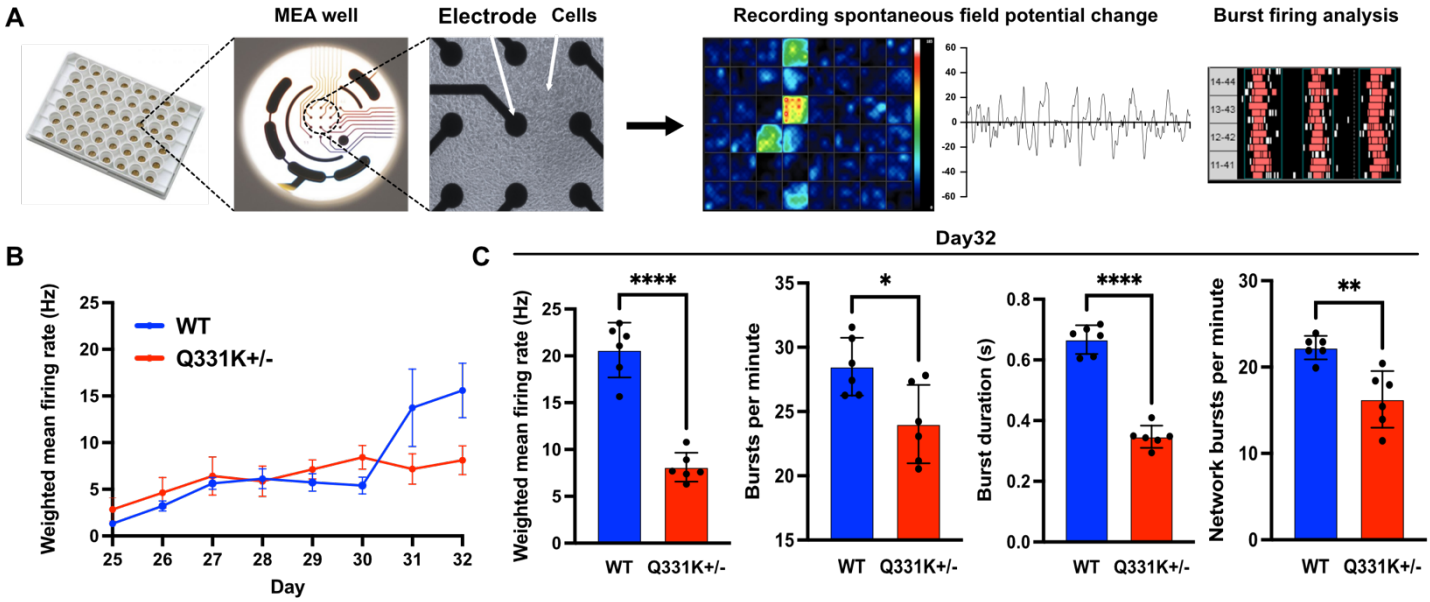

Figure 3.5 The electrophysiological function of WT and Q331K+/- neurons (A) Illustration of MEA experiment (B) Longitudinal comparison of action potential firing frequencies in WT and Q331K+/- neurons from day25 to day 32. (C) Side-by-side comparison of various aspect of electrophysiology of neurons in both groups at the day of peak functionality (Day32). In the presented data, error bars represent standard deviation, and *p<0.05, **p<0.005, ****p<0.0001.

3.4.3 Spinal astrocytes are successfully differentiated from WT and TDP43$^{Q331K+/-}$ iPSCs

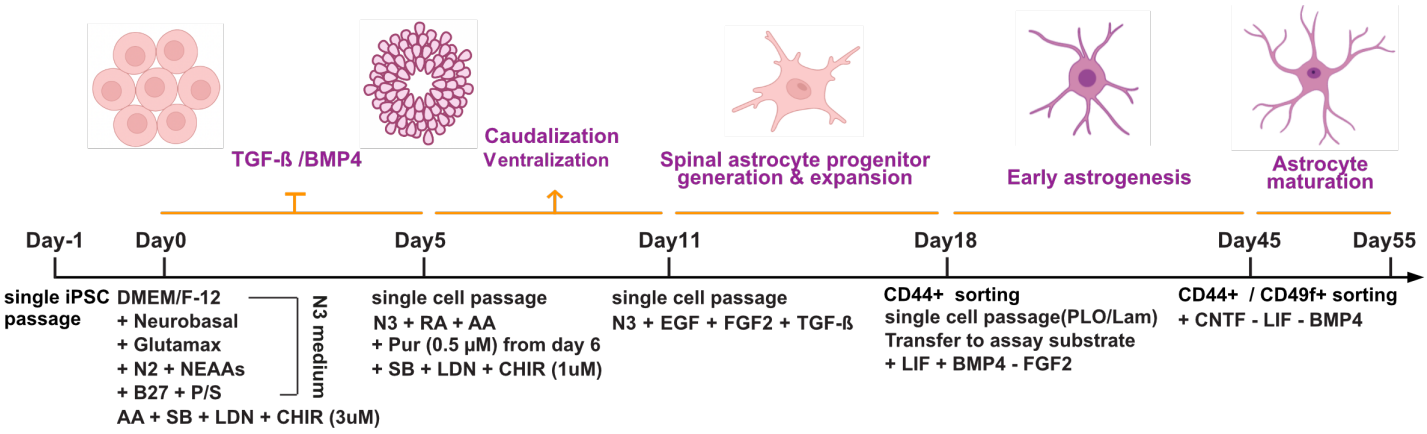

Figure 3.6 The spinal astrocyte differentiation scheme adapted from Tchieu *et al*

Human iPSC cultures (WT and TDP43$^{Q331K+/-}$) were differentiated into astrocytes by suppressing neurogenesis while activating spinal astrogenic transcription factors through a series of small molecules treatment. **[Figure 3.6]** The iPSCs were differentiated into regionally unspecified neural progenitors by day 11 using the same protocol for motor neuron differentiation, since the astrocytes and neurons share the same progenitors (neuroepithelial cells) at the early embryogenic stage. The progenitors in natural

environment are fate-restricted to differentiate into neurons and the rest of them proliferates for astrogenesis by turning on the gliogenic transcriptional switches (JAK-STAT pathway) while repressing pro-neural transcription factors after completing the neurogenic phase.[19–21] Thus, we followed their native developmental sequence by temporally optimizing the small molecule treatment scheme at each of the differentiation phases. From day 11 to day 18, the progenitors are expanded by treating fibroblast growth factor (FGF2) and epidermal growth factor (EGF) before inducing astrogenic transcriptions. The TGF-β was additionally treated at this phase, since the TGF-β was recently reported as an upstream activator to induce NF1A (Nuclear Factor 1A) gene expression which induces glial competency.[22] The study demonstrated a transient but not chronic expression of NF1A effectively increased the expression of glial specific cytoskeletal marker GFAP (Glial Fibrillary Acidic Protein) by temporarily lengthening the concomitant G1 phase. At day 18, the culture medium switched to astrocyte induction medium having LIF and BMP4 for daily feeding until day 24 passage. LIF is a cytokine in interleukin-6 family, secreted from neurons to help notch to turn on the JAK-STAT signal. BMP4 induces the formation of SMAD1-STAT3 transcription factor complex that transactivates the astrogenic genes such as STAT3, CD44, AMOG.[23] The cells at day 25 were sorted with antibodies against CD44 to remove neuronal population (CD44-) and further differentiate the CD44+ early astrogenic progenitors. The post-sorted cells were passaged every 6 days to maintain the initial density in culture. The CD44+ cells exhibited polarized morphology but a non-neuronal shape of cytoskeleton projection, characterized by a large cytoplasmic area with a protoplasmic shape. **[Figure 3.7A]**

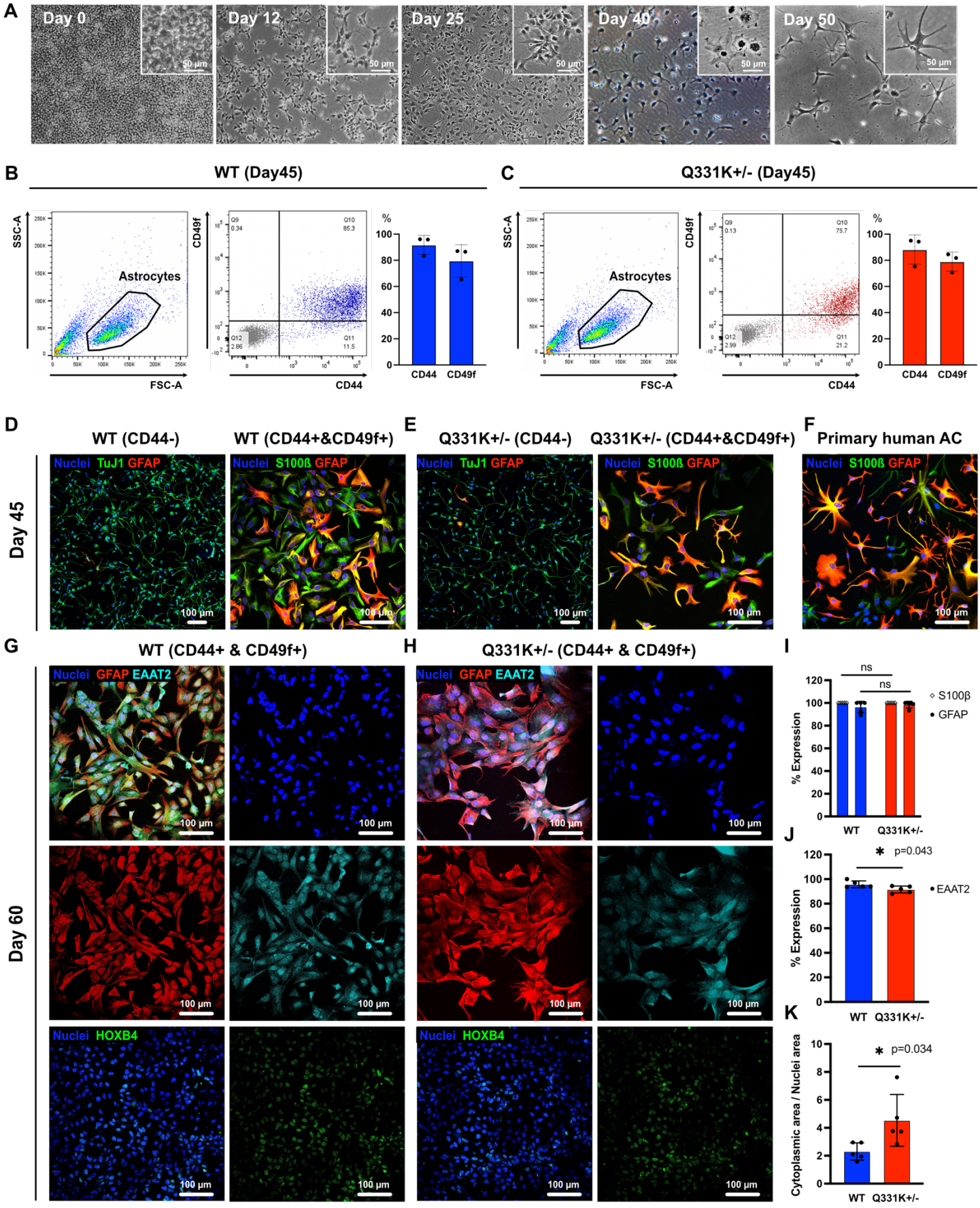
A
Day 0
Day 12
Day 25
Day 40
Day 50
50 µm
B
WT (Day45)
C
Q331K+/- (Day45)
SSC-A
FSC-A
Astrocytes
CD49f
CD44
Q9 0.34
Q10 85.3
Q12 2.86
Q11 11.5
Q9 0.13
Q10 75.7
Q12 2.99
Q11 21.2
%
CD44
CD49f
D
WT (CD44-)
WT (CD44+&CD49f+)
E
Q331K+/- (CD44-)
Q331K+/- (CD44+&CD49f+)
F
Primary human AC
Day 45
Nuclei TuJ1 GFAP
Nuclei S100ß GFAP
100 µm
G
WT (CD44+ & CD49f+)
H
Q331K+/- (CD44+ & CD49f+)
Day 60
Nuclei GFAP EAAT2
Nuclei HOXB4
I
ns
S100β
GFAP
% Expression
WT
Q331K+/-
J
* p=0.043
EAAT2
K
* p=0.034
Cytoplasmic area / Nuclei area

Figure 3.7 The identification of iPSC-derived astrocytes post live cell sorting (A) time course morphological change of differentiating astrocytes from day 0 to day 50 after sorting. FACS sorting result of (B) WT culture and (C) Q331K+/- mutant culture using antibodies against CD44 and CD49f. Difference in protein expression and morphology of CD44- cells with the CD44+ / CD49f+ astrocytes from (D) WT and (E) Q331K mutant iPSCs at day 45. (F) Reference image of primary human astrocytes stained against the same antibodies. Matured astrocyte marker and ventral spinal marker expression of (G) WT and (H) Q331K+/- culture at day 60. Quantification of (I) S100β, GFAP (J) EAAT2 expression and (K) cytoskeletal size comparison of the differentiated astrocytes in both groups. In the presented data, error bars represent standard deviation, and *p<0.05, ns not significant.

At day 45, the cells were sorted again with CD44 and CD49f antibodies which are integrin-binding proteins expressed on the early and late stage of astrocytes, respectively. Barbar *et al* demonstrated the CD49f to be exclusively expressed on matured astrocytes' surface but not on other glia or neurons through comprehensive single-cell RNA sequencing analysis.[24] The majority of day 45 cells in both WT and mutant groups expressed CD44 (>84%) and CD49f (>79%), verifying a successful differentiation of astrocytes despite having the mutation. **[Figure 3.7B, 3.7C]** The CD44+ and CD49f+ double positive cells were plated on the PLO/Laminin coated substrate for further maturation until the assay date. The plated cells showed apparent morphological differences with the CD44- cells of which majorities of the cell expressed neuronal marker βIII-tubulin (TuJ1). **[Figure 3.7D, 3.7E].** The CD44+ & CD49f+ cells at day 45 showed similar morphological development and heterogeneity with those of the primary human astrocytes **[Figure 3.7F]**. The astrocytes were further matured for 15 more days post-sorting, until reaching the stage of expressing Excitatory Amino Acid Transporter 2 (EAAT2). The majority of WT and Q331K+/- astrocytes expressed S100β and GFAP, which are calcium binding protein expressed from early astrocyte progenitors and intermediate filament protein expressed from the later stage of astrogenesis, respectively **[Figure 3.7G, 3.7H, 3.7I]**. The uniform expression of HOXB4 in their nuclei further verified the ventral spinal identity of the sorted cells **[Figure 3.7G, 3.7H]**. The percentage of cells expressing EAAT2 in WT astrocytes was higher than that in mutant astrocytes on the same day, implying the extracellular glutamate uptake function might be compromised via the Q331K +/- mutation in astrocytes.**[Figure 3.7G, 3.7H, 3.7J]** Additionally, GFAP-stained cytoskeletal area of mutant astrocytes was larger than that of normal astrocytes **[Figure 3.7K]**, which agrees with

previous findings that various ALS-patient-derived astrocytes have hypertrophic phenotypes in common.[25]

3.4.4 Electrophysiological function of neurons are affected by the co-cultured astrocytes in unexpected way

Next, we sought to compare the electrophysiological function of neurons under the presence of WT and Q331K+/- mutant astrocytes. We generated 4 pairs of astrocyte/neuron co-culture (WT MN + WT AC, WT MN + mutant AC, mutant MN + WT AC, mutant MN + mutant AC) by adding day 45 astrocytes to the same number of motor neurons plated on the MEA wells on the differentiation day 25 which is after their neurogenic phase, and daily recorded the firing behavior of neurons for 10 days. Unlike the hypothesis we made, the WT astrocytes did not improve the electrophysiological function of WT neurons, rather decreasing the firing frequency, and Q331K+/- mutant astrocytes showed a similar effect on the firing frequency of WT neurons. **[Figure 3.8A]** Conversely, the mutant neurons which were initially compromised on their firing function presumably due to the downstream effect of TARDBP mutation showed an increasing pattern of the firing frequency when cultured with both groups of astrocytes, regardless of their genotypes. **[Figure 3.8B]** On the final day of recording, this trend was more obvious showing that the neuronal firing frequency was not affected by the mutation status of astrocytes. In both groups of neurons, adding WT and mutant astrocytes induced a similar trend of firing frequency change, implying the response to the astrocytic input is highly regulated by the intrinsic mutation of neurons. **[Figure 3.8C, 3.8D]** However, it is unclear why the addition of normal astrocytes impairs the firing function of WT neurons, and the reason for the functional improvement of mutant neurons after co-culturing with mutant astrocytes. We will discuss more of the possible reasons for this counterintuitive observation in the following discussion section.

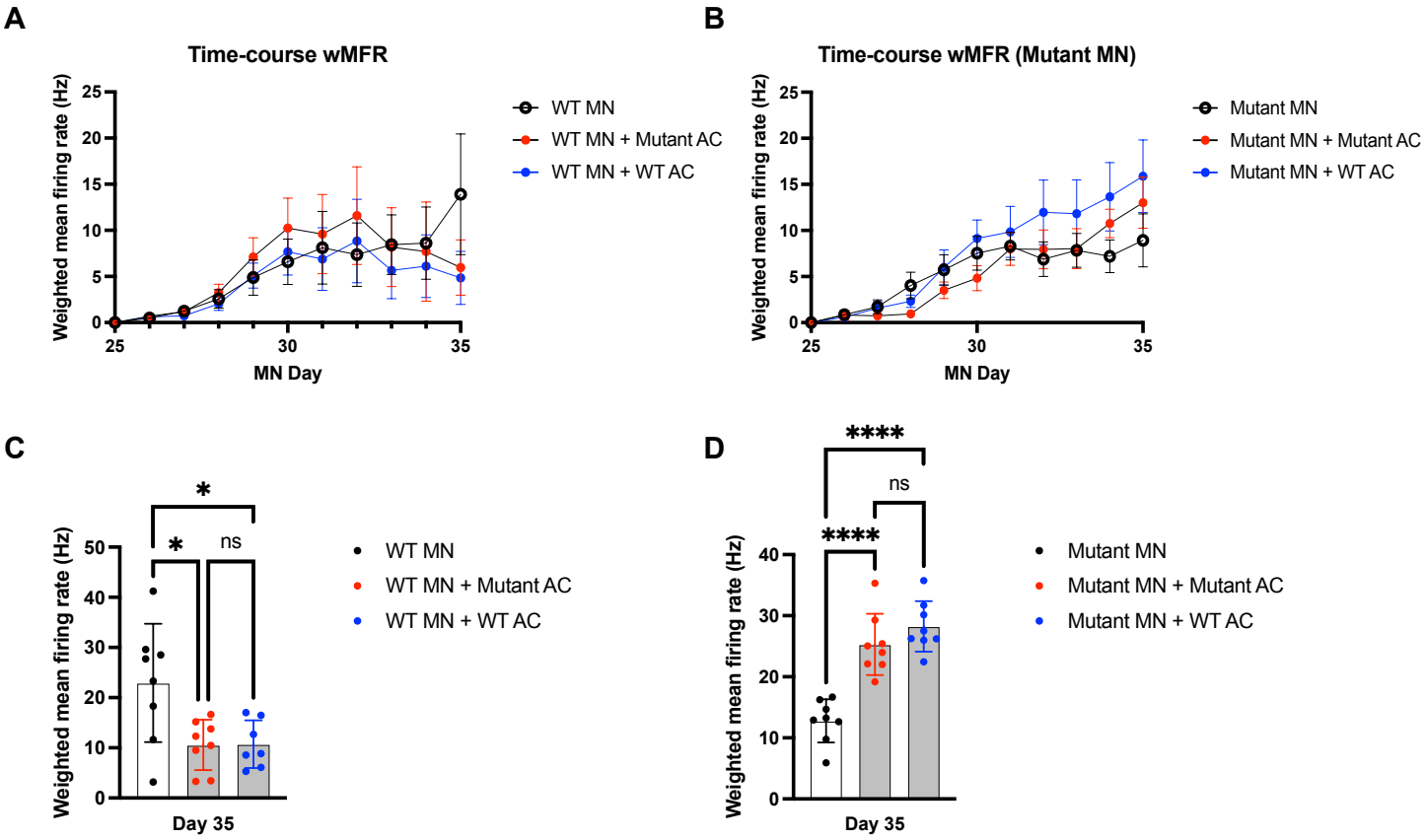

Figure 3.8 The electrophysiological function of WT and Q331K+/- neurons after astrocyte addition The representative trace of time-course mean firing rate change of WT motor neurons with WT and mutant astrocyte co-culture **(A)** and mutant motor neurons with the same set of astrocyte co-culture **(B)**. The consolidated data of the neuronal firing frequency at the last day of the MEA assay for three batches of experiment for WT motor neurons **(C)** and mutant motor neurons **(D)**. In the presented data, error bars represent standard deviation, and *p<0.05, ****p<0.0001, ns not significant.

3.5 Discussion

The WTC11 iPSCs developed and shared by Bruce Conklin's group (Gladstone Institute, CA) were used to generate normal ventral spinal neurons and isogenic astrocytes. For ventral spinal neuron differentiation, the iPSCs were treated with a series of induction mediums containing morphogens for driving neural progenitors followed by adding ventralizing and caudalizing factors at the defined temporal window for specifically priming progenitor cells into the desired lineage of neurons. The homogeneous expression of Nestin and PAX6 on day 18 cells confirmed the successful generation of regionally unspecified neural progenitors with a minimal amount of contaminating cells from different germ layers. Also, the culture was highly enriched with the neural rosettes by day 12-15, resembling

the early neural tube formation *in vivo* spinal cord development. The day 18 passaged cells were further treated with neural maturation factors until the homogeneity assessment via flow cytometry on day 25 with antibodies against CD271 (P75NTR) and CD44. CD271 is a transmembrane neurotrophin receptor protein enriched on neurons, for which the downstream signals control the neuronal differentiation, growth, and death during their life cycle.[26] CD44 is a hyaluronic binding transmembrane receptor protein that works for cell-surface adhesion, known to be minimally expressed on neurons but highly on the differentiating glia.[27–29] Both WT and mutant cells were highly expressing CD271 (80~83%) whereas CD44 expression was negligible, demonstrating the enrichment of neuron population in the day 25 culture. The motor neuron-specific transcriptional factor Islet-1 was partially expressed on the neurons in both groups, indicating the possible inclusion of ventral interneurons in the cultures, though more detailed subpopulation analysis is required. In spite of having a pure population of neurons by day 25 of culture, a small number of non-neuronal cells in both groups gradually proliferated to form a mixed culture with the post-mitotic neurons around day 40.

We next analyzed the TDP-43 expression pattern to investigate whether the mutation in the TARDBP gene causes cytoplasmic aggregation of the TDP-43 in neurons. The cultures at day 25,32,40 were fixed and stained against human TDP-43 protein and quantified their cytoplasmic protein expression in both groups. Additionally, we have compared their TDP-43 mRNA expression level at multiple time points to compare the overall TARDBP gene transcription level throughout their development. Surprisingly, we did not observe an evident difference in the expression pattern of the TDP-43 between the WT and Q331K+/- mutant cells and both of their TDP-43 were well localized in the nuclei at all assay time points. This indicates that the misallocation and/or aggregation of the TDP-43 observed in the post-mortem tissue of ALS patients may not be driven by the inherent mutation in neurons but needs an extracellular trigger to turn on the pathologic signal. Since the numbers of evidence verified that cytoplasmic TDP-43 inclusion is a pathogenic factor rather than merely a downstream disease phenotype, it is critical to elucidate specific non-neuron autonomous preconditions

deriving their TDP-43 proteinopathy. Interestingly, the absolute amount of TDP-43 transcript in mutant cells post-differentiation was significantly larger than WT, in contrast to the similarities in the protein localization pattern. This might be due to the compensation mechanism of the impaired gene to quantitatively make up the deficiency of protein activity but more studies are required to understand this aberrantly elevated level of the TARDBP transcript in mutant cells.

Next, the functionalities of the differentiated neurons in both groups were evaluated by the MEA experiment. We daily recorded their spontaneous field potential traces from day 25 to 32 upon continuous ionic stimulation naturally occurring inside of the culture medium. Both of the cultures were able to fire comparable action potentials with mean firing frequencies of 5~7 Hz by day 30 but the mean firing rate of WT neurons outpaced the mutant neurons distinctively from day 31. The electrophysiology of the day32 WT and mutant cultures exhibited apparent differences in terms of individual firing frequency, burst firing frequency, burst duration, and network burst firing frequency which measures the interneural signaling abilities in culture. The result suggests that the TDP-43 mutation in neurons *per se* could affect their electrophysiological function, implying an extensive downstream effect of having a mutation in RNA binding protein.

We sought to understand how their baseline function could be affected by the astrocytic input. For astrocyte differentiation, we utilized the spinal neuron differentiation protocol for generating regionally unspecified progenitors based on the fact that the spinal astrocytes are generated from the same progenitors with neurons. To optimize the astrogenesis process, we have tested a diverse morphogen treatment scheme with varying conditions including sequence and duration of astrogenic factors (LIF, BMP4, TGF-β, CNTF) addition and treating concentration. The final protocol was established based on the result of CD49f and CD44 protein expression %, which was proven to effectively discriminates the astrocytes from other glia and neurons. CD49f is a laminin-binding protein, recently discovered as a novel astrocyte marker by Barbar *et al*.[24] The authors showed negligible expression of the surface protein in immature astrocytes, oligodendrocytes and neurons, but

exclusively on matured astrocytes. As mentioned, CD44 is an effective surface marker to sort glial cells from heterogeneous neuroglial culture, since the protein is enriched on the glial cell membrane but not on neurons. We have used both protein markers to evaluate the differentiation status as well as selectively sort differentiated astrocytes for the downstream experiments. The consistent FACS result of over 80% of CD49f and CD44 positivity in day 45 culture verified the successful induction of astrocytes by the time.

The similar expression level of both surface markers and S100β, GFAP, HOXB4 in WT and Q331K+/- mutant culture demonstrated the mutation does not significantly hinder ventral spinal astrogenesis. However, since fewer of the mutant astrocytes expressed EAAT2 than WT astrocytes, one of the downstream phenotypes of TDP-43 mutation might be the damaged extracellular glutamate clearing ability. Additionally, the cell body size of mutant astrocytes was significantly larger than that of WT cells, which agrees with the previous observations of hypertrophic astrocytes explanted from neurodegenerative animal tissue.[25] To analyze more comprehensive downstream phenotypes of TDP-43 mutation in astrocytes, functional assessment such as intracellular calcium release, extracellular glutamate absorption, and clearance of reactive oxygen species along with the side-by-side transcriptomic comparison of mutant astrocytes with WT counterparts are required.

Lastly, we co-cultured the differentiated motor neurons with astrocytes, both for WT and Q331K+/- mutant group to investigate how the astrocyte addition alters neuronal electrophysiology. We hypothesized that the normal astrocytes will increase the firing rate of co-cultured WT and mutant neurons, whereas mutant astrocytes exert the opposite effect. However, the MEA analysis showed the modality of the response to the astrocyte addition was more dependent on the mutation status of neurons. WT motor neurons showed an impaired firing function under the effect of astrocytes regardless of their mutation status. Conversely, mutant motor neurons showed an increasing trend of firing function with both WT and mutant astrocytes. This unexpected result might be attributed to the insufficient maturity of iPSC-derived astrocytes, since the canonical markers we used for cell type

identification are unable to tell us whether they are ready to interact with neurons, although this hypothesis still cannot fully explain the opposing trend of firing behavior in WT and mutant neurons with astrocytes. Another possible reason is the unoptimized co-culture condition (e.g. medium composition, neuron to astrocyte ratio co-culture timing for each cell type, feeding cycle) since culture condition could dominate the neuron's physiology and mask the astrocytic input. Thus, it is necessary to verify whether the electrophysiological outcome came from neuroglial interaction or any other extrinsic factor(s) before making a conclusion about this study.

3.6 Conclusion

In this study, we successfully differentiated spinal motor neurons and astrocytes from both WT and Q331K+/- mutant iPSC cultures, using protocols adapted from the recent literature. The WT and mutant motor neurons showed a comparable phenotype in terms of TDP-43 expression, intracellular calcium flux, and axonal trafficking of mitochondria but a significant difference in electrophysiological function. The WT motor neurons showed much more frequent spontaneous firing than the mutant group, implying the potential pathologic role of TARDBP mutation in ion channel misregulation. The differentiated astrocytes from both groups of iPSCs also showed phenotypic differences in protein expression and morphology. However, the neuroglial co-culture experiment showed that neurons' functional response to the astrocyte addition was more affected by neurons' intrinsic mutation status, rather than that of astrocytes. Both groups of astrocytes decreased the firing frequency of WT motor neurons, but increased the firing frequency of the mutant motor neurons. To understand the underlying physiology of this unexpected result, it is necessary to compare the gene expression profile of adult primary astrocytes to that of iPSC-astrocytes to understand if they are ready to regulate the nearby neurons. Moreover, the optimization process of the neuroglial co-culture experiment is required to more accurately recapitulate their physiological interaction *in vivo*.

3.7 Reference

1. Nagai, M. *et al.* Astrocytes expressing ALS-linked mutated SOD1 release factors selectively toxic to motor neurons. *Nature Neuroscience* **10**, 615–622 (2007).
2. Tripathi, P. *et al.* Reactive Astrocytes Promote ALS-like Degeneration and Intracellular Protein Aggregation in Human Motor Neurons by Disrupting Autophagy through TGF-β1. *Stem Cell Reports* **9**, 667–680 (2017).
3. Tong, J. *et al.* Expression of ALS-linked TDP-43 mutant in astrocytes causes non-cell-autonomous motor neuron death in rats. *EMBO Journal* **32**, 1917–1926 (2013).
4. Phatnani, H. P. *et al.* Intricate interplay between astrocytes and motor neurons in ALS. *Proceedings of the National Academy of Sciences of the United States of America* **110**, (2013).
5. Yamanaka, K. & Komine, O. The multi-dimensional roles of astrocytes in ALS. *Neuroscience Research* vol. 126 31–38 (2018).
6. Izrael, M., Slutsky, S. G. & Revel, M. Rising Stars: Astrocytes as a Therapeutic Target for ALS Disease. *Frontiers in Neuroscience* vol. 14 (2020).
7. Hall, C. E. *et al.* Progressive Motor Neuron Pathology and the Role of Astrocytes in a Human Stem Cell Model of VCP-Related ALS. *Cell Reports* **19**, 1739–1749 (2017).
8. Guttenplan, K. A. *et al.* Knockout of reactive astrocyte activating factors slows disease progression in an ALS mouse model. *Nature Communications* **11**, (2020).
9. Pansarasa, O. *et al.* Sod1 in amyotrophic lateral sclerosis: “ambivalent” behavior connected to the disease. *International Journal of Molecular Sciences* **19**, 1–13 (2018).
10. Wang, W. *et al.* The inhibition of TDP-43 mitochondrial localization blocks its neuronal toxicity. *Nature Medicine* **22**, 869–878 (2016).
11. Parkin, G. M., Udawela, M., Gibbons, A. & Dean, B. Glutamate transporters, EAAT1 and EAAT2, are potentially important in the pathophysiology and treatment of schizophrenia and affective disorders. *World Journal of Psychiatry* **8**, 51–63 (2018).
12. Guttenplan, K. A. *et al.* Knockout of reactive astrocyte activating factors slows disease progression in an ALS mouse model. *Nature Communications* **11**, (2020).
13. Walker, A. K. *et al.* ALS-associated TDP-43 induces endoplasmic reticulum stress, which drives cytoplasmic TDP-43 accumulation and stress granule formation. *PLoS ONE* **8**, (2013).
14. Xu, Z. S. Does a loss of TDP-43 function cause neurodegeneration? *Molecular Neurodegeneration* **7**, 1 (2012).
15. Suk, T. R. & Rousseaux, M. W. C. The role of TDP-43 mislocalization in amyotrophic lateral sclerosis. *Molecular Neurodegeneration* vol. 15 (2020).
16. Smith, A. S. T. *et al.* Human Induced Pluripotent Stem Cell-Derived TDP-43 Mutant Neurons Exhibit Consistent Functional Phenotypes Across Multiple Gene Edited Lines Despite Transcriptomic and Splicing Discrepancies. *Frontiers in Cell and Developmental Biology* **9**, (2021).
17. Du, Z. W. *et al.* Generation and expansion of highly pure motor neuron progenitors from human pluripotent stem cells. *Nature Communications* **6**, (2015).
18. Amoroso, M. W. *et al.* Accelerated high-yield generation of limb-innervating motor neurons from human stem cells. *Journal of Neuroscience* **33**, 574–586 (2013).

19. TCW, J. *et al.* An Efficient Platform for Astrocyte Differentiation from Human Induced Pluripotent Stem Cells. *Stem Cell Reports* **9**, 600–614 (2017).

20. Chandrasekaran, A., Avci, H. X., Leist, M., Kobolák, J. & Dinnyés, A. Astrocyte differentiation of human pluripotent stem cells: New tools for neurological disorder research. *Frontiers in Cellular Neuroscience* vol. 10 (2016).

21. Magistri, M. *et al.* A comparative transcriptomic analysis of astrocytes differentiation from human neural progenitor cells. *European Journal of Neuroscience* **44**, 2858–2870 (2016).

22. Tchieu, J. *et al.* NFIA is a gliogenic switch enabling rapid derivation of functional human astrocytes from pluripotent stem cells. *Nature Biotechnology* **37**, 267–275 (2019).

23. Fukuda, S. *et al.* Potentiation of Astrogliogenesis by STAT3-Mediated Activation of Bone Morphogenetic Protein-Smad Signaling in Neural Stem Cells. *Molecular and Cellular Biology* **27**, 4931–4937 (2007).

24. Barbar, L. *et al.* CD49f Is a Novel Marker of Functional and Reactive Human iPSC-Derived Astrocytes. *Neuron* **107**, 436-453.e12 (2020).

25. Li, K., Li, J., Zheng, J. & Qin, S. Reactive astrocytes in neurodegenerative diseases. *Aging and Disease* vol. 10 664–675 (2019).

26. Sajanti, A. *et al.* A comprehensive p75 neurotrophin receptor gene network and pathway analyses identifying new target genes. *Scientific Reports* **10**, (2020).

27. Cai, N., Kurachi, M., Shibasaki, K., Okano-Uchida, T. & Ishizaki, Y. CD44-positive cells are candidates for astrocyte precursor cells in developing mouse cerebellum. *Cerebellum* **11**, 181–193 (2012).

28. Liu, Y. *et al.* CD44 expression identifies astrocyte-restricted precursor cells. *Developmental Biology* **276**, 31–46 (2004).

29. Naruse, M., Shibasaki, K., Yokoyama, S., Kurachi, M. & Ishizaki, Y. Dynamic Changes of CD44 Expression from Progenitors to Subpopulations of Astrocytes and Neurons in Developing Cerebellum. *PLoS ONE* **8**, (2013).

Chapter 4. The Pathologic Role of IFNγ-induced Neuroinflammation on ALS Development

- This chapter has been published in the following manuscript

Changho Chun, Jung Hyun Lee, Mark Bothwell, Paul Nghiem, Alec S.T. Smith* and David L. Mack*, **'Interferon-γ Elicits Pathological Hallmarks of ALS in Human Motor Neurons'** *BioRxive* (2022)

4.1 Abstract

Neuroinflammation is an established factor contributing to amyotrophic lateral sclerosis (ALS) pathology, implicating the possible detrimental effects of inflammatory cytokines to motor neurons. The RNA/DNA-binding protein TDP-43 has emerged as a pivotal actor in ALS, because TDP-43 mutations cause familial ALS and loss of nuclear TDP-43, associated with its redistribution into cytoplasmic aggregates (TDP-43 proteinopathy), in motor neurons occurs in 97% of ALS cases. However, mechanisms linking neuroinflammation to TDP-43 mis-localization have not been described. Programmed death-ligand 1 (PD-L1) is an immune-modulatory protein, highly expressed on cell surfaces following acute inflammatory stress. To determine which inflammatory cytokines might impact motor neuron function, seven cytokines known to be elevated in ALS patients' cerebrospinal fluid were tested for their effects on PD-L1 expression in human iPSC-derived motor neurons. Among the tested cytokines, only interferon-**γ** (IFN-**γ**) was found to strongly promote PD-L1 expression. Thus, we hypothesized that excessive exposure to IFN-**γ** may contribute to motor neuron degeneration in ALS. We observed that neuronal populations exposed to IFN-**γ** exhibited severe TDP-43 cytoplasmic aggregation and excitotoxic behavior correlated with impaired neural firing activity, hallmarks of ALS pathology, in both normal and ALS mutant ($TARDBP^{Q331K+/-}$) neurons. Single-cell RNA sequencing revealed possible mechanisms for these effects. Motor neurons exposed to IFN-**γ** exhibited an extensive shift of their gene expression profile toward a neurodegenerative phenotype. Notably, IFN-**γ** treatment induced aberrant expression levels for 70 genes that are listed in the recent literature as being dysregulated in ALS. Additionally, we found that genes related to neuronal electrophysiology, protein aggregation, and TDP-43 mis-regulation were abnormally expressed in IFN-**γ** treated cells. Moreover, IFN-**γ** induced a significant reduction in the expression of genes that encode indispensable proteins for neuromuscular synapse development and maintenance, implying that cytokine

exposure could directly impair signal transmission between motor axons and muscle membranes. Our findings suggest that IFN-**γ** could be a potent upstream pathogenic driver of ALS and provide potential candidates for future therapeutic targets to treat sporadic forms of ALS, which account for roughly 90% of reported cases.

4.2 Introduction

Amyotrophic lateral sclerosis (ALS) is a neurodegenerative disease that primarily attacks motor neurons, leading to progressive and ultimately fatal denervation of skeletal muscle throughout the body. Familial mutations are implicated as the cause for roughly 10% of ALS cases, while the pathologic origin of the other 90% remains unclear.[1,2] Drugs currently approved for use in ALS patients in the USA and/or Europe prolong patients' lives by only a few months, leaving the disease intractable.[1] Most patients do not develop neuromuscular symptoms until their 50s or 60s, regardless of the cause. However, the disease progresses rapidly once patients become symptomatic, with the average life expectancy of patients reported as less than 5 years after symptom onset.[1,2]

A common pathologic feature of ALS is dysfunction of the RNA/DNA-binding protein, TDP-43. It has been suggested that TDP-43 plays a central, but poorly understood, role in ALS etiology since mutations of the gene encoding TDP-43, TARDBP, segregate with disease in some cases of familial ALS, and loss of nuclear TDP-43, associated with aberrant cytoplasmic accumulation of TDP-43 aggregates, is present in 97% of both familial and non-familial forms of ALS.[3–5]

Neuroinflammation is known to be a major factor in ALS progression and inflammatory cytokine action may switch from a neuroprotective to a neurotoxic role as the disease develops.[6–8] Although previous studies have shown that activated peripheral immunity could acutely damage motor neurons' survival and function, the molecular drivers of inflammatory stress and the following neurodegenerative consequences in neurons are unclear.[7,9–12] To assess the capacity of motor neurons to respond to various neuroinflammatory cytokines, we examined their effects on expression of Programmed death-ligand 1 (PD-L1), a cell surface protein, that is highly expressed by many cell types in response to exposure to a variety of inflammatory cytokines. PD-L1 plays a key role in immune escape by activating its cognate receptor, PD-1 on immune cells.[13] We, therefore, investigated the influence of pro-inflammatory cytokines, known to be increased in ALS patients' cerebrospinal fluid, on expression levels of PD-L1. We used both WT and ALS mutant ($TARDBP^{Q331K+/-}$) iPSC-derived motor neurons for the cytokine screening assay, to compare their response.

We showed that interferon-**γ** (IFN-**γ**), was the only cytokine, among those tested, that strongly promotes neuronal PD-L1 expression in both groups. Although IFN-**γ** contributes to normal brain development and has been suggested to influence neurodevelopmental disorders such as autism and schizophrenia,[14] a role for IFN-

γ in ALS etiology has not been explored. Importantly, we report that IFN-**γ** treated motor neurons in both normal and TARDBP$^{Q331K+/-}$ groups recapitulated pathologic hallmarks of ALS, such as hyperexcitation followed by loss of neuronal firing ability and cytoplasmic aggregation of TDP-43.

In order to reveal mechanisms that might mediate the effects of IFN-**γ** exposure and TARDBP$^{Q331K+/-}$ genotype on motor neuron ALS pathophysiology, we employed single-cell RNA sequencing to identify genes that are differentially expressed in response to IFN-**γ** exposure or TARDBP mutation, individually or in concert. The results of our transcriptomic analysis suggest that IFN-**γ** could be a potent neurodegenerative cue to induce ALS pathogenic processes and reveal possible mechanisms linking IFN-**γ** exposure to TDP-43 proteinopathy. Collectively, our findings suggest that compounds capable of inhibiting IFN-**γ**-mediated signaling in neurons may constitute promising targets for future immunotherapeutic drugs to prevent the progression of neurodegeneration in both familial and sporadic forms of ALS.

4.3 Materials and Methods

4.3.1 Maintenance of human iPSC lines

WTC11 (WT, Q331K+/-) iPSCs were frozen in mFreSR medium (Stem Cell Technologies) and stored under cryogenic conditions in liquid nitrogen. 10 cm dishes were treated with Matrigel (Thermo Fisher Scientific) diluted 1 to 60 in DMEM/F12 medium (Thermo Fisher Scientific) and incubated at 37^{o}C/ 5% CO_2 overnight. On the day of plating, vials of cells were removed from liquid nitrogen storage and incubated in a 37^{o}C water bath for 3 minutes. The content of the vial (1 mL) was then transferred to a 15 mL centrifuge tube and centrifuged for 3 minutes at 300 g. The supernatant was aspirated and cells were resuspended in fresh mTeSR (Stem Cell Technologies) supplemented with 10 μM Y-27632 (Thermo Fisher Scientific), a specific inhibitor of Rho kinase activity. Prepared Matrigel plates were then aspirated, washed with PBS containing Ca^{2+} and Mg^{2+} (Thermo Fisher Scientific), and the cell suspension was then plated evenly over the prepared culture surface. Y-27632 was removed from the culture medium the first day after plating and cells were fed daily with fresh mTeSR from then on. Cells were incubated at 37^{o}C/ 5% CO_2 until iPSC colonies filled the field of view when visualized using an

Eclipse TS100 microscope (Nikon) fitted with a 10X lens. At this point, medium was aspirated and replaced with TrypLE 1x solution (Invitrogen), incubated in 37°C/ 5% CO_2 for 5 minutes. The detached cell colonies were dissociated with gentle trituration with P1000 pipette, followed by adding the same volume of PBS with calcium and magnesium. The cell suspension was spun down and resuspended in fresh mTeSR with mild trituration to gently break up cell clusters. The cell suspension was then split across the desired number of Matrigel-coated plates and returned to the incubator. During continued culture, any iPSC colonies displaying irregular boundaries, significant space between cells or low nuclear to cytoplasmic ratios were carefully marked and removed from culture using a fire-polished, sterile glass pipette.

4.3.2 Differentiation of iPSCs into ventrospinal motor neurons

Human iPSCs were passaged onto Matrigel-coated 6-well plates as described above and incubated at 37°C/ 5% CO_2 in mTeSR until they reached ~50% confluency. At this point, cultures were differentiated into regionally unspecified neural progenitor cells using a monolayer differentiation method. Briefly, the undifferentiated day0 cells were treated with dual-SMAD inhibitors, SB431532 and LDN193189, as well as ascorbic acid (AA). CHIR99021 was added to the medium for the purpose of activating the Wnt pathway, which has been proven to enhance neuroepithelial differentiation and proliferation. At day 5, cultures were treated with All-trans retinoic acid (RA) for caudalization and the SHH agonist Purmorphamine, to give ventralization cues to the cells. On day 11, cells were passaged onto fresh Matrigel coated 6-well plates and treated with RA and AA until day 18 to expand the neural progenitor population. These cells were then passaged at 100,000 cells/ cm^2 onto 0.01% poly-L-ornithine (Sigma-Aldrich) and 5 µg/mL laminin (Sigma-Aldrich)-coated surfaces and exposed to culture conditions promoting motor neuron differentiation. Specifically, cells were fed with 10 ng/mL of neurotrophic factors (BDNF, GDNF, IGF-1 from R&D systems, NT3 from Stem Cell Technologies), ascorbic acid (2.27 µM). During all stages of differentiation, a basal medium consisting of a 1:1 mix of Neurobasal medium and DMEM/F12, supplemented with B27, Glutamax, N2, Non-essential amino

acids, and penicillin-streptomycin, was used. All cells used in the described experiments were differentiated from WTC11 colonies between passages 45 and 55.

4.3.3 Cytokine treatment

WT and TARDBP$^{Q331K+/-}$ mutant iPSC-derived neurons were exposed to 7 different cytokines, treated from day 23 to day 25 of the ventrospinal neuron differentiation method described above. Recombinant human and mouse IFNα, IFNγ, IL-4, IL-6, IL-1β, IL-17, and TNF-α were used at concentrations depicted in Figure 1B. All of the cytokines were purchased from R&D Systems.

4.3.4 Co-culture of CD8+ T cells and iPSC-derived motor neurons

Whole blood was collected into 10 mL BD Vacutainer Plastic Collection Tubes with Sodium Heparin and inverted multiple times. To isolate PBMCs, whole blood was gently layered over a double volume of Ficoll in a Falcon tube and centrifuged for 30-40 minutes at 400g without a brake. Four layers formed, each containing different cell types - the uppermost layer contained plasma, which was removed by pipetting. The second layer contained PBMCs and these cells were gently removed using a pipette and added to PBS to wash off any remaining platelets. The pelleted cells were then counted and the percentage viability estimated using Trypan blue staining. A 96 well cell culture plate was coated with a CD3-specific Ab (OKT3, eBioscience for human T cells) and 5 μg/mL concentrations of PD-L1-Ig for control experiments. For co-culture of CD8$^+$ T cells and iPS derived motor neurons, the culture plate was coated with poly-L-ornithine, laminin, and a CD3-specific Ab sequentially. Human CD8$^+$ T cells were purified from PBMCs freshly isolated from whole blood using CD8a$^+$ T cell isolation kit II, human (Miltenyi Biotec.). Purity was confirmed to be over 90 % by flow cytometry. The T cells were labeled with 1μM CFSE, quenched by cold FBS, and incubated in plates coated with CD3-specific Ab. Human iPSC-derived neurons were cocultured with CD8$^+$ T cells purified from PBMCs at a 1:1 ratio (Neurons : CD8$^+$ T cells) for 5 days in culture medium with CD3 stimulation. On day 5 after stimulation, cells were stained with an Ab against CD8-APC and then analyzed for CFSE dilution by flow cytometry.

4.3.5 Flow cytometry

The following antibodies were used for flow cytometry analysis: PD-L1 (29E.2A3, BioLegend), CD44 (C44Mab-5, BioLegend), and CD8 (SK1, BioLegend). The stained cells were analyzed using a BD FACS Calibur flow cytometer. For each sample, 10,000 events were recorded and histograms were plotted. The percentages of cells were calculated using FlowJo software (Treestar, Ashland, OR).

4.3.6 Immunocytochemistry

Cells were fixed in 4% paraformaldehyde for 15 minutes and permeabilized in 0.2% Triton-x solution, followed by blocking with 5% goat serum in PBS for 1 hour at room temperature. Cells were then incubated with primary antibodies diluted in 0.5% BSA in PBS overnight at 4°C. The next day, cells were washed 3 times with PBS. They were then incubated in a secondary antibody solution containing secondary antibodies diluted in 0.5% BSA in PBS overnight at 4°C. Counterstaining was performed with Vectashield containing DAPI (Vector Labs). Images were taken at the Garvey Imaging Core at the University of Washington's Institute for Stem Cell and Regenerative Medicine using a Leica SP8 Confocal System on an inverted microscope platform. 12-bit 2048x2048 pixel images were acquired with Leica LAS X software. Antibodies used in this study were as follows: mouse anti-Islet1 (1 in 200, DSHB), rabbit anti-β III tubulin (1 in 500, Sigma Aldrich), rabbit anti-TDP43 (1 in 200, Invitrogen), goat anti-ChAT (1 in 200, R&D Systems), Alexafluor-488 conjugated goat-anti-mouse secondary antibody (1:500, Invitrogen), Alexafluor-594 conjugated goat-anti-rabbit secondary antibody (1:500, Invitrogen) and Alexafluor-647 conjugated Donkey-anti-goat secondary antibody (1:500, Invitrogen).

4.3.7 Electrophysiology

Population level function in motor neuron cultures was assessed using 48-well multielectrode arrays (MEA) in conjunction with the Maestro MEA system (Axion Biosystems). Day 21 cells were plated on Cytoview 48 well plates (Axion Biosystems) at the density of 100,000 cells per well. Plated cells were then subjected to daily cytokine and blocking antibody treatment using fresh medium from the next day onwards. Electrophysiological recordings were taken every day from day 22 to day 40 for

all experimental groups. During data acquisition, standard recording settings for spontaneous neuronal spikes were used (Axis software, version 2.5), and cells were maintained at 37°C/ 5% CO_2 throughout the 2-minute recording period. The standard settings have 130 × gain, and record from 1 to 25 000 Hz, with a low-pass digital filter of 2 kHz for noise reduction. In all experiments, spike detection was set at 5x the standard deviation of the noise and network burst detection was recorded if at least 25% of the electrodes in a given well showed synchronous activity. Reported results were calculated by averaging all of the electrodes in each well, then averaging data from duplicate wells.

4.3.8 Quantitative real-time PCR

We extracted total RNA from cells using Trizol (Invitrogen). After checking RNA purity and concentration, RNA was reverse transcribed to cDNA using the iScript SuperMix reagent (BioRad). Primers (IDT) were diluted in nuclease-free water with PowerUp SYBR Green master mix (Applied Biosystems) and qPCR performed on the Applied Biosystems 7300 machine. The following primers were used human β-actin: forward, 5' -ACTCTTCCAGCCTTCCTTCC- 3', reverse, 5' -CAATGCCAGGGTACATGGTG- 3'; human PD-L1: forward, 5' -GGAAATTCCGGCAGTGTACC- 3', reverse, 5' -GAAACCTCCAGGAAGCCTCT- 3'; human IFI27: forward, 5' – TGGAATGCCACGGAATTAACC - 3', reverse, 5' - GCCACAACTCCTCCAATCAC - 3'; human IFIT2: forward, 5'-CACTGCAACCATGAGTGAGA - 3', reverse, 5' – AGGTTGCACATTGTGGCTTT- 3'; human PLAAT4: forward, 5' – CCGCTGTAAACAGGTGGAAA - 3', reverse, 5' - CCGCTGTAAACAGGTGGAAA - 3'; human CRABP1: forward, 5' - AAGGTCGGAGAAGGCTTTGA- 3', reverse, 5' - AGTGGCTAAACTCCTGCACT- 3'; human KCND2: forward, 5'- CCTTCTTCTGCTTGGACACG-3', reverse, 5'- TCTGTCATCACCAGCCCAAT-3'; human SCN9A: forward, 5'- AGGACCTCAGAGCTTTGTCC-3', reverse, 5'- AAGTCACTGCTTGGCTTTGG-3'; human PRPH: forward, 5'- CTCAAGCAGAGGTTGGAGGA-3', reverse, 5'- CGTGCAGCTTCTTGAGGAAC-3'; human TPBG: forward, 5' - GCCTCGTCCAACAACCATAC- 3', reverse, 5' - CACCTCTTCGCCTCTTGTTG- 3'; human BST2: forward, 5' - CCATCTCCTGCAACAAGAGC- 3', reverse, 5' – TGCATCCAGGGAAGCCATTA - 3'; human PBX3: forward, 5'- TTACCAAGGGTCCCAAGTCG-3', reverse, 5'- GTAGCCTCCCGTCTGATTGA-3'; human C9orf16: forward, 5'- GCAGAATACGCTGCCATCAA-3', reverse, 5'- CGTGGAGGTGGTCATTCTTC-3'; human p53: forward, 5'- CCCAAGCAATGGATGATTTGA-3', reverse, 5'- GGCATTCTGGGAGCTTCATCT-3'; human p21: forward, 5'- GGCAGACCAGCATGACAGATT-3', reverse, 5'- GCGGATTAGGGCTTCCTCT-3'; human PUMA:

forward, 5'- CCTGGAGGGTCCTGTACAATCT-3', reverse, 5'- GCACCTAATTGGGCTCCATCT-3'; human pri-miR-34a: forward, 5'- CCAGAACAGTTCCTGCTGC-3', reverse, 5'- TTAGCTGGTGCTCTCAGAC-3'. Relative RNA levels were calculated from Ct values.

4.3.9 Single cell RNA sequencing

Single cells differentiated from WT and Q331K+/- mutant iPSC-derived neurons with or without IFN**γ** treatment were collected on day 32, to generate total 4 independent single cell libraries. Following single cell dissociation using TrypLE (Thermo Fisher Scientific), cells were filtered through a 70 μm filter and spun down at 1200 rpm for 5 minutes. The single cell pellet was resuspended in neuron maintenance medium at a maximum concentration of 2,000,000 cells/mL, followed by measuring cell viability using the Countess II automated cell counter (Invitrogen), which confirmed over 91% viability of cells in all groups. Cells were spun down at 1200 rpm for 5 minutes again and resuspended in PBS + 0.04% BSA at a concentration of 15,000 cells/16.5 μL to target harvesting 10,000 recovered cells per library. cDNAs of single cells from each group were barcoded with 10x Genomic's Chromium Next GEM Chip G Single Cell Kit and Chromium Next GEM Single Cell 3' Kit v3.1, by following manufacturer's protocol. Constructed libraries were loaded to the Tapestation (Agilent) to quantify the cDNA amount and confirm fragmentation status, followed by sequencing with the Illumina NextSeq2000 at the Genomics core with the University of Washington's Institute for Stem Cell and Regenerative Medicine. The sequencing was performed at an estimated read depth of 10,000 reads/cell. Sequenced FASTQ reads were initially processed using CellRanger v.3 software with settings recommended by the manufacturer (10X Genomics).

4.3.10 Transcriptomic data analysis

Read alignment, filtering, barcode counting, and unique molecular identifier (UMI) counting was performed using CellRanger data processing software provided by 10x Genomics. The feature barcoded matrix was obtained for further gene expression analysis with Seurat V4.0. The quantitative summary of sequencing was obtained from the CellRanger as follows: 1) The sequencing of single

cells from WT culture without IFN**γ** stimulation detected 1,911 genes per cell, 4,105 UMI per cell, and 21,312 mean reads per cell. 2) The sequencing of single cells from WT culture with IFN**γ** stimulation detected 1,833 genes per cell, 3,726 UMI per cell, and 16,427 mean reads per cell. 3) The sequencing of single cells from Q331K+/- mutant culture without IFN**γ** treatment detected 1,651 genes per cell, 3,443 UMI per cell, and 18,452 mean reads per cell. 4) The sequencing of single cells from Q331K+/- mutant culture with IFN**γ** treatment detected 1,858 genes per cell, 3,803 UMI per cell, and 20,319 mean reads per cell. For the comparative gene expression analysis, the integration of single-cell data described by Stuart *et al.* was applied on the basis of the Seurat algorithm. Before applying the integration, cells with low UMI counts, doublets, and cells with relatively high mitochondrial DNA content were removed. The cleared datasets were subsequently normalized in order to correct for differences in read depth and library size, using Seurat's "LogNormalize" function which divides feature counts of the cell by its total counts, followed by multiplying the scale factor. Then, the integration method included in Seurat v.4 aligned the shared cell populations across multiple datasets to identify cells that are in a matched biological state in each library, which allows comparative gene expression analysis across the selected libraries to be performed. The PCA was performed with the integrated data post normalization, followed by running the "RunUMAP" function to generate 2-dimensional UMAP projections using the top principal components detected in the dataset. "FindConveredMarkers" function in Seurat identified conserved cell type markers for generating the feature plots with the "FeaturePlot" function. The clusters were annotated by analyzing the list of conserved marker genes in each cluster with the gene ontology database, The Human Protein Atlas, and the PanglaoDB. Differential gene analysis was performed by using the "FindMarkers" function in Seurat, and the result was displayed with volcano plots, heatmaps, and violin plots to visually highlight the contrast in gene expression across the selected transcriptomic datasets.

4.4 Results

4.4.1 IFN-γ significantly elevates PD-L1 expression on iPSC-derived motor neurons

We established a differentiation protocol, using small molecules, for generating induced pluripotent stem cell (iPSC)-derived ventrospinal motor neuron populations, essentially as described by Smith *et al*.[15,16] Furthermore, we previously employed CRISPR-Cas9-mediated gene editing techniques to introduce a pathogenic Q331K mutation into the TARDBP gene locus of the WTC11 iPSC line, creating an ALS (TDP-43 mutant) line and an isogenic control pair.[15] In this study, these iPSCs were induced to generate human spinal motor neurons with wildtype (WT) and TARDBP$^{Q331K+/-}$ genotypes. We assessed whether exposure of neurons with these two genotypes to inflammatory cytokines affected expression of PD-L1. Neurons were exposed to IFNα, IFN-**γ**, IL-4, IL-6, IL-1β, IL-17, or TNFα for 3 days (post-neuronal induction), which are the inflammatory cytokines reported to be most significantly increased in ALS patients.[17,18] **[Figure 4.1A, 4.1B]** Of the 7 listed cytokines, only IFN-**γ** promoted a significant increase in PD-L1 expression, and this was consistent across both WT and Q331K+/- populations. [**Figure 4.1C]**

Does PD-L1 in motor neurons function as a suppressor of cytotoxic T cell attack as it does in many cancer cell types? To address this question, we isolated T cells from a normal donor's blood sample and labeled them with a carboxyfluorescein succinimidyl ester (CFSE), which covalently attaches a fluorescent label to the amines of cellular proteins. IFN-**γ** treated neurons were co-cultured with CFSE labeled $CD8^+$ T cells for 5 days in the presence of anti-CD3, a marker of T cell proliferation. Labeled T cells without neurons were used as controls in the presence of anti-CD3 or in the presence of both anti-CD3 and PD-L1-Fc proteins. PD-L1-Fc inhibited the proliferation of $CD8^+$ T cells by approximately 30%. [**Figure 4.1D]** As shown in the same figure, IFN-**γ** treated neurons also reduced $CD8^+$ T cell proliferation but only by approximately 10%, suggesting that the level of PD-L1 expression in motor neuron achieved by IFN-**γ** exposure is only modestly immunosuppressive.

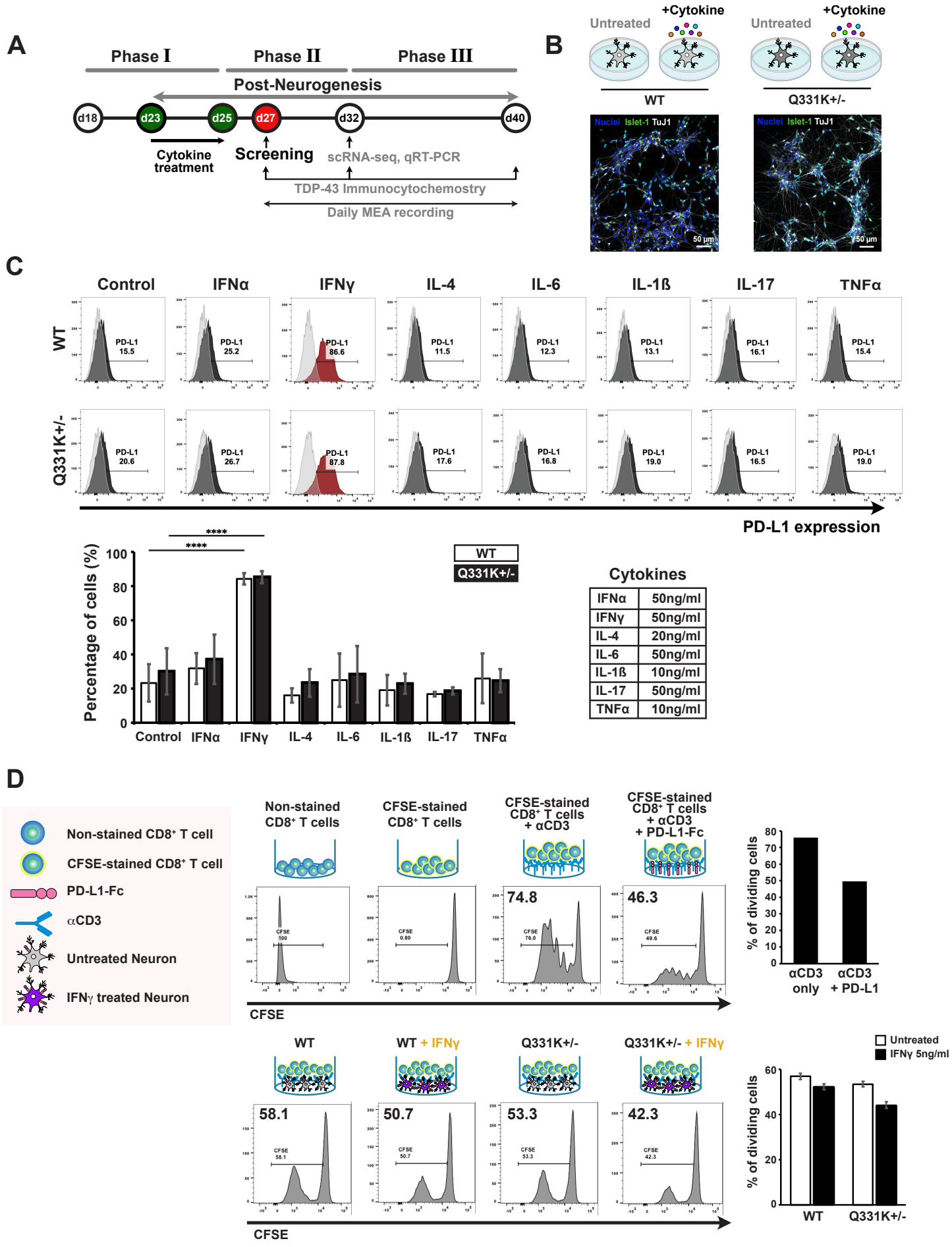
A
Phase I
Phase II
Phase III
Post-Neurogenesis
d18
d23
d25
d27
d32
d40
Cytokine treatment
Screening
scRNA-seq, qRT-PCR
TDP-43 Immunocytochemistry
Daily MEA recording
B
Untreated
+Cytokine
WT
Q331K+/-
Nuclei Islet-1 TuJ1
50 µm
C
Control
IFNα
IFNγ
IL-4
IL-6
IL-1ß
IL-17
TNFα
WT
Q331K+/-
PD-L1
PD-L1 expression
Percentage of cells (%)
WT
Q331K+/-
Cytokines
IFNα 50ng/ml
IFNγ 50ng/ml
IL-4 20ng/ml
IL-6 50ng/ml
IL-1ß 10ng/ml
IL-17 50ng/ml
TNFα 10ng/ml
D
Non-stained CD8⁺ T cell
CFSE-stained CD8⁺ T cell
PD-L1-Fc
αCD3
Untreated Neuron
IFNγ treated Neuron
Non-stained CD8⁺ T cells
CFSE-stained CD8⁺ T cells
CFSE-stained CD8⁺ T cells + αCD3
CFSE-stained CD8⁺ T cells + αCD3 + PD-L1-Fc
74.8
46.3
CFSE
% of dividing cells
αCD3 only
αCD3 + PD-L1
WT
WT + IFNγ
Q331K+/-
Q331K+/- + IFNγ
58.1
50.7
53.3
42.3
Untreated
IFNγ 5ng/ml

Figure 4.1 IFN-γ elevates PD-L1 expression in both WT and TARDBP mutant iPSC-derived spinal motor neurons. (A) Experiment timeline for motor neuron differentiation and downstream assays. (B) Schematic illustration of 4 experimental groups and culture images of WT and mutant neurons before cytokine treatment. (C) Cell surface PD-L1 expression after IFNα, IFNγ, IL-4, IL-6, IL-1β, IL-17, and TNFα treatment in iPSC-derived cells during phase II. Representative flow cytometry histograms (top) and quantification of flow cytometry analyses (bottom left). Error bars, S.D. (n=3, biological replicates). The table shows the concentrations of the treated cytokines (bottom right). (D) Suppression of $CD8^+$ T cell proliferation by co-culture with IFN-γ-treated neurons. Schematic of the cells and antibodies used (left panel). CFSE-labeled $CD8^+$ T cells were stimulated by incubating them in anti-CD3-coated plates for 5 days, in the absence or presence of IFN-γ-treated iPSC-derived neurons. Quantification of CFSE-labeled $CD8^+$ T cell proliferation is depicted in each histogram (middle panels) and summarized in the bar graph (right panel).

4.4.2 IFN-γ exposure hyperactivates neurons followed by a complete loss of their firing function

Having verified that motor neurons are particularly sensitive to IFN-γ, we investigated whether this inflammatory cytokine might contribute to the electrophysiological dysfunction of motor neurons associated with ALS. We assessed function of iPSC-derived motor neuron cultures, with both WT and $TARDBP^{Q331K+/-}$ genotypes, via multi-electrode arrays (MEAs), which enable recording of spontaneous field potential changes from cultured neurons in a non-destructive and non-invasive manner. **[Figure 4.2A)** We treated neurons daily with 3 different concentrations of IFN-γ (0.5 ng/mL, 5 ng/mL, 50 ng/mL) from days 23 to 40 post neuronal induction while recording the neuron's firing activity across the same culture period. **[Figure 4.2B]** The time-course analysis of the mean firing rate shows a distinct difference in the firing pattern between untreated and IFN-γ-treated neurons. Untreated neurons showed a gradual increase in the firing rate as they matured for both the normal and mutant groups and maintained firing rates above 5 Hz from day 27 until the end of phase 2. However, neurons treated with IFN-γ above 5 ng/mL showed a drastic increase in the firing rate from day 27, reaching higher than 30 Hz by day 32, followed by a sharp decline in the firing rate subsequently. As a consequence of IFN-γ exposure, both WT and mutant groups completely lost their firing ability by day 38. **[Figure 4.2C]**

Although IFN-γ treatment was the major driver of this aberrant firing behavior, we also observed a notable difference in firing patterns between IFN-γ untreated WT and mutant neurons. The TARDBP mutant neurons tended to exhibit more active firing patterns than WT neurons early in the recording period. However, they started to exhibit impaired firing ability from day 31 and this trend was maintained until the end of the recording period. Notably, the firing frequency of mutant neurons was significantly

lower than that of WT neurons at day 38. This result suggests that electrophysiological impairment could be one of the downstream pathologic effects of TARDBP mutation in neurons, which agrees with previous studies.[15,19] **[Figure 4.2C]** However, since IFN-**γ** exposure induced a much more pronounced impairment of neuronal electrophysiology, regardless of mutation status, the data suggest that IFN-**γ**-mediated inflammatory stress in the neurons may be a potent trigger of both inherited and acquired forms of neurodegenerative disease. [**Figure 4.2D]**

This "hyperactivation followed by silencing" pattern was consistently observed in both WT and mutant neurons exposed to IFN-**γ** above 5 ng/ml. The weighted mean firing rate consistently showed a significant increase in firing frequency followed by a sudden drop, whereas untreated controls were still able to fire in the last phase of recording. **[Figure 4.2E]** In neuronal cultures, neural circuit formation can lead to synchronization of neural activity, detected as "burst" firing on MEAs.[16,20,21] The differentiation protocol employed for these studies specifies neurons with ventral spinal cord identity, including interneurons as well as motor neurons, and the presence of interneurons was confirmed by our RNAseq analysis (data not shown). Consequently, these cultures have the potential to generate neuronal networks *in vitro*. We therefore monitored network burst firing behavior in these cultures to understand whether IFN-**γ** treatment altered inter-neuronal signaling. We observed an increase in the burst firing frequency of both WT and mutant neurons during the mid-phase, but the contribution of IFN-**γ** to this change was limited. However, the burst firing ability of mutant neurons was dramatically reduced in the last phase, regardless of IFN-**γ** treatment. IFN-**γ** -treated WT neurons showed dose-dependent decreases in burst firing ability in this same phase. **[Figure 4.2F]** Similarly, we observed an increase in network burst firing frequency for both groups of neurons in the mid-phase of the recording. As expected, prolonged exposure to 50 ng/mL IFN-**γ** produced evidence of decaying network burst firing activity in both groups by the end of the culture period. However, exposure to 5 ng/mL IFN-**γ** affected neurons harboring mutant TARDBP more strongly than WT neurons. **[Figure 4.2G]**

Taken together, we observed that electrophysiological function of cultured neurons is affected by both TARDBP mutation and IFN-**γ**-mediated stress. However, the physiologic influence of IFN-**γ** treatment surpassed the inherent mutation in terms of the strength of its effect on firing patterns. We found that normal neurons were similarly vulnerable to continuous IFN-**γ**-mediated inflammatory stress, strongly suggesting that IFN-**γ** could be a critical pathogenic driver of sporadic ALS, which accounts for the majority of patient cases.

4.4.3 Prolonged IFN-γ exposure triggers cytoplasmic TDP-43 mis-localization

Does IFN-**γ** exposure contribute to triggering the cytoplasmic mis-localization of TDP-43, which is a defining hallmark of ALS? To address this question, we treated both WT and mutant neurons with 5 ng/mL IFN-**γ** for 15 days following the neurogenic phase of differentiation and immunostained the culture with anti-TDP-43 on days 25, 32, and 40 to monitor its expression and subcellular localization. **[Figure 4.3A]** Interestingly, we did not observe cytoplasmic TDP-43 mis-localization at any examined time-point in either WT or TARDBP mutant neurons without IFN-**γ** treatment. However, IFN-**γ** exposure led to prominent cytoplasmic accumulation and aggregation of TDP-43, in both groups of neurons. This phenotype was not observed until day 40, suggesting that TDP-43 mis-localization may require an accumulation of inflammatory stress over time to trigger the phenotype. **[Figure 4.3B]** Although the WT neurons developed a significant TDP-43 proteinopathy in response to IFN-**γ** exposure, the degree of the phenotype was more severe for TARDBP$^{Q331K+/-}$ mutant cells. This result indicates that the TARDBP mutation generates neurons that are more susceptible to cytoplasmic TDP-43 aggregation in response to inflammatory stress. **[Figure 4.3C]**

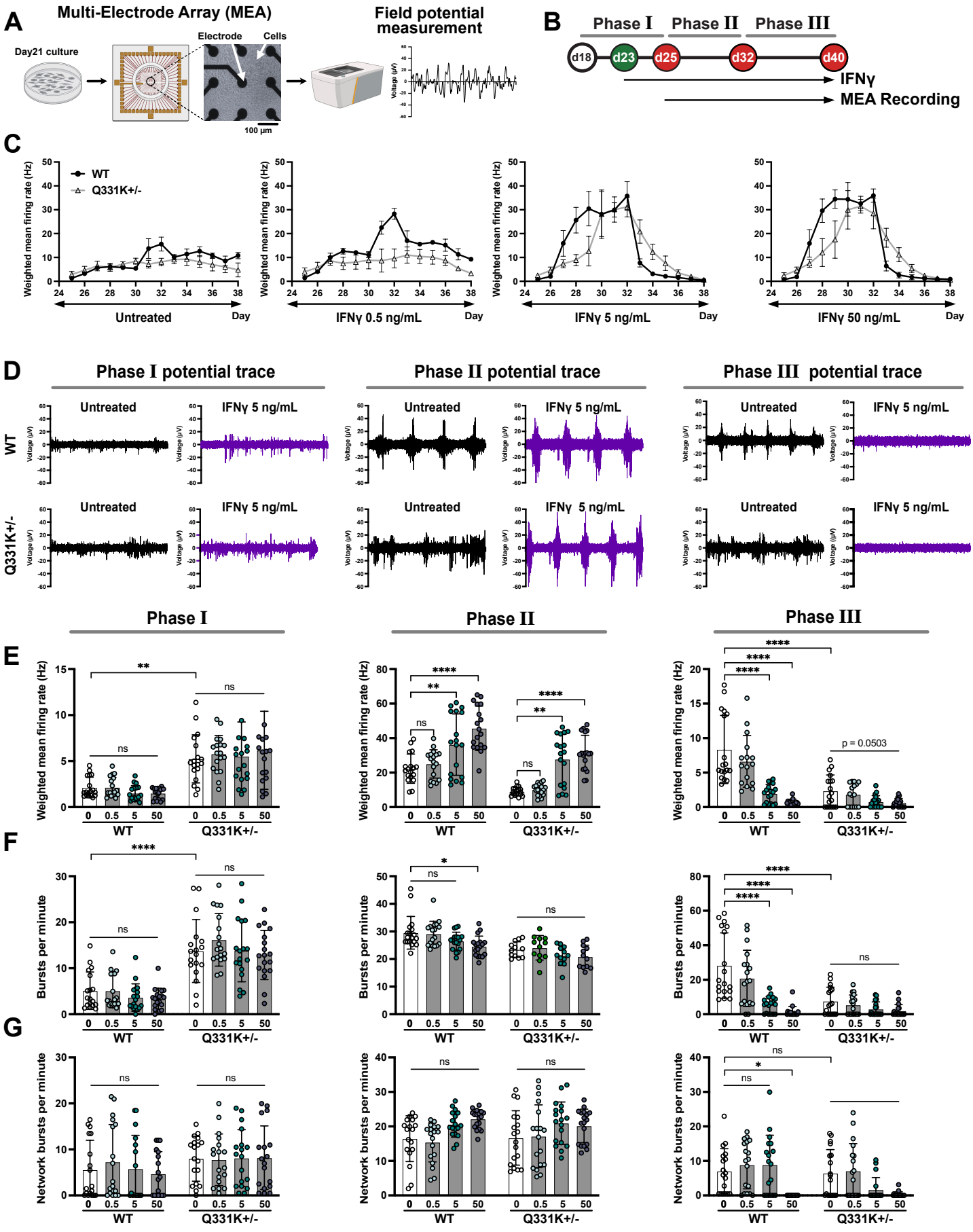
A
Multi-Electrode Array (MEA)
Day21 culture
Electrode
Cells
100 µm
Field potential measurement
B
Phase I
Phase II
Phase III
d18
d23
d25
d32
d40
IFNγ
MEA Recording
C
WT
Q331K+/-
Weighted mean firing rate (Hz)
Untreated
IFNγ 0.5 ng/mL
IFNγ 5 ng/mL
IFNγ 50 ng/mL
Day
D
Phase I potential trace
Phase II potential trace
Phase III potential trace
Untreated
IFNγ 5 ng/mL
WT
Q331K+/-
E
Phase I
Phase II
Phase III
Weighted mean firing rate (Hz)
p = 0.0503
F
Bursts per minute
G
Network bursts per minute
0
0.5
5
50
WT
Q331K+/-
ns

Figure 4.2 IFN-γ treatment induces aberrant electrophysiological activity in WT and TARDBP mutant iPSC-derived neuronal populations. (A) Illustration of the MEA experiment. (B) Experiment time line for the IFN-γ treatment and neuronal electrophysiology recordings. (C) Representative plot for time-course weighted mean firing frequency of the neurons. High concentration IFN-γ treated neurons show aberrant increase in firing rate during phase II, followed by an acute silencing in phase III. (D) Field potential trace of the neurons from each condition showing aberrant electrophysiological progression in response to IFN-γ treatment. Collective summary of phase-dependent electrophysiology of neurons for (E) weighted mean firing rate, (F) burst firing frequency, and (G) network burst firing frequency under the different stimulation conditions and mutation statuses. (Error bars S.D., n = 3 biological replicates; *P < 0.05, ***P<0.001, ****P<0.0001, ns=not significant; two-way ANOVA)

4.4.4 Impact of IFN-γ exposure on the p53 pathway

TDP-43 promotes the function of p53, a key mediator of cell death across many diseases. Maor-Nof *et al.* recently reported that p53 could be a critical regulator of neurodegeneration in *C9orf72* mutant ALS, which is the most common subtype of familial ALS and is known to promote TDP-43 proteinopathy.[22,23] Hence, we further investigated the activation of p53 under the same conditions as in Figure 3B. We employed qRT-PCR to examine the expression of mRNA encoding p53, as well as its downstream effectors, p21, PUMA, and pri-miR-34a. **[Figure 4.3D]** In the WT condition, expression of the p53 pathway genes was low at initial stages of culture, but p21 expression was increased in a time-dependent manner following IFN-γ treatment. Interestingly, the expression of those p53 pathway genes in cells bearing mutant TDP-43 all increased in a time-dependent manner, regardless of IFN-γ exposure, indicating that mutant TDP-43 activates the p53 pathway, even in the absence of extensive cytoplasmic TDP-43 mis-localization. Since p53 pathway activation is a common response to various types of cellular stress, this result suggests that the presence of mutant TDP-43 could drive an intracellular stress response to turn on p53 signaling in neurons, whereas IFN-γ-mediated inflammatory stress elicits significant TDP-43 proteinopathy in both WT and Q331K+/- mutant neurons. **[Figure 3E]**

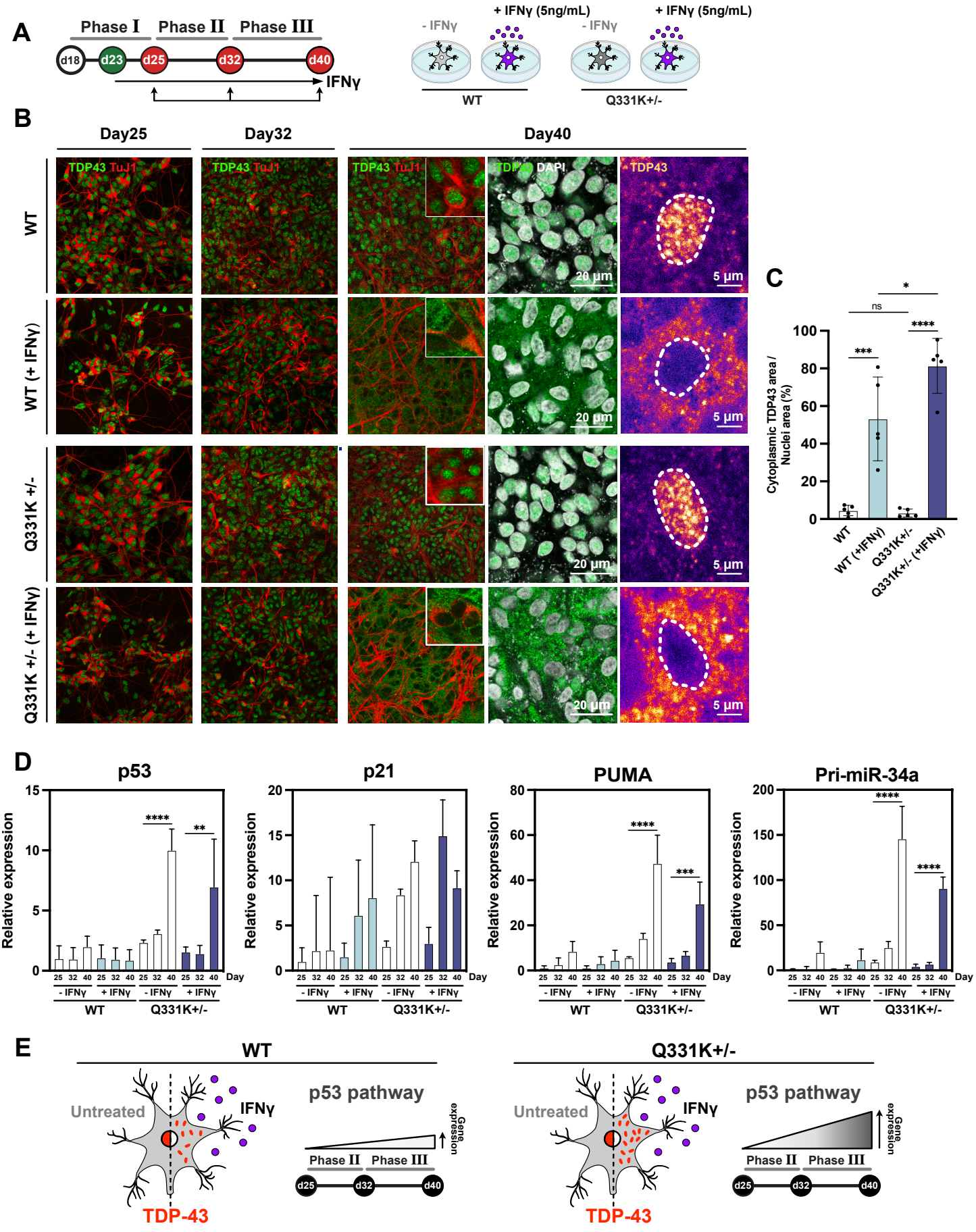
A
Phase I
Phase II
Phase III
d18
d23
d25
d32
d40
IFNγ
- IFNγ
+ IFNγ (5ng/mL)
WT
Q331K+/-
B
Day25
Day32
Day40
WT
WT (+ IFNγ)
Q331K +/-
Q331K +/- (+ IFNγ)
TDP43 TuJ1
TDP43 DAPI
TDP43
20 µm
5 µm
C
Cytoplasmic TDP43 area / Nuclei area (%)
ns
*
***
****
WT
WT (+IFNγ)
Q331K+/-
Q331K+/- (+IFNγ)
D
p53
p21
PUMA
Pri-miR-34a
Relative expression
Day
- IFNγ
+ IFNγ
WT
Q331K+/-
E
WT
Q331K+/-
Untreated
IFNγ
TDP-43
p53 pathway
Gene expression
Phase II
Phase III
d25
d32
d40

Figure 4.3 IFN-γ treatment triggers TDP-43 proteinopathy, whereas TARDBP mutation increases the basal activity of the p53 signaling pathway. (A) Experiment timeline of the immunocytochemistry and gene expression assays. (B) Immunocytochemistry assay of WT and TARDBP mutant cultures showing significant cytoplasmic translocation and aggregation of TDP-43 protein in response to IFN-**γ** stimulation at the later phases of both cultures. (C) Quantitative analysis of cytoplasmic TDP-43 translocation for each experimental condition. Time-course qRT-PCR analysis for each experimental group to quantify the expression of (D) p53, p21 (the early transcriptional target of p53 signaling), PUMA (a proapoptotic gene induced by p53), and Pri-miR-34a (a p53-regulated microRNA). An apparent trend in p53 pathway activation is observed with TARDBP mutation, whereas IFN-**γ** stimulation plays a limited role on this pathway. (E) Schematic summary of the phenotypic observation in each condition. (Error bars S.D., n = 3 biological replicates; *P < 0.05, ***P<0.001, ****P<0.0001, ns=not significant; one-way ANOVA)

4.4.5 Exposure to IFN-γ significantly alters the transcriptomic profile of both WT and TARDBP mutant motor neurons

Functional effects of IFN-**γ** are primarily mediated by JAK1/2 dependent activation of STAT1/2 transcription factors. Therefore, to gain insight into the mechanisms responsible for IFN-**γ** effects on electrophysiological dysfunction and TDP-43 cytoplasmic mis-localization, we characterized the transcriptional changes induced by exposure of motor neurons to IFN-**γ**. WT and Q331K+/- mutant neurons were treated with IFN-**γ** (5 ng/mL) for 10 days (days 22 to 32 post neuronal induction) directly following the neurogenic phase of differentiation, and subjected to single-cell RNA-sequencing on the last day of stimulation. We generated four single cell libraries defined by mutation status and IFN-**γ** treatment. **[Figure 4.4A]** Population analysis showed that motor neurons constituted 37.7% and 40.0% of WT and Q331K+/- mutant populations, respectively. The majority of non-neuronal cells in both groups were early glial progenitors and their gene expression profiles were all affected by IFN-**γ** treatment. **[Figure 4.4B]** Further cluster annotation, based on homeobox (HOX) gene expression patterns, indicated that both WT and Q331K+/- mutant motor neuron populations expressed regional identities specific to the upper spinal cord. (data not shown)

Motor neuron stimulation by IFN-**γ** generated 672 (WT) and 430 (Q331K+/-) differentially expressed genes (DEGs) compared to untreated controls. Interestingly, 613 DEGs appeared between the IFN-**γ** stimulated WT and Q331K+/- motor neurons, implying a potential role for the TDP-43 mutation in mediating neuronal responses to IFN-**γ**. We also found 327 DEGs between the WT and Q331K+/- neurons that were not exposed to IFN-**γ**, indicating that the TDP-43 mutation exerted a significant impact on cultured motor neuron's downstream gene expression profiles. **[Figure 4.4C]**

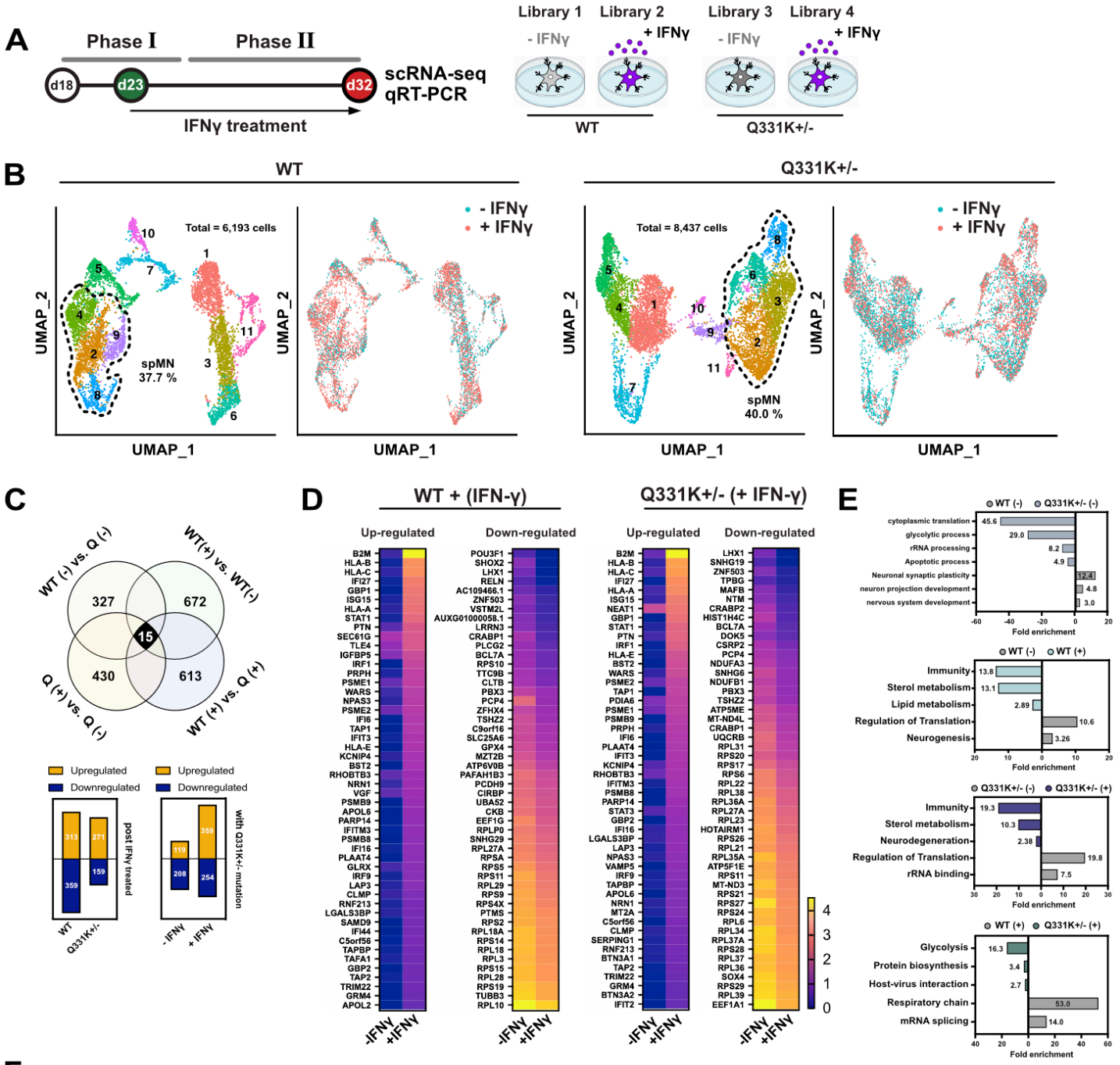
A
Phase I
Phase II
d18
d23
d32
scRNA-seq
qRT-PCR
IFNγ treatment
Library 1
Library 2
Library 3
Library 4
- IFNγ
+ IFNγ
WT
Q331K+/-
B
WT
Q331K+/-
Total = 6,193 cells
Total = 8,437 cells
spMN
37.7 %
spMN
40.0 %
UMAP_1
UMAP_2
C
WT (-) vs. Q (-)
WT(+) vs. WT(-)
Q (+) vs. Q (-)
WT (+) vs. Q (+)
327
672
15
430
613
Upregulated
Downregulated
post IFNγ treated
with Q331K+/- mutation
WT
Q331K+/-
-IFNγ
+IFNγ
D
WT + (IFN-γ)
Q331K+/- (+ IFN-γ)
Up-regulated
Down-regulated
E
WT (-)
Q331K+/- (-)
WT (+)
Q331K+/- (+)
cytoplasmic translation
glycolytic process
rRNA processing
Apoptotic process
Neuronal synaptic plasticity
neuron projection development
nervous system development
Immunity
Sterol metabolism
Lipid metabolism
Regulation of Translation
Neurogenesis
Neurodegeneration
rRNA binding
Glycolysis
Protein biosynthesis
Host-virus interaction
Respiratory chain
mRNA splicing
Fold enrichment
F
Q331K+/- (-) > WT (-)
WT (+) > WT (-)
Q331K+/- (+) > Q331K+/- (-)
Q331K+/- (+) > WT (+)
GO: Cytoplasmic Translation
GO: Immunity
GO: Immunity
GO: Glycolysis
RPL24
RPL21
RPL39
RPL36A
RPL34
B2M
HLA-B
HLA-C
IFI27
GBP1
HLA-A
ENO1
TPI1
PGAM1
ENO2
PGK1
Log2FC
P-value (-Log10)

Figure 4.4 IFN-γ treatment induces inflammatory gene expression in both WT and TARDBP mutant iPSC-derived motor neurons. (A) Experiment timeline of IFN-γ treatment and gene expression analysis. The schematic illustration shows the library constitution for the single-cell RNA sequencing experiment. (B) UMAP clustering of both cultures shows the populational distribution of the differentiated cells. (C) The number of DEGs in each pairwise comparison. (+) indicates culture with IFN-γ treatment and (–) indicates untreated controls. Q indicates Q331K+/- mutant group. (D) Heatmap of top 50 DEGs based on the fold change post IFN-γ treatment in both WT and mutant motor neurons. Scale indicates relative gene expression level in each group. Gene counts per cell were normalized for their total counts over all genes and logarithmized. (E) Gene ontology (GO) analysis of the DEGs generated in each pairwise comparison. (F) The top 5 DEGs included in the selected GO terms in each pairwise comparison. > denotes the listed genes are more expressed in the left group than in the control group on the right.

A heatmap of the top 50 DEGs in each group shows that IFN-γ exposure significantly increased inflammatory gene expression and decreased ribosomal protein gene expression in both WT and Q331K+/- motor neurons. A notable elevation of B2M (ß-2-microglobulin) expression was observed in both WT and Q331K+/- motor neurons in response to IFN-γ treatment. B2M is a component of MHC-1 (Major Histocompatibility Complex-I) class molecules. They are expressed in all nucleated cells and are responsible for presenting foreign peptide fragments on the cell surface, which bind CD8+ T cells to trigger an immediate immune response. ß-2-microglobulin is a critical mediator of MHC-1 surface expression, verified using a B2M-defienct mouse model that rarely presents MHC-1 on the cell surface and exhibits poor development of CD8+ T-cells.[24,25] The significant increase of B2M expression in our culture model demonstrated that IFN-γ elicits an acute inflammatory response from treated motor neurons. In addition, a sharp increase of HLA-A, HLA-B, and HLA-C expression in WT and Q331K+/- neurons, which encodes human leukocyte antigens that correspond to MHC-I class, confirmed that the IFN-γ-mediated inflammatory response constituted a major upstream driver of gene expression change in both groups of motor neurons. **[Figure 4.4D]**

Gene ontology analysis was performed using the DEGs that arose from 4 different pairs of gene expression data, to generally characterize the nature of the effects. Changes in gene expression due to the TARDBP mutation were mainly related to cytoplasmic translation, glycolytic processes, and neuronal synaptic plasticity. Within the cytoplasmic translation GO term, ribosomal proteins (including RPL24, RPL21, RPL39, RPL34, and RPL36A) were up-regulated in mutant neurons. These data mirror the sequencing results previously reported from primary excitatory neurons harboring a *C9orf72*

mutation, which is responsible for the most frequent form of familial ALS.[26] DEGs arising from IFN-**γ** treatment were primarily related to immunity, sterol metabolism, and regulation of translation in both WT and mutant neurons. However, mutant neurons exposed to IFN-**γ** exhibited significant differences in the expression levels of genes related to glycolysis, respiratory chain, and mRNA splicing, when compared to WT motor neurons receiving the same concentration of IFN-**γ**. **[Figure 4.4E, 4.4F]**

4.4.6 IFN-γ drives gene expression changes characteristic of neurodegeneration.

We sought to ascertain whether exposure to IFN-**γ** promoted the expression of ALS-related transcripts in cultured motor neurons and, if so, how the trend differed from that caused by the TARDBP$^{Q331K+/-}$ mutation. We compared the identified DEGs individually to lists of the ALS risk genes recently identified by applying a machine learning algorithm to ALS GWAS data and molecular profiling of iPSC-derived motor neurons.[27] **[Figure 4.5A]** We found a significant overlap between the 4 sets of DEGs with those risk genes. In particular, we found 72 DEGs related to ALS pathology, derived by IFN-**γ** exposure. The result confirms that cytokine exposure puts cultured neurons on to a neurodegenerative pathway, which could potentially lead to the development of an ALS phenotype, although the IFN-**γ** did not induce motor neuron death in either WT or mutant groups. **[Figure 4.5B, 4.5C]**

The most significantly mis-regulated DEGs in each pairwise comparison, and the GO analysis results for those genes, revealed a distinct effect of Q331K mutation and IFN-**γ** exposure on motor neuron function, suggesting that the functional behavior of these cells is more greatly affected when both factors are present. **[Figure 4.5D, 4.5E]** In summary, IFN-**γ** treatment significantly altered the gene expression profile of both WT and Q331K mutant motor neurons in a manner that could lead to the development of ALS phenotypes. **[Figure 4.5F]**

From the list of genes exhibiting greater than two-fold differential expression for each pairwise comparison, we employed qPCR to confirm and more precisely quantify the extent of differential expression of genes that are particularly relevant to neurodegeneration. We found that apoptotic genes,

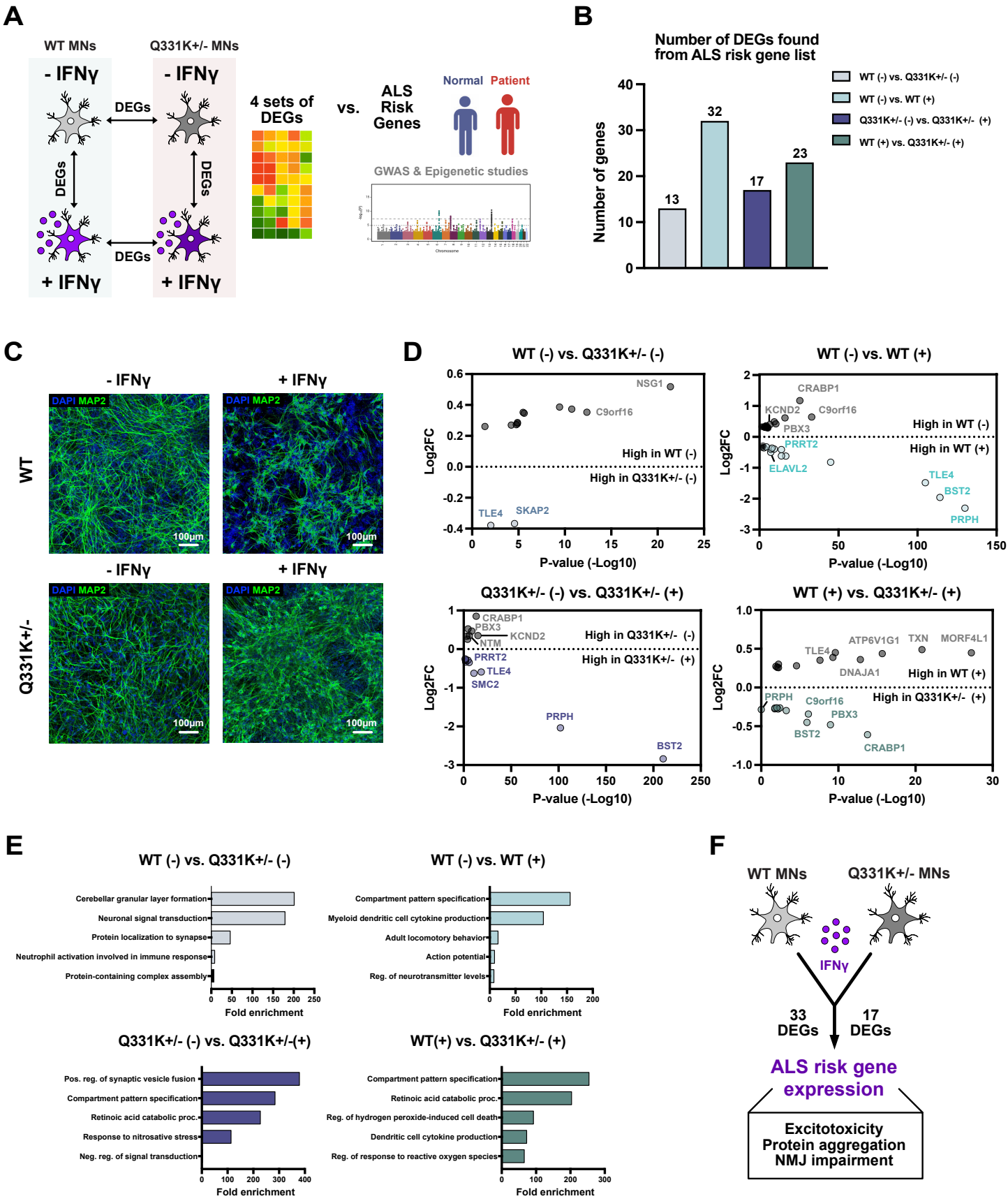
A
WT MNs
Q331K+/- MNs
- IFNγ
- IFNγ
DEGs
DEGs
DEGs
DEGs
+ IFNγ
+ IFNγ
4 sets of DEGs
vs.
ALS Risk Genes
Normal
Patient
GWAS & Epigenetic studies
B
Number of DEGs found from ALS risk gene list
Number of genes
40
30
20
10
0
13
32
17
23
WT (-) vs. Q331K+/- (-)
WT (-) vs. WT (+)
Q331K+/- (-) vs. Q331K+/- (+)
WT (+) vs. Q331K+/- (+)
C
- IFNγ
+ IFNγ
WT
Q331K+/-
DAPI MAP2
100μm
D
WT (-) vs. Q331K+/- (-)
NSG1
C9orf16
High in WT (-)
High in Q331K+/- (-)
TLE4
SKAP2
Log2FC
P-value (-Log10)
WT (-) vs. WT (+)
CRABP1
KCND2
C9orf16
PBX3
PRRT2
ELAVL2
High in WT (-)
High in WT (+)
TLE4
BST2
PRPH
Q331K+/- (-) vs. Q331K+/- (+)
CRABP1
PBX3
NTM
KCND2
PRRT2
TLE4
SMC2
High in Q331K+/- (-)
High in Q331K+/- (+)
PRPH
BST2
WT (+) vs. Q331K+/- (+)
ATP6V1G1
TXN
MORF4L1
TLE4
DNAJA1
High in WT (+)
PRPH
C9orf16
PBX3
BST2
CRABP1
High in Q331K+/- (+)
E
WT (-) vs. Q331K+/- (-)
Cerebellar granular layer formation
Neuronal signal transduction
Protein localization to synapse
Neutrophil activation involved in immune response
Protein-containing complex assembly
Fold enrichment
WT (-) vs. WT (+)
Compartment pattern specification
Myeloid dendritic cell cytokine production
Adult locomotory behavior
Action potential
Reg. of neurotransmitter levels
Fold enrichment
Q331K+/- (-) vs. Q331K+/-(+)
Pos. reg. of synaptic vesicle fusion
Compartment pattern specification
Retinoic acid catabolic proc.
Response to nitrosative stress
Neg. reg. of signal transduction
Fold enrichment
WT(+) vs. Q331K+/- (+)
Compartment pattern specification
Retinoic acid catabolic proc.
Reg. of hydrogen peroxide-induced cell death
Dendritic cell cytokine production
Reg. of response to reactive oxygen species
Fold enrichment
F
WT MNs
Q331K+/- MNs
IFNγ
33 DEGs
17 DEGs
ALS risk gene expression
Excitotoxicity
Protein aggregation
NMJ impairment

Figure 4.5 The IFN-γ-induced transcriptomic changes promote an ALS phenotype in motor neurons. (A) The schematic illustration shows how the analysis was performed. (B) DEGs found from each comparison were compared with the previously reported risk genes for various neurodegenerative disease states. The number of risk genes on the y axis shows how many of the reference risk genes for each disease were overlapped with the DEGs generated by either mutation or IFN-γ treatment. (C) The immunostaining images show that IFN-γ treatment does not induce notable cell death in both groups of culture. (D) The fold-change and p-value of selected DEGs for each comparison that have a significant role in neurodegeneration based on the recent literature. (E) GO analysis results for the subgroup of DEGs that are known to increase the risk of ALS development. (F) Illustration summary of the discovery delineated in the figure. (+) indicates culture with IFN-γ treatment and (–) indicates untreated controls.

such as IFI27, IFIT2, and PLAAT4, were highly elevated in response to IFN-γ treatment but were unaffected by the Q331K mutation. **[Figure 4.6A]** We also confirmed decreasing CRABP1 gene expression following IFN-γ exposure. CRABP1 is an essential component of neuromuscular junction (NMJ) development and maintenance via the CRABP1-CaMKII-Agrn pathway. Its reduced expression in IFN-γ treated cells indicates that this cytokine may directly impair the stability and function of muscle innervation by motor neurons. **[Figure 4.6B]** Moreover, the list of DEGs in IFN-γ treated cells compared with controls included genes encoding ion channel proteins responsible for regulating neuronal electrophysiology. RNA-seq and qRT-PCR data both implicated that the genes for the voltage-gated potassium channel KCND2 and the sodium channel SCN9A were mis-regulated in a direction that might promote neuronal excitotoxicity. **[Figure 4.6C]** The significant increase in expression of PRPH that encodes the neuron-specific intermediate filament protein, peripherin, is interesting because over-expression of peripherin in motor neurons promotes neuronal cell death, and peripherin is a component of ubiquitinated inclusions and of axon spheroids in ALS.[28–30] Given that the overexpression of WT peripherin causes protein aggregation and motor neuron degeneration in transgenic mice, our result implies that exposure to IFN-γ could drive adoption of similar phenotypes in human motor neurons. Similarly, the decrease of TPBG observed following cytokine treatment indicates that IFN-γ could increase the risk of protein aggregation since the ablation of TPBG is known to promote alpha-synuclein aggregation in a mouse model of neurodegeneration. **[Figure 4.6D]** Lastly, we found significantly altered expression for ALS risk genes under IFN-γ exposure, such as BST2, PBX3, and C9orf16, which

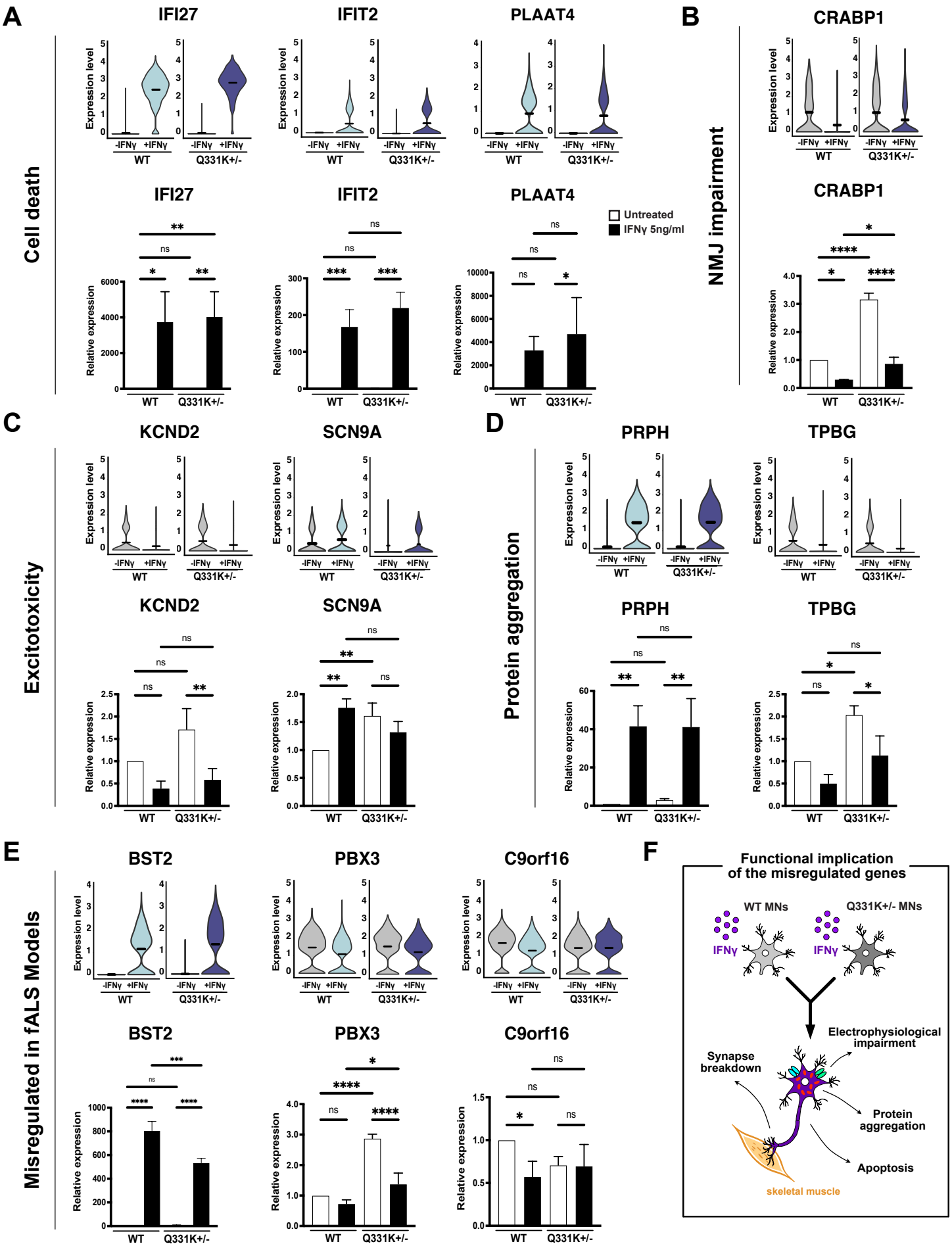
A
Cell death
IFI27
IFIT2
PLAAT4
Expression level
-IFNγ +IFNγ
WT
Q331K+/-
Relative expression
Untreated
IFNγ 5ng/ml
B
NMJ impairment
CRABP1
C
Excitotoxicity
KCND2
SCN9A
D
Protein aggregation
PRPH
TPBG
E
Misregulated in fALS Models
BST2
PBX3
C9orf16
F
Functional implication
of the misregulated genes
WT MNs
Q331K+/- MNs
IFNγ
Electrophysiological
impairment
Synapse
breakdown
Protein
aggregation
Apoptosis
skeletal muscle

Figure 4.6 qRT-PCR verification of the selected DEG expression categorized by their functional implications in motor neurons. Comparison of RNAseq and qRT-PCR assay results for the DEGs potentially responsible for cell death (A), NMJ impairment (B), excitotoxicity (C), and protein aggregation (D). (E) Additional DEGs known to be mis-regulated in familial ALS models, in which aberrant expression was caused by IFN-**γ** treatment. (F) Schematic summary of the potential implications for the listed DEGs driving neurodegenerative phenotypes. (Error bars S.D., n = 3 biological replicates; *P < 0.05, ***P<0.001, ****P<0.0001, ns=not significant; two-way ANOVA)

have been reported to be mis-regulated in various familial ALS models although their pathologic function is yet to be identified. **[Figure 4.6E]** In summary, IFN-**γ** exposure promoted gene expression changes that are likely to induce electrophysiological impairment, neuromuscular synapse breakdown, protein aggregation, and apoptotic cell death. **[Figure 4.6F]**

4.5 Discussion

In this study, we found that only IFN-**γ**, among cytokines tested, increases the expression of immune-modulatory protein PD-L1 in both WT and Q331K+/- mutant motor neurons. Other pro-inflammatory cytokines known to be elevated in ALS patient cerebrospinal fluid were not able to induce the PD-L1 up-regulation, our data suggest that motor neurons might be particularly sensitive to IFN-**γ**. We hypothesized that an inflammatory response leading to excessive exposure of spinal cord motor neurons to IFN-**γ** could elicit expression of a neurodegenerative phenotype. The source of neuroinflammation-associated IFN-**γ** that may affect motor neurons remains to be fully charactered. T cells are a major source of IFN-**γ** secretion, although NK cells, glia and even neurons can produce IFN-**γ**.[31] T cell infiltration of the CNS parenchyma occurs only in a few types of acute inflammation. A T cell population resides constitutively associated with the choroid plexus, where it may secrete IFN-**γ** into the CSF. Importantly, CSF of ALS patients exhibits an expansion of a T cell subpopulation expressing eomesodermin, which drives IFN-**γ** expression.[32] IFN-**γ** is permeable to the blood spinal barrier, particularly in the cervical region, implying that T cells impacted by peripheral inflammation might expose motor neurons to IFN-**γ**.[33–35] Moreover, Bonney *et al* showed that IFN-**γ** even promotes its permeability to the blood-brain barrier, implying that uncontrolled IFN-**γ** secretion may broadly affect the physiology of the entire CNS.[36] Finally, peripherally projecting motor axons lie outside the blood

brain barrier. Exposure of sympathetic axons to IFN-**γ** mediates axonal STAT1 phosphorylation and transport of these activated transcription factors to the somatic nucleus.[37] If a similar retrograde IFN-**γ** axonal signaling pathway exists in motor neurons, T cell-generated IFN-**γ** circulating peripherally might affect motor neurons.

We examined the capacity of IFN-**γ** exposure to elicit two hallmarks of ALS – impaired neurophysiological function of motor neurons and mis-localization of TDP-43 in cytoplasmic aggregates, and observed the occurrence of both, in agreement with our hypothesis. We found that the electrophysiological function of neurons bearing a TARDBP mutation and exposed to IFN-**γ** was significantly impaired, and the impact of the cytokine treatment surpassed the effect of the mutation. The cytokine-treated neurons showed a 'hyperexcitation and silencing' pattern (regardless of whether or not they expressed a TARDBP mutation) that resembled the excitotoxic behavior of neurons in the mid-phase of ALS. Although further follow-up studies are required, downregulated genes encoding the potassium channels and abnormal elevation of genes for sodium channel proteins could be responsible for their functional damage.

We further studied whether TDP-43 proteinopathy, another pathologic hallmark of ALS, could be induced by IFN-**γ** treatment. The continuous treatment of IFN-**γ** triggered a severe cytoplasmic aggregation of TDP-43 in both WT and mutant neurons at late stages of culture. No such phenotype was induced at any time point by the presence of the TARDBP mutation alone, although the severity of the IFN-**γ** triggered phenotype was more pronounced in the mutant groups. This result implies that mis-localization of TDP-43 requires an upstream trigger beyond mutation in the TARDBP gene, but does not discount the possibility that the mutation in TARDBP does contribute to the development of a pathologic phenotype.

Our single-cell RNA sequencing analysis revealed that IFN-**γ** triggers a significant transcriptomic alteration in both WT and Q331K+/- mutant neurons that trends toward the development of an ALS phenotype and suggests several specific mechanisms by which increased IFN-**γ** transcriptional

signaling in motor neurons might impair electrophysiological function and promote TDP-43 mis-localization. Among the DEGs arising from IFN-**γ** treatment, we identified genes known to be aberrantly expressed in familial ALS, as well as potential drivers of cell apoptosis, protein aggregation, excitotoxicity, and NMJ breakdown, implying that cytokine exposure may induce a broad range of ALS pathological hallmarks, even in motor neurons that do not bear mutations in TDP-43. Since many DEGs identified in familial ALS mouse models were also mis-regulated in our normal motor neurons after simply treating with IFN-**γ**, we could postulate that the mutation may work as a potential upstream trigger to induce secretion of IFN-**γ**, which in turn drives neurodegenerative gene expression in motor neurons.

We found that IFN-**γ** induces an abnormal expression of motor neuron-specific genes responsible for regulating NMJ development and maintenance. CRABP1 is a retinoic acid-binding protein, that was recently found to regulate motor function via maintenance of the NMJ through the CRABP-CaMKII-Agrin axis. Lin *et al*. showed that CRABP1 knock-out mice exhibited adult-onset ALS-like phenotypes and developed significantly impaired NMJs followed by motor axon degeneration, which was rescued after the re-expression of the gene.[38] It is notable that, in our hands, CRABP1 expression was dramatically reduced in both genotypes of motor neurons under exposure to IFN-**γ**, indicating that excessive immunological activity might contribute to the development of sporadic forms of ALS via direct targeting of the neuromuscular synapse. PRPH encodes a neuronal intermediate filament protein, peripherin. Mutations in this gene lead to the enrichment of one of the three splice variants observed in human patients (Per28), which causes a disruption of neurofilament assembly and is associated with the development of an ALS phenotype.[28] Peripherin levels are significantly elevated in patients with motor neuron disease and the protein accumulates in the majority of axonal inclusion bodies in ALS patient motor neurons.[28–30,39] Given that motor neurons are highly polarized cells with extremely long axons, the regulation of cytoskeletal genes is of critical importance in the axonal trafficking of organelles and biomolecules, which directly affects motor neuron survival and function.

PRPH also localizes to Bunina bodies, which are intraneuronal protein inclusions, suggesting that an increase in peripherin expression may cause protein aggregation in motor neurons.[28] Xiao *et al*. showed that overexpression of PRPH induces self-aggregation and causes motor neuron degeneration in transgenic mice. In our experiments, the significant increase of PRPH in motor neurons exposed to IFN-**γ** raises two important questions: 1) Does increased PRPH in neurons disrupt axonal trafficking and degenerate neurons in a retrograde manner? 2) Does PRPH also induce cytoplasmic aggregation of TDP-43? TPBG encodes trophoblast glycoprotein and a deficiency in this protein induces the aggregation of alpha-synuclein in mice. Although TPBG mis-regulation is more directly linked to Parkinson's disease, the downstream effect of decreased TPBG expression in motor neurons may be worth investigating in order to establish a better understanding of its potential role in developing a broad range of neurodegenerative phenotypes.

Regardless, there still are important questions that to be answered to better understand the pathologic role of TDP-43 proteinopathy on ALS development. First, more studies are required to understand the pathologic consequence of severe TDP-43 cytoplasmic aggregations induced by IFN-**γ** in motor neurons. Second, speculative mechanisms mentioned here linking particular DEGs to IFN-**γ**-mediated protein aggregation need to be experimentally tested. Finally, we still do not understand the exact role of TARDBP mutations in aggravating the disease phenotype once initiated by cytokine exposure.

We additionally investigated whether the p53 pathway, a cell death mediator gene that is known to be mis-regulated in familial ALS is turned on by IFN-**γ** treatment. Given that p53 is one of TARDBP's downstream target genes, we postulated that the p53 pathway could be initiated by IFN-**γ**-induced TDP-43 proteinopathy. However, IFN-**γ** stress did not induce p53 signaling. Instead, the presence of a TARDBP mutation strongly upregulated p53 pathway genes in a time-dependent manner, indicating that the p53 pathway is directly affected by the mutation status of TDP-43.

We believe these results raise important questions, the answers to which could lead to a better understanding of the pathogenic role of aberrant immunity-mediated neurodegeneration, which could be a key component driving rapid disease progression in ALS. For example, it is currently unclear whether the inflammatory reaction occurs at the axon terminal, the periphery of the patient's body, before spreading the pathologic effect to neuronal cell bodies in a retrograde manner. Finally, it would be valuable to investigate the neuron-autonomous pathologic role of PD-L1, besides its immune-modulatory function, since recent studies have revealed that exogenous PD-L1 treatment to mouse sensory neurons significantly impairs their firing ability without having any influence on the immune response.[40] Therefore, understanding the neuron-autonomous role and downstream signaling path of PD-L1-mediated neuromodulation could be a critical step towards understanding the mechanism of the IFN-**γ**-induced neurodegeneration.

4.6 Conclusion

Our findings strongly suggest that IFN-**γ** is a potent driver of neuroinflammation that induces the adoption of ALS phenotypes in both WT and TARDBP mutant spinal motor neurons. We found that IFN-**γ** treatment not only induces a significant increase in functional PD-L1 and inflammatory gene expression but also extensively shifts motor neuron's gene expression towards a diverse array of neurodegenerative features. We found that continuous exposure to IFN-**γ** alters motor neuron phenotypes in a manner that mirrors changes observed in ALS. Both WT and TARDBP mutant iPSC-derived motor neurons showed a dramatic decay of firing frequency coupled with an increase in cytoplasmic TDP-43 aggregation following IFN-**γ** treatment. However, the mutant neurons exhibited more severe phenotypes for both features, suggesting a role for the mutation in exacerbating the inflammatory stress response. We further confirmed that IFN-**γ** exposure triggered transcriptomic alterations that suggest movement towards expression of a neurodegenerative phenotype in motor neurons. Thus, our study provides strong evidence for a pathogenic link between IFN-**γ**-mediated inflammation and subsequent neurodegeneration in spinal motor neurons that mirrors ALS pathology.

These results suggest that immunomodulatory compounds may constitute strong targets for ameliorating symptoms in both sporadic and familial forms of ALS.

4.7 Reference

1. Hardiman, O. *et al.* Amyotrophic lateral sclerosis. *Nature Reviews Disease Primers* **3** (2017)
2. Masrori, P. & van Damme, P. Amyotrophic lateral sclerosis: a clinical review. *European Journal of Neurology* **27** (2020)
3. Watkins, J. A., Alix, J. J. P., Shaw, P. J. & Mead, R. J. Extensive phenotypic characterization of a human TDP-43Q331K transgenic mouse model of amyotrophic lateral sclerosis (ALS). *Sci. Rep.* **11** (2021)
4. Yuan, Z. *et al.* TDP-43 Mutations in Familial and Sporadic Amyotrophic Lateral Sclerosis. *Science* **319** (2008)
5. Arseni, D. *et al.* Structure of pathological TDP-43 filaments from ALS with FTLD. *Nature* **601** (2022)
6. Estes, M. L. & McAllister, A. K. How neuroinflammation contributesto neurodegeneration. *Science* **353 (**2016)
7. Hooten, K. G., Beers, D. R., Zhao, W. & Appel, S. H. Protective and Toxic Neuroinflammation in Amyotrophic Lateral Sclerosis. *Neurotherapeutics* **12** (2015)
8. Beers, D. R. & Appel, S. H. Immune dysregulation in amyotrophic lateral sclerosis: mechanisms and emerging therapies. *The Lancet Neurology* **18** (2019)
9. Liddelow, S. A. *et al.* Neurotoxic reactive astrocytes are induced by activated microglia. *Nature* **541** (2017)
10. Coque, E. *et al.* Cytotoxic CD8+ T lymphocytes expressing ALS-causing SOD1 mutant selectively trigger death of spinal motoneurons. *Proc. Natl. Acad. Sci.* **116** (2019)
11. Liu, J. & Wang, F. Role of neuroinflammation in amyotrophic lateral sclerosis: Cellular mechanisms and therapeutic implications. *Frontiers in Immunology* **8** (2017)
12. Chun, C., Smith, A. S. T., Bothwell, M. & Mack, D. L. *The Role of Extracellular Vesicles in the Progression of ALS and Their Potential as Biomarkers and Therapeutic Agents with Which to Combat the Disease*. *IntechOpen, Book chapter review* (2020)
13. Wu, Y., Chen, W., Xu, Z. P. & Gu, W. PD-L1 distribution and perspective for cancer immunotherapy—blockade, knockdown, or inhibition. *Front. Immunol.* **10** (2019)
14. Warre-Cornish, K. *et al. Interferon-γ signaling in human iPSC-derived neurons recapitulates neurodevelopmental disorder phenotypes*. *Sci. Adv.* **6** (2020)
15. Smith, A. S. T. *et al.* Human Induced Pluripotent Stem Cell-Derived TDP-43 Mutant Neurons Exhibit Consistent Functional Phenotypes Across Multiple Gene Edited Lines Despite Transcriptomic and Splicing Discrepancies. *Front. Cell. Dev. Biol.* **9** (2021)
16. Smith, A. S. T. *et al.* HDAC6 Inhibition Corrects Electrophysiological and Axonal Transport Deficits in a Human Stem Cell-Based Model of Charcot-Marie-Tooth Disease (Type 2D). *Adv. Biol.* **6** (2022)
17. Chen, X., Hu, Y., Cao, Z., Liu, Q. & Cheng, Y. Cerebrospinal fluid inflammatory cytokine aberrations in Alzheimer's disease, Parkinson's disease and amyotrophic lateral sclerosis: A systematic review and meta-analysis. *Frontiers in Immunology* **9** (2018)
18. Dreger, M., Steinbach, R., Otto, M., Turner, M. R. & Grosskreutz, J. Cerebrospinal fluid biomarkers of disease activity and progression in amyotrophic lateral sclerosis. *Journal of neurology, neurosurgery, and psychiatry* **93** (2022)

19. Chand, K. K. *et al.* Defects in synaptic transmission at the neuromuscular junction precede motor deficits in a TDP-43Q331K transgenic mouse model of amyotrophic lateral sclerosis. *FASEB Journal* **32** (2018)

20. Müller, J. *et al.* High-resolution CMOS MEA platform to study neurons at subcellular , cellular, and network levels. *Lap. Chip.***15** (2017)

21. Smith, A. S. T. *et al.* NanoMEA: a versatile platform for high-throughput analysis of structure-function relationships in human stem cell-derived excitable cells and tissues. *Nano Lett.* **20** (2020)

22. Vogt, M. A. *et al.* TDP-43 induces p53-mediated cell death of cortical progenitors and immature neurons. *Sci. Rep.* **8** (2018)

23. Maor-Nof, M. *et al.* p53 is a central regulator driving neurodegeneration caused by C9orf72 poly(PR). *Cell* **184** (2021)

24. Glas, R., Ohlen, C., Hoglund, P. & Karre, K. The CD8 + T Cell Repertoire in/~z-microglobulin-deficient Mice Is Biased towards Reactivity Against Self-Major HistocompatibiHty Class I. *J.Exp.Med*. **179** (1994)

25. Koller, B. H., Marrack, P., Kappler, J. W. & Smithies, O. Normal Development of Mice Deficient in B2M, MHC Class1 Proteins, and CD8+ T cells. *Science* **248**(1990)

26. Balendra, R. & Isaacs, A. M. C9orf72 -mediated ALS and FTD : multiple pathways to disease. *Nat. Rev. Neurol.* **14** (2018)

27. Zhang, S. *et al.* Genome-wide identification of the genetic basis of amyotrophic lateral sclerosis. *Neuron* **110** (2022)

28. Xiao, S. *et al.* An aggregate-inducing peripherin isoform generated through intron retention is upregulated in amyotrophic lateral sclerosis and associated with disease pathology. *Journal of Neuroscience* **28** (2008)

29. He, C. Z. & Hays, A. P. Expression of peripherin in ubiquinated inclusions of amyotrophic lateral sclerosis. *J. Neurol. Sci* .**217** (2004)

30. Beaulieu, J.-M., Nguyen, M. D. & Julien, J.-P. *Late Onset Death of Motor Neurons in Mice Overexpressing Wild-Type Peripherin*. *The Journal of Cell Biology* **147** (1999)

31. Aebischer, J. *et al.* IFNγ triggers a LIGHT-dependent selective death of motoneurons contributing to the non-cell-autonomous effects of mutant SOD1. *Cell Death Differ.* **18** (2011)

32. Yazdani, S. *et al.* T cell responses at diagnosis of amyotrophic lateral sclerosis predict disease progression. *Nat. Comm.* **13** (2022)

33. Mizuno, T. *et al.* Interferon-γ directly induces neurotoxicity through a neuron specific, calcium-permeable complex of IFN-γ receptor and AMPA GluRl receptor. *The FASEB Journal* **22** (2008)

34. Pan, W., Banks, W. A. & Kastin, A. J. *Permeability of the blood-brain and blood-spinal cord barriers to interferons*. *Journal of Neuroimmunology* **76** (1997)

35. Goverman, J. Autoimmune T cell responses in the central nervous system. *Nature Reviews Immunology* **9** (2009)

36. Bonney, S. *et al.* Gamma Interferon Alters Junctional Integrity via Rho Kinase, Resulting in Blood-Brain Barrier Leakage in Experimental Viral Encephalitis. *mBio* **10** (2019)

37. Song, R. *et al.* Two modes of the axonal interferon response limit alphaherpesvirus neuroinvasion. *mBio* **7** (2016)

38. Lin, Y. L. *et al.* CRABP1-CaMKII-Agrn regulates the maintenance of neuromuscular junction in spinal motor neuron. *Cell Death Differ.* (2022)

39. Corrado, L. *et al.* A novel peripherin gene (PRPH) mutation identified in one sporadic amyotrophic lateral sclerosis patient. *Neurobiol. Aging* **32** (2011)

40. Chen, G. *et al*. PD-L1 inhibits acute and chronic pain by suppressing nociceptive neuron activity via PD-1. *Nat. Neurosci.* **344** (2017)

Chapter 5. Evaluate the physiological relevance of the iPSC-spinal motor neurons by comparing transcriptomic trajectories of differentiating *in vitro* culture to that of the developing human spinal cord ventral horn

5.1 Abstract

Advances in neurodegenerative disease modeling with human iPSC-derived cells provided an unprecedented opportunity to recreate the disease pathophysiology in human tissue. Since the first iPSC-spinal neurons were generated in 2010, several differentiation protocols have been developed to generate spinal neurons that better mirror their native counterparts. However, those protocols in common generate a mixture of an undefined subpopulation of neurons, with unknown transcriptomic profiles and developmental statuses of various non-neuronal byproducts. Current in vitro differentiation protocols still lack in detail on how to provide those signals in the correct spatiotemporal manner but rely on the daily provision of induction morphogens and growth factors that have extremely short half-lives without fully understanding their mechanism of action for inducing neurogenic signaling cascades in vivo. Moreover, there is a minimal understanding of which stage the iPSC-spinal neurons correspond to the native developmental pathways, and how the neuronal composition and gene expression profile is different from those of the native spinal cord ventral horn. These overall shortcomings make the representation of iPSC-spinal neurons questionable, significantly hindering the extensive application of the *in vitro* culture for disease modeling. To address these critical shortcomings, we longitudinally analyzed the transcriptome of the developing iPSC-ventral spinal neurons at a single cell level, to compare it with that of the developing human spinal cord ventral horn. We analyzed the longitudinal expression of marker genes identifying critical cell types in the ventral spinal cord development, to assess the physiological relevance of neurodevelopment in culture. Particularly, we focused on analyzing the subpopulations of neurons generated through our iPSC differentiation protocol, by

quantifying the key marker gene expressions for the different ventral spinal neuron types. In the future analysis, we will also perform a side-by-side transcriptomic comparison of the *in vitro* data with that obtained from fetal spinal cord ventral horn at various gestational stages, to map their gene expression trajectories. We expect this comprehensive transcriptomic matching will provide us with an important molecular clue to enhance our current spinal neuron differentiation protocol to more accurately mimic native ventral spinal neuron development. Furthermore, this initial transcriptomic study will provide us an invaluable insight into how and when we should co-culture them to the developing iPSC-derived skeletal muscle, for generating functional human NMJ in the future to model NMDs as a whole.

5.2 Introduction

The progressive pathology of NMDs is driven by defects in more than one neuronal subtype.[1,2] The interaction of these neuronal subpopulations in the ventral horn of the spinal cord is essential for normal development, long-term survival, and function throughout life.[2,3] Moreover, the exquisitely designed inter-neuronal crosstalk may affect their transcriptomic profiles during spinal cord development.[4–7] However, the current iPSC-spinal neuron differentiation protocols were built upon an insufficient understanding of the temporal window of native neurodevelopment. In addition, in vitro neural differentiation protocols rely on the daily addition of small molecule cocktails without having information on the molecular kinetics at each stage of inductions.[1,3,8,9] Consequently, we have been producing unknown subpopulations of neurons and contaminating cell mixtures that are not likely to mirror that of the native spinal cord ventral horn. Moreover, we have no idea how the transcriptomic profiles of each of the neurons differentiated in vitro are different from those of their native counterparts. Therefore, we posit that our inability to consistently generate the correct ratio of neuronal subtypes and transcriptomic status, and have them survive and continue to function long-term is caused by inaccurate inductive signals that do not mimic the exquisite spatiotemporal signaling gradients during embryonic development. This shortcoming has been a major roadblock to understanding the native biology and pathophysiology of the system as a whole.

In an attempt to recapitulate the spatially and temporally dynamic mixture of neuronal subtypes in vivo, we need to create an iPSC-derived human spinal cord ventral horn by mimicking the structural organization and morphogen gradients established during de novo rostral/caudal and dorsal/ventral patterning. Specifically, we hypothesize developmental pathway as well as how their neuronal transcriptome and subtype composition are different.

In this final aim, we analyzed the gene expression profile of differentiating iPSC culture from an undifferentiated state to day45 of post-mitotic neuronal state. The cellular composition at each critical stage of their development was analyzed to confirm they are on the correct neurogenic pathway. Additionally, we analyzed their transcriptome to understand which subpopulation of spinal neurons were generated, using known marker genes for those neurons. Moreover, we studied whether the neurons express a set of essential genes required for neuromuscular development since the NMJ develops through the reciprocal signaling of motor neurons and skeletal muscle from the initial developmental stage. In future works with this aim, we will perform a side-by-side single-cell transcriptomic comparison of neuronal subtypes differentiating *in vitro* to human fetal spinal cord neurons at multiple gestational stages. We will establish an iterative workflow of identifying fetal neuronal clusters with distinct transcriptional signatures that then drives the refinement of our *in vitro* differentiation protocol. We expect this comprehensive dataset will provide us with an important temporal guidance map of signaling cues that drive the critical stages of native neurogenesis. It will also tell us how to provide kinetically accurate stimulation to each stage of differentiating iPSC, leading to generating a much more physiologically relevant population of ventral spinal neurons. Additionally, this advancement in ventral spinal neuron differentiation will fuel our future studies like the creation of an iPSC-derived neuromuscular tissue for a more comprehensive pathophysiological study of NMDs at a tissue level.

5.3 Materials and Methods

5.3.1 Differentiation of iPSCs into spinal motor neurons

Human iPSCs (WTC11) were passaged onto Matrigel-coated 6-well plates as described above and incubated at 37ºC/ 5% CO_2 in mTeSR until they reached ~50% confluency. At this point, cultures were differentiated into regionally unspecified neural progenitor cells using a monolayer differentiation method adapted from Smith *et al*.[13] Briefly, the undifferentiated day0 cells were treated with dual-SMAD inhibitors, SB431532 and LDN193189, as well as ascorbic acid (AA). CHIR99021 was added to the medium for the purpose of activating the Wnt pathway, which has been proven to enhance neuroepithelial differentiation and proliferation. At day 5, cultures were treated with All-trans retinoic acid (RA) for caudalization and the SHH agonist Purmorphamine, to give ventralization cues to the cells. On day 11, cells were passaged onto fresh Matrigel coated 6-well plates and treated with RA and AA until day 18 to expand the neural progenitor population. These cells were then passaged at 100,000 cells/ cm^2 onto 0.01% poly-L-ornithine (Sigma-Aldrich) and 5 µg/mL laminin (Sigma-Aldrich)-coated surfaces and exposed to culture conditions promoting motor neuron differentiation. Specifically, cells were fed with 10 ng/mL of neurotrophic factors (BDNF, GDNF, IGF-1 from R&D systems, NT3 from Stem Cell Technologies), ascorbic acid (2.27 µM). During all stages of differentiation, a basal medium consisting of a 1:1 mix of Neurobasal medium and DMEM/F12, supplemented with B27, Glutamax, N2, Non-essential amino acids, and penicillin-streptomycin, was used. All cells used in the described experiments were differentiated from WTC11 colonies between passages 45 and 55.

5.3.2 Immunocytochemistry

Cells were fixed in 4% paraformaldehyde for 15 minutes and permeabilized in 0.2% Triton-x solution, followed by blocking with 5% goat serum in PBS for 1 hour at room temperature. Cells were then incubated with primary antibodies diluted in 0.5% BSA in PBS overnight at 4°C. The next day, cells were washed 3 times with PBS. They were then incubated in a secondary antibody solution containing secondary antibodies diluted in 0.5% BSA in PBS overnight at 4°C. Counterstaining was performed with Vectashield containing DAPI (Vector Labs). Images were taken at the Garvey Imaging

Core at the University of Washington's Institute for Stem Cell and Regenerative Medicine using a Leica SP8 Confocal System on an inverted microscope platform. 12-bit 2048x2048 pixel images were acquired with Leica LAS X software. Antibodies used in this study were as follows: mouse anti-Islet1 (1 in 200, DSHB), rabbit anti-β III tubulin (1 in 500, Sigma Aldrich), rabbit anti-PAX6 (1 in 200, Invitrogen), goat anti-Nestin (1 in 200, Invitrogen), Alexafluor-488 conjugated goat-anti-mouse secondary antibody (1:500, Invitrogen), Alexafluor-594 conjugated goat-anti-rabbit secondary antibody (1:500, Invitrogen) and Alexafluor-647 conjugated Donkey-anti-goat secondary antibody (1:500, Invitrogen).

5.3.3 Single cell RNA sequencing

Single cells were collected on the motor neuron differentiation day3,5,8,11,15,18,21,24,27 and stored in LN2 until the day of library generation. The single cells on the differentiation day 30,35,40,45,50 were stagger-cultured from the different starting dates to run the library generation experiment on the same day without freeze-thawing step. Total of 15 samples from different differentiation day are divided into three groups to generate three multiplexed libraries with Chromium NextGem library construction kit (10x Genomics) to proceed with serial sequencing due to the capacity limit. Specifically, the generated cDNAs of single cells from each group were barcoded with 10x Genomics' Chromium Next GEM Chip G Single Cell Kit and Chromium Next GEM Single Cell 3' Kit v3.1, by following the manufacturer's protocol. Constructed libraries were loaded to the Tapestation (Agilent) to quantify the cDNA amount and confirm fragmentation status, followed by sequencing with the Illumina NextSeq2000 (P3 reagent) at the Genomics core with the University of Washington's Institute for Stem Cell and Regenerative Medicine. The sequencing was performed at an estimated read depth of 10,000 reads/cell. Sequenced FASTQ reads were initially processed using CellRanger v.3 software with settings recommended by the manufacturer (10X Genomics).

5.3.4 Transcriptomic data analysis

Read alignment, filtering, barcode counting, and unique molecular identifier (UMI) counting was performed using *CellRanger* data processing software provided by 10x Genomics. The feature barcoded matrix was obtained for further gene expression analysis with Seurat V4.0.6. The quantitative summary of sequencing was obtained from the *CellRanger*. For the comparative gene expression analysis, cells with low UMI counts, doublets, and cells with relatively high mitochondrial DNA content were removed. The cleared datasets were subsequently normalized in order to correct for differences in read depth and library size, using Seurat's "LogNormalize" function which divides feature counts of the cell by its total counts, followed by multiplying the scale factor. The PCA was performed with the integrated data post-normalization, followed by running the "RunUMAP" function to generate 2-dimensional UMAP projections using the top 10 principal components detected in the dataset. For the cluster annotation, a marker gene list was obtained from the literature published by Rayon et al. The data visualization was performed with codes provided by Seurat (scatter plots, feature plots, heatmaps, violin plots) and Graphpad prism (bar plots). For the gene ontology analysis, ShinyGo V 0.76.2 was used.

5.4 Results

5.4.1 Human spinal motor neurons are successfully differentiated from WTC11 WT iPSCs

The *in vitro* spinal motor neuron differentiation process involves four major induction stages as illustrated in the previous section. Briefly, the undifferentiated pluripotent stem cells are initially treated with small molecules (SB431542, LDN193189) that inhibit the mesodermal pathway and induce early neuroectodermal fate. Du et al additionally found that activation of WNT by using CHIR99021 promotes the enrichment of neuroepithelial cells as well as their proliferation in the early progenitor phase. We adapted these protocols for optimizing the initial neuroectodermal induction from day 0 to day 5 in culture, mimicking the regionally unspecified neural tube formation in vivo The second phase of the differentiation involves a further patterning of the neuroepithelial cells within the dorso-ventral and rostro-caudal axis to specifically derive them into the ventral spinal neurons. The dorso-ventral

patterning depends on the gradient of sonic hedgehog (SHH) signaling generated from noto cord below the neural tube. The high concentration of SHH molecules induces ventralization of the precursor cells whereas dorsalization mainly occurs where the SHH signal phases out. Additionally, SHH gradient determines the generating ratio of motor neurons to interneurons, the two major neuron types in the ventral horn of the spinal cord. We used purmorphamine, a potent SHH agonist with varying concentrations for adjusting the level of ventralization as the differentiation proceeds. For rostro-caudal patterning, previous studies have demonstrated that all-trans retinoic acid (RA) is a key regulator of caudalization by controlling the expression pattern of HOX genes. Therefore, the introduction timing, duration, and gradient of RA and SHH treatment combinatorically determines the regional identity of spinal neurons during early spinal cord development. We treated RA from day 6 to day 18 at which the initial neural induction was assumed to be completed. The early progenitors expanded mainly from day 11 to day 18 to enrich the culture with the neural precursor population that expresses Nestin and Pax6.**[Figure 5.1A, 5.1B]** To induce neural maturation without having the neurotrophic support from glia, we provided human recombinant brain-derived neurotrophic factor (BDNF), glial-derived neurotrophic factor (GDNF), ciliary neurotrophic factor (CNTF) together with the Insulin-like growth factor-1 (IGF-1) daily basis from day 18 to the end of the culture. The day25 culture expressed lateral motor column marker ISL-1 with significant growth of neurites, indicating the cells are on the motor neuron differentiation track. **[Figure 5.1C]** Pax6.**[Figure 5.1A, 5.1B]** To induce neural maturation without having the neurotrophic support from glia, we provided human recombinant brain-derived neurotrophic factor (BDNF), glial-derived neurotrophic factor (GDNF), ciliary neurotrophic factor (CNTF) together with the Insulin-like growth factor-1 (IGF-1) daily basis from day 18 to the end of the culture. The day25 culture expressed lateral motor column marker ISL-1 with significant growth of neurites, indicating the cells are on the motor neuron differentiation track. **[Figure 5.1C]**

5.4.2 Longitudinal single-cell RNA sequencing provided overall transcriptomic view of the differentiation

To run the longitudinal sequencing analysis, we collected 1 million cells from each culture, for every three days from day0 to day30, and kept frozen in -150 °C until the assay date. From day30 to day50, we collected the same number of cells for every 5 days but used fresh culture due to the low viability of late-stage neurons after defrosted. The total 15 multiplexed libraries from iPSC to day50 of culture were generated with 10x Chromium 3' library construction kit for sequencing run. The pooled library solution was sequenced with Illumina 1000/2000 P3 cartridge kit. We first analyzed the

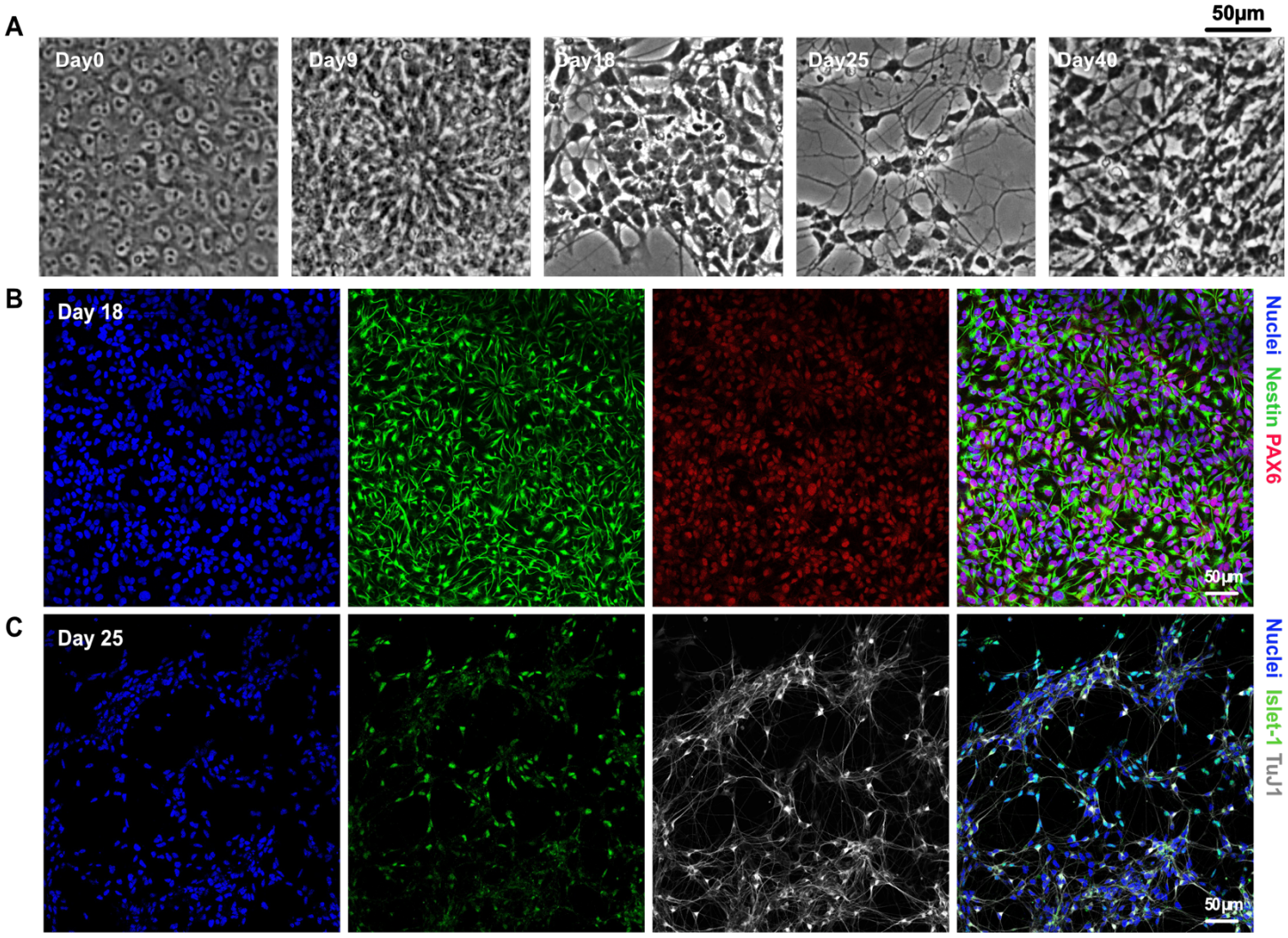

Figure 5.1 Expression of protein markers at each stage of spinal motor neuron differentiation (A) Morphological development of neurons during the differentiation and the time points of single cell collection (B) Day 18 progenitor cells express the intermediate filament Nestin and paired box protein-6 (PAX6), a canonical marker of early neural precursor cells. (C) Day 25 neurons show the early neuron marker Islet-1, mainly expressed in the lateral motor neurons, and beta tubulin, the pan-neuronal marker.

sequencing result of libraries at 4 critical time points, iPSC, day18, day24, day30 to understand the initial picture of the differentiation status. **[Figure 5.2A]** The number of cells recovered for sequencing was 5,608 on average, with more cells recovered from the day 30 culture than other groups, presumably due to the fewer cell death that occurred in the live cell culture. Throughout those points, 54,120 total readings per cell were made on average, and the number of genes detected was 4,961 per cell on average. **[Figure 5.2B]**

To understand cell type diversity in each sample, we performed clustering analysis using UMAP algorithm embedded in Seurat v4.0.6. The clustering resulted in generating 8 (iPSC), 9 (day18), 13 (day24), and 12 (day30) different clusters in each group. The result showed a close proximity of clusters for iPSC and day18 culture, which implies the majority of cells share common genes and are on a similar track of the differentiation process, whereas the day24 culture showed a bifurcated clustering trend which became more evident in the day30 culture, implies the cells were divided into two main lineages as the differentiation proceeds. **[Figure 5.2C]**

As expected, the undifferentiated culture highly expressed canonical pluripotency markers such as OCT4, CNMD, and NANOG although there was a variance among the level of these marker expressions in culture. We also found a high % of cells expressing SOX2, which is a transcription factor expressed both in stem cells and early ectoderm. Interestingly, 11.58% of the iPSC culture expressed early neural progenitor marker MAP2, implying some of the stem cells are losing their stemness but auto-differentiated into the ectodermal lineage, which is known as a default pathway of germ layer differentiation. Further analysis revealed that those cells (mainly in cluster 6 of the iPSC library) were much less expressing pluripotency markers but shifted to ectoderm even without receiving any induction cues of differentiation. (data not shown)

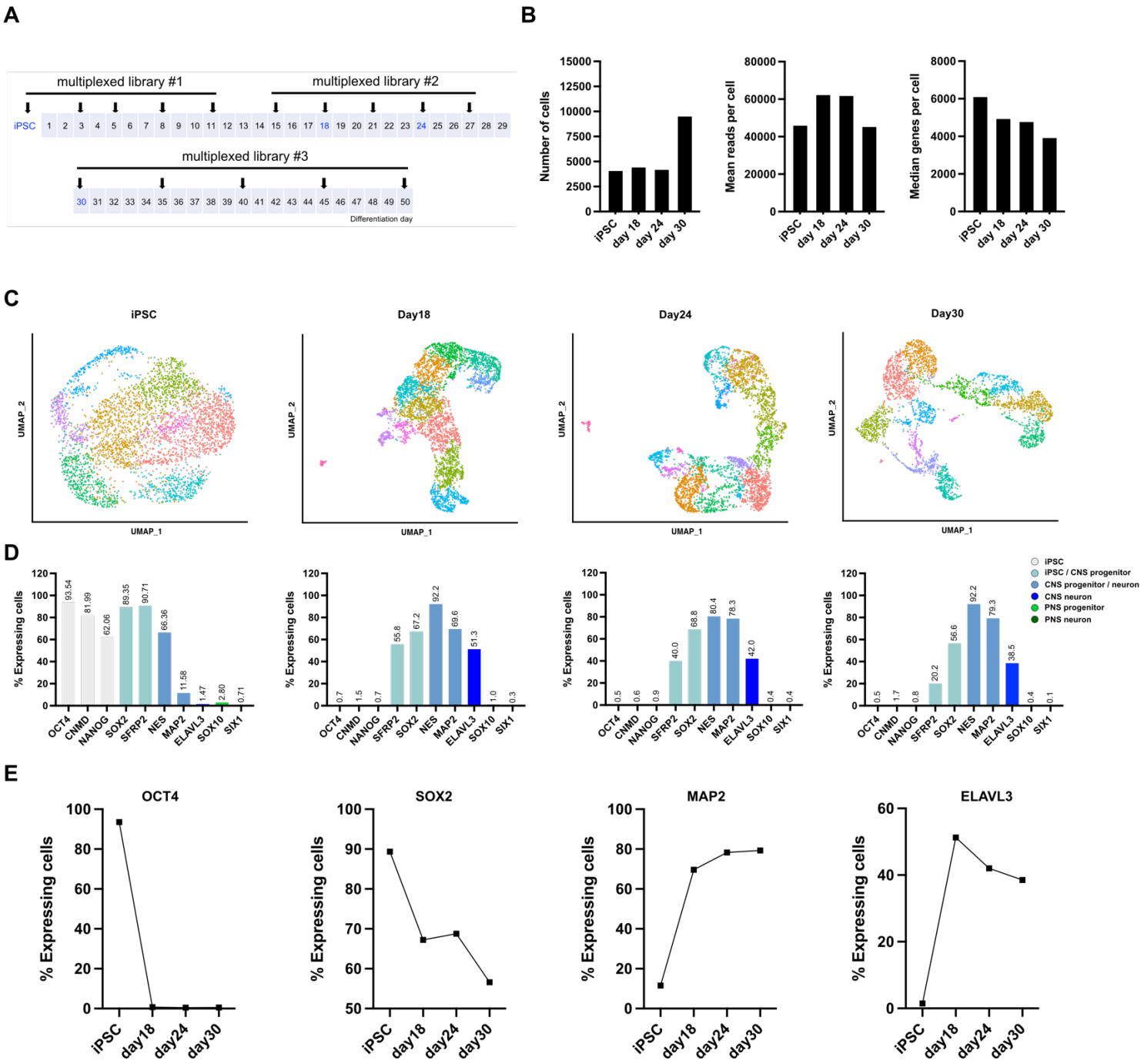

Figure 5.2 The trend of critical marker gene expression for the libraries at 4 critical differentiation time points
(A) Timeline of the single cell collection for library preparation (B) Sequencing metric distribution from 4 different libraries. The number of cells sequenced, total molecules detected per cell, and the number of genes discovered from each cell. (C) UMAP clustering analysis shows each stage of culture is composed of 9~13 different clusters based on their gene expression similarities. (D) Quantitative analysis of critical marker genes at each stage of differentiation. The cell types based on each marker gene expression were categorized as iPSC, iPSC/CNS progenitor, CNS progenitor/neuron, CNS neuron, PNS progenitor, and PNS neuron. (E) Time course change of marker gene expression. OCT4 = pluripotency marker, SOX2 = pluripotency / ectoderm marker, MAP2 = CNS progenitor & neuron marker, ELAVL3 = CNS neuron marker. The % expressing cells is the ratio of cells expressing each marker to the total cells in the culture.

From day18 culture, pluripotency marker expression disappeared in all clusters, indicating the entire culture completely lost its pluripotency but differentiated into the specific lineage of cells. The day 18 cells showed high expression of SFRP2 and SOX2, which shows the culture is likely to be dominated by cells from ectoderm, where the neural precursors are made. At the same time, those cells with highly expressed Nestin and MAP2, strongly imply that most cells are successfully differentiated at least into neural precursors, although further analysis for the cell type annotation is required to specify their subclasses. Surprisingly, over 50% of day18 cells were also expressing CNS neuron markers, ELAVL3, and STMN2, which we expected to see from the later stage of differentiation. Given that both gene expression is known to well discriminate post-mitotic neurons from early neural precursors, a significant expression of them in culture verifies the differentiation process occurs faster than we expected. In the day30 culture, we saw a substantial reduction in SFRP2 and SOX2 but a similar level of MAP2 and ELAVL3 which indicate the neurogenic process may reach the plateau state. However, we need to employ more specific marker genes to better understand where the cells are on their developmental track. Although not a significant change, the decrease of ELAVL3 expression after day18 may need more explanation to understand their developmental status better. **[Figure 5.2D, 5.2E]**

We further sought to understand how the day18 culture is different from a later stage of differentiation, first by analyzing the ratio of neural precursors to neurons. We picked day27 culture for the side-by-side comparison with day18 culture since it has been the first evaluation time-point of the differentiation. We found a significant difference in their gene expression profile presented by UMAP clustering analysis. **[Figure 5.3A, 5.3B]** Although the faster pace of differentiation than we expected, we found the day18 culture is still enriched with neural progenitors expressing SOX2, many of which were disappeared in the day 27 culture but mostly replaced by MAP2 positive population. We confirmed this finding by analyzing more of the marker genes, such as MKI67, NEFL, NEFM, and NRG1. The high expression of SOX2, NEX, and MKI67 in the cells at the left region of the UMAP verified the early precursors are confined to those clusters. Conversely, MAP2, ELAVL3, STMN2, NEFL, NEFM, and

NRG1 were exclusively expressed in the cells of the rest of the region, making clear segregation of progenitors and post-mitotic neuronal populations.**[Figure 5.3C]** We confirmed that high expression of neuronal markers in clusters 1,4,7,11 in day27 culture **[Figure 5.3D]**, which were having spinal cord identity verified by high expression of HOX genes. The day 27 neurons were mainly expressing HOX3 to HOX9, showing the differentiated neurons have hindbrain to cervical identity in the spinal cord. **[Figure 5.3E]** We further studied the subpopulation of the day27 neurons by using markers for V0, V1, V2, and V3 interneurons and motor neurons. Only a few cells expressed markers for V0 and V1 interneurons but a notable number of cells expressed the V2 interneuron marker ASCL1, and V3 interneuron marker NKX2-2 and SIM1 which all work as transcriptional factors. As expected, more than half of the neuronal population expressed at least one of the motor neuron marker genes, which verifies the neuronal clusters are enriched with motor neurons. The result indicating the protocol can generate more population of V2, and V3 interneurons and motor neurons than another subclass of ventral spinal neurons. **[Figure 5.3F]** The UMAP subgroup clustering of ELAVL3 and STMN2 positive population confirmed that 4 clusters are expressing pan-neuronal markers. **[Figure 5.4A, 5.4B]** cluster 6 and 7 were enriched with V2 and V3 interneurons with more V2 interneurons in cluster 7 and more of V3 interneurons in cluster 6. **[Figure 5.4C, 5.4D]** We also found that cluster 6 has SLC18A3 and CHAT-positive motor neuron populations, suggesting that a single cluster is not simply comprised of one type of neurons but a mixture of multiple neuronal subtypes. We did not see a notable expression of canonical spinal motor neuron marker expression, ISL1, and MNX, which is known to be transiently expressed. However, high expression of marker genes for cholinergic neurons verifies that clusters 0 and 6 are enriched with motor neurons. **[Figure 5.4E, 5.4F]**

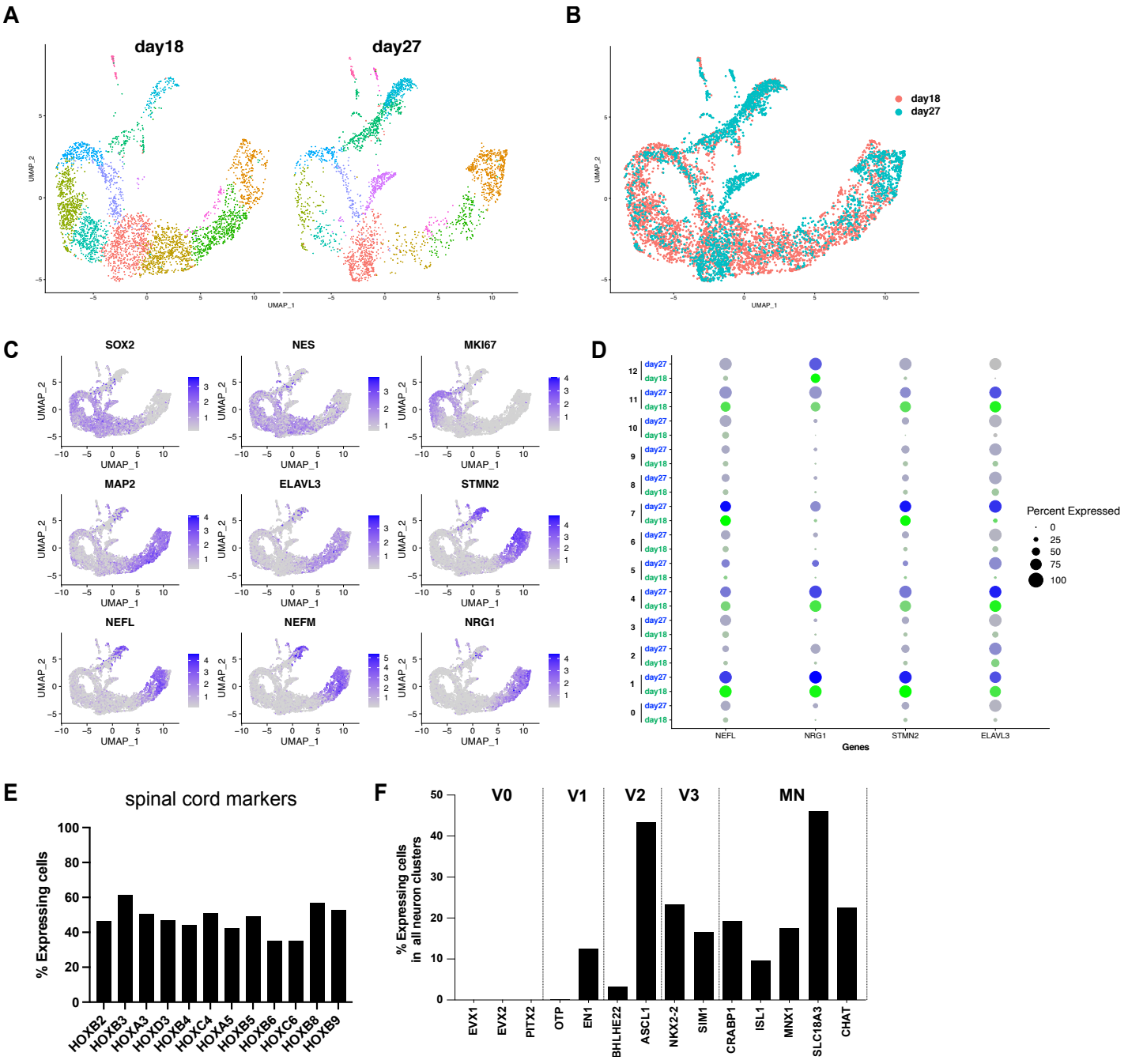

Figure 5.3 Gene expression analysis of day18 and day27 culture (A) Side-by-side UMAP comparison of day18 and day27 cultures (B) superimposed UMAP figure of those cultures show a distinct difference in the single cell gene expression (C) The featured plot shows a bifurcate expression pattern of neural progenitor markers (left) and post-mitotic neuron markers (right) in the integrated UMAP (D) The neuronal gene expression pattern in each cluster of day18 and day27 culture (E) Quantitative analysis of HOX gene expressions verifies the spinal cord identity of the differentiated day27 neurons (F) Sub-neuronal population analysis of the day27 culture with marker genes for V0,V1,V2,V3 ventral interneurons and motor neurons. The neurons in the day27 culture did not express genes for the dorsal horn of the spinal cord.

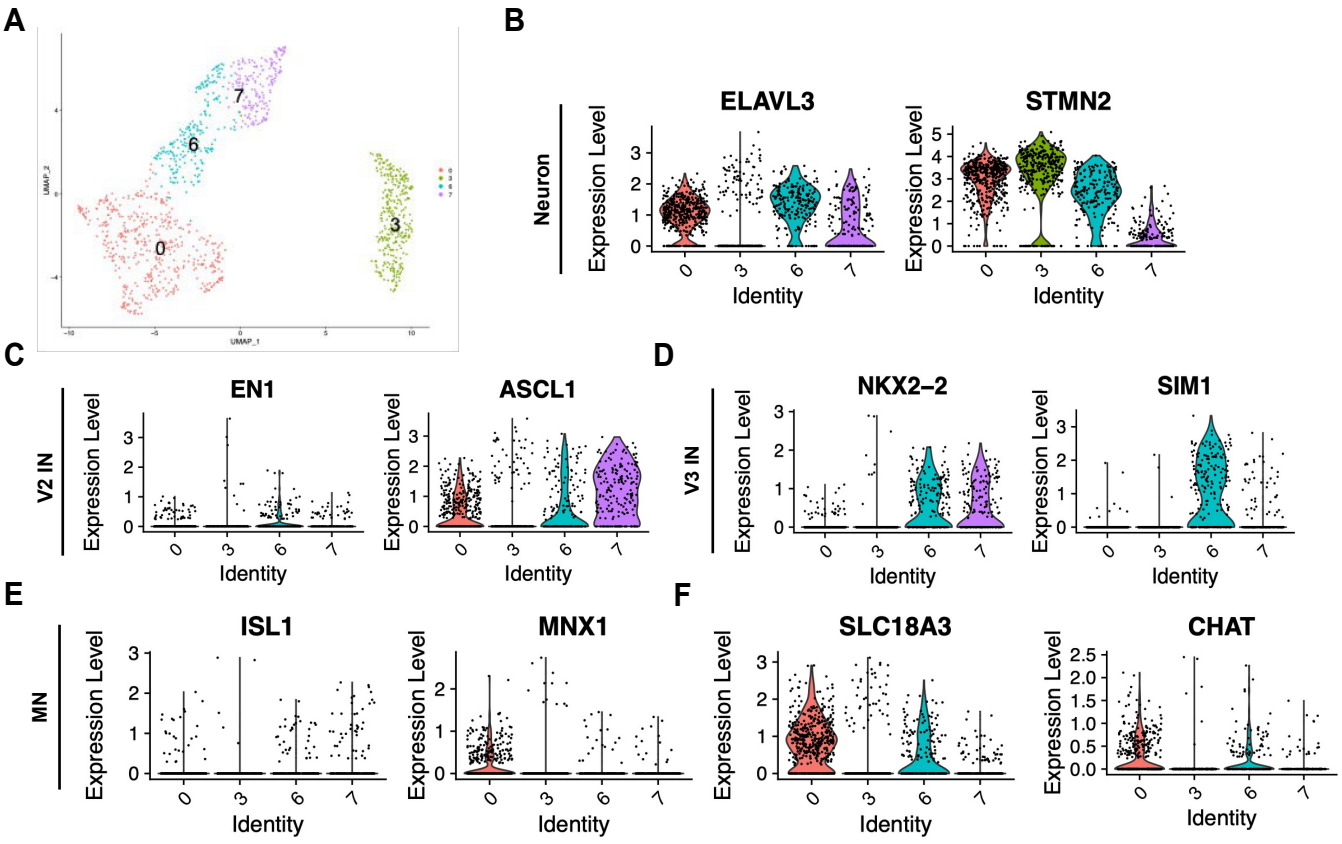

Figure 5.4 Marker gene expression in each neuronal cluster (A) UMAP of subgroups expressing neuronal markers (B) Pan-neuronal marker ELAVL3 and STMN2 expression in cluster 0,3,6,7. (C) V2 interneuron marker expression (D) V3 interneuron marker expression (E) Motor neuron marker expression in cluster 0,3,6,7.

Next, we compared the gene expressions of the day27 neuron clusters to that of the developing human spinal cord. We used the raw data shared by Rayon *et al* (2021), to reproduce figures of transcriptomic expression. We found the native spinal cord made the more clear transition of neural progenitors to neurons by CS19, demonstrated by the evident increase of cells expressing MAP2, ELAVL3, and STMN2, and a decrease of NES. On the other hand, the day27 culture was still enriched with SOX2 and NES-positive cells, which implies the cells in the day27 culture are still under active neurogenesis. **[Figure 5.5A, 5.5B]** Further comparison of marker expression for interneuron and motor neurons revealed more notable differences in the subpopulation of ventral neurons generated in each culture. The NKX2-2 and SIM1 level shows that *in vitro* differentiation makes much more V3 interneurons than *in vivo*, within this period of native spinal cord development.

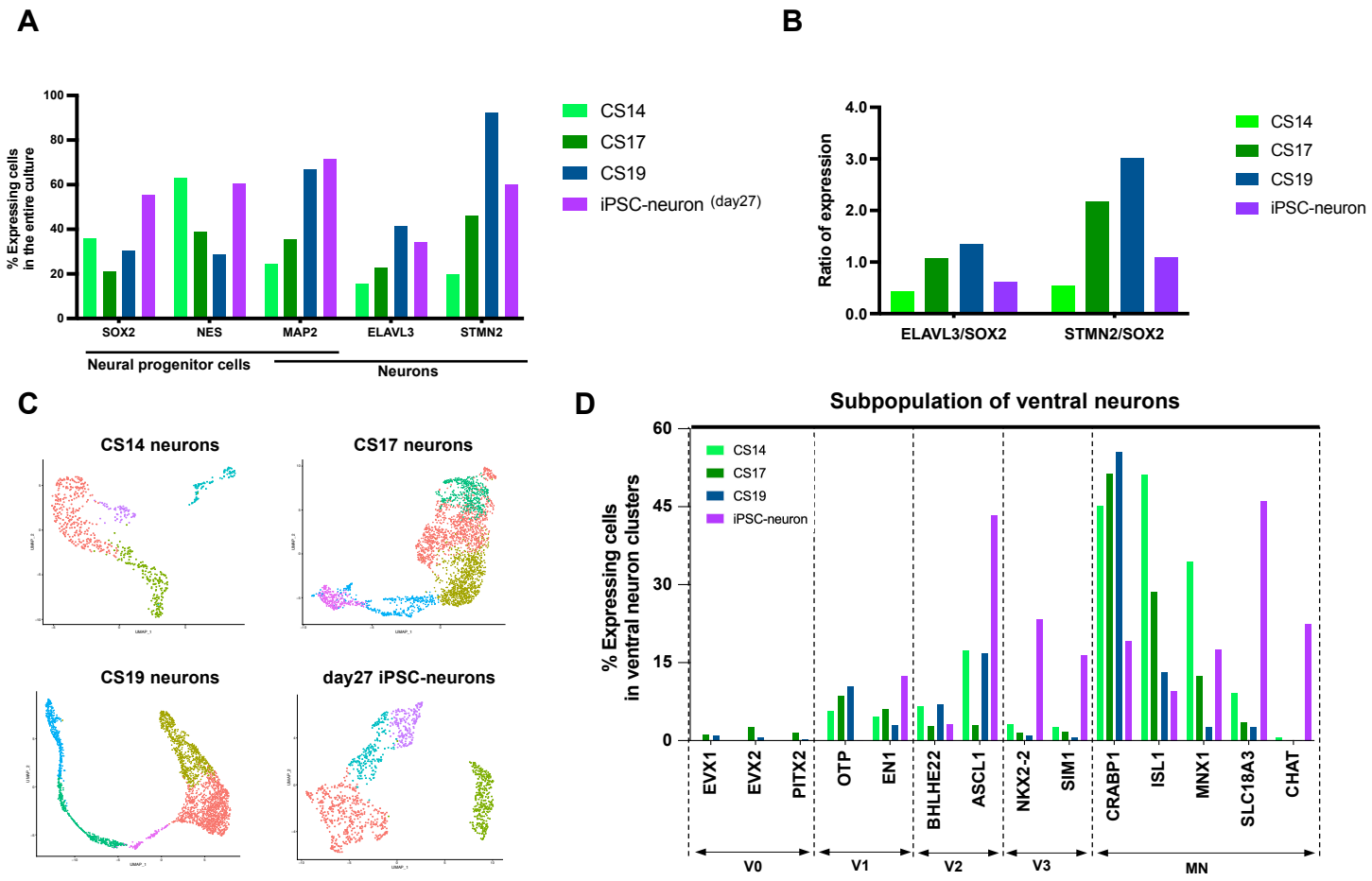

Figure 5.5 Gene expression comparison of day 27 in vitro culture with those of developing human spinal cord at the Carnegie stage 14,17,19. (A) Population % expressing neural progenitor and pan-neuronal marker genes. (B) The ratio of cell expression genes for neurons to progenitors shows the day27 culture resembles more of the CS14. (C) UMAP of the developing human spinal cord (D) % expressing cells in each culture for the selected marker genes in the ventral population.

Spinal motor neurons in each cluster also showed clear disparities in CRABP1, SLC18A3, and CHAT expressions. We found the day27 culture showed a much lower level of CRABP1 gene than in any of the three developmental stages *in vivo*, whereas the SLC18A3 and CHAT level was extremely higher *in vitro* differentiation than *in vivo* cases. **[Figure 5.5C, 5.5D]**

5.5 Future works

In addition to the initial set of results presented above, we aim to perform a more in-depth analysis of the raw dataset obtained from the whole 15 libraries in vitro to reveal the unknown transcriptomic dynamics along the motor neuron differentiation. Moreover, we will suggest how the current iPSC-spinal motor neuron differentiation protocol should be improved to generate a

physiologically relevant population of spinal motor neurons, particularly to develop the first functional human NMJ in a dish with iPSC-derived skeletal muscle. To this end, we will perform an extensive transcriptomic trajectory analysis with Monocle 3 algorithm to map the chronological gene expression change in pseudo-time, followed by selecting critical gene sets for the motor function to track how the transcripts are expressed along the differentiation timeline. Moreover, we will compare the result with that of the developing human spinal cord we will collect, to better understand the physiological relevance of iPSC-derived ventral spinal neurons. We expect this comprehensive side-by-side transcriptomic comparison will provide significant insight into the field of neuromuscular disease modeling research, to ultimately develop more reliable therapeutic approaches in the near future.

5.6 Reference

1. Ho, R. *et al.* Cross-Comparison of Human iPSC Motor Neuron Models of Familial and Sporadic ALS Reveals Early and Convergent Transcriptomic Disease Signatures. *Cell Syst* **12**, 159-175.e9 (2021).

2. Blum, J. A. *et al.* Single-cell transcriptomic analysis of the adult mouse spinal cord reveals molecular diversity of autonomic and skeletal motor neurons. *Nat Neurosci* **24**, 572–583 (2021).

3. Thiry, L., Hamel, R., Pluchino, S., Durcan, T. & Stifani, S. Characterization of Human iPSC-derived Spinal Motor Neurons by Single-cell RNA Sequencing. *Neuroscience* **450**, 57–70 (2020).

4. Chen, S. *et al.* Optimized methods for rapidly dissecting spinal cords and harvesting spinal motor neurons with high survival and purity from rats at different embryonic stages. *Journal of Spinal Cord Medicine* **41**, 281–291 (2018).

5. Zhang, Q. *et al.* Single-cell analysis reveals dynamic changes of neural cells in developing human spinal cord. *EMBO Rep* **22**, (2021).

6. Fu, Y., Rusznák, Z., Herculano-Houzel, S., Watson, C. & Paxinos, G. Cellular composition characterizing postnatal development and maturation of the mouse brain and spinal cord. *Brain Struct Funct* **218**, 1337–1354 (2013).

7. Delile, J. *et al.* Single cell transcriptomics reveals spatial and temporal dynamics of gene expression in the developing mouse spinal cord. *Development (Cambridge)* **146**, (2019).

8. Lin, C. Y. *et al.* IPSC-derived functional human neuromuscular junctions model the pathophysiology of neuromuscular diseases. *JCI Insight* **4**, (2019).

9. Hawrot, J., Imhof, S. & Wainger, B. J. Modeling cell-autonomous motor neuron phenotypes in ALS using iPSCs. *Neurobiology of Disease* vol. 134 Preprint at https://doi.org/10.1016/j.nbd.2019.104680 (2020).

Chapter 6. Conclusions and Future Directions

The research presented in this dissertation illustrates the physiological role of non-neuron autonomous factors such as astrocytes and inflammatory cytokines on neuromodulation using iPSC-derived spinal motor neurons. We believe this work has many implications for future neuromuscular disease modeling efforts. We established a protocol to generate human spinal motor neurons in culture, and suggested a way to evaluate their developmental status at a single cell level to improve the physiological relevance of the in vitro model. Moreover, our approach to understanding neurons' physiological dependency in normal and diseased conditions provided comprehensive insight to better understand neurodegenerative drivers and suggested potential immunotherapy targets to combat the disease. Specifically, in the first aim study, we found the iPSC-neurons' survival and electrophysiological function can be highly improved by treating the normal astrocyte's extracellular vesicles in a dose-dependent manner, which contains a variety of neuroprotective nucleic acids and proteins verified by the cargo profile analysis. In the second aim study, we showed that pro-inflammatory stress induced by the continuous treatment of interferon-γ extensively alters the transcriptomic profile of motor neurons toward the neurodegenerative direction. Interestingly, the stressed motor neurons exhibited pathologic hallmarks of ALS such as electrophysiological excitotoxicity and cytoplasmic TDP-43 aggregation. This result strongly implies that excessive exposure of the spinal cord to the inflammatory cytokine could derive a severe level of peripheral neurodegeneration. Finally, this dissertation study also includes an extensive analysis of iPSC-derived ventral spinal neuron's physiological relevance by performing longitudinal transcriptomic profiling along their differentiation, to provide an objective view of how well the iPSC-derived neurons recapitulate the developmental status of their native counterpart.

These efforts have potential implications to create new approaches for understanding the upstream pathology of many types of NMDs in a comprehensive manner since they commonly show aberrant glial activity and excessive immune infiltration during the course of disease development. The

result presented in this study implies that the therapeutic efforts may need to be focused on regulating non-neuron autonomous factors which could potentially promote explosive neurodegeneration. In future studies, we aim to elucidate the signaling mechanism of neurodegeneration derived from dysregulated immunity and glial activity to identify therapeutic sites to immunologically block the pathogenic signaling cascade. Additionally, we aim to construct 3D human NMD models in a dish with more reliable iPSC-derived motor neurons and skeletal muscle as a high-throughput platform of drug discovery, to accurately assess the therapeutic efficacy of the candidate therapeutic molecules at the functional tissue level.